Élő sejtek és kopolimer bevonatok kezelése zöld tea polifenollal (EGCg): dinamikai vizsgálatok jelölésmentes bioszenzorokkal

DOI:10.18136/PE.2016.623

Péter Beatrix Éva

- Doktori (PhD) értekezés -

Pannon Egyetem – Molekuláris- és Nanotechnológiák Doktori Iskola

Magyar Tudományos Akadémia Műszaki Fizikai és Anyagtudományi Intézet

Témavezető:

Dr. Horváth Róbert

Budapest, 2016

Living cells and copolymer coatings exposed to green tea polyphenol (EGCg): dynamic investigations using label-free optical biosensors

Beatrix Éva Péter

- Ph.D. thesis-

University of Pannonia– Doctoral School of Molecular- and Nanotechnology

Hungarian Academy of Sciences, Institute of Technical Physics and Materials Science

Supervisor:

Dr. Róbert Horváth

Budapest, 2016

Living cells and copolymer coatings exposed to green tea polyphenol (EGCg): dynamic investigations using label-free optical biosensors

Értekezés doktori (PhD) fokozat elnyerése érdekében

Írta:

Péter Beatrix Éva

Készült a Pannon Egyetem – Molekuláris- és Nanotechnológiák Doktori Iskolájában

Témavezető: Dr. Horváth Róbert

Az értekezést témavezetőként elfogadásra javaslom:

Dr. Horváth Róbert: igen / nem ……..

(aláírás)

A jelölt a doktori szigorlaton …… %-ot ért el.

Az értekezést bírálóként elfogadásra javaslom:

Bíráló neve: ……. igen / nem ……..

(aláírás)

Bíráló neve: ……. igen / nem ……

(aláírás)

A jelölt az értekezés nyilvános vitáján …… %-ot ért el.

……

Bíráló Bizottság elnöke

A doktori (PhD) oklevél minősítése ……

……

EDT elnöke

Veszprém,……..

TABLE OF CONTENTS

PhD értekezés kivonata

A zöld tea egyik hatóanyaga, az epigallokatekin-gallát (EGCg) hatásait már régóta vizsgálják, és számos esetben derült fény egészséget megőrző tulajdonságaira, többek között arra, hogy csökkenti a rák kialakulásának, az áttétek képződésének, illetve a szív, -és érrendszeri betegségek kockázatát, csökkenti a vérnyomást, koleszterinszintet és vércukrot, gyorsítja az anyagcserét, továbbá egyes tanulmányok szerint segít a vírusok és baktériumok elleni védekezésben is. Pozitív hatásairól rengeteg publikáció beszámol, azonban a szakirodalomban ellentmondásos adatok, eredmények is fellelhetők. Ennek oka valószínűleg az, hogy az EGCg kis molekulatömegű és rendkívül instabil anyag. Ezen tulajdonságai miatt jelöléses módszerekkel problémás, nehézkes lehet e polifenol vizsgálata. A szakirodalomban az esetek túlnyomó részében jelöléses módszereket alkalmaztak, így tehát hiánypótló munkának is nevezhető ezen különleges hatóanyag jelölésmentes technnikákkal történő vizsgálata.

A jelölésmentes bioszenzorok és képalkotó technikák robbanásszerű fejlődésen mentek keresztül az utóbbi években; a biológiai alapkutatásokban csak most kezdődött a kiaknázásuk, a műszerek egyre érzékenyebbek, alkalmazásuk új utakat nyithat meg a biológiai alapkutatásokban és biotechnológiai alkalamzásokban. Az említett technikák fontos előnye, hogy a méréseket valós időben, jelölő anyagok, festékek nélkül tudjuk megvalósítani, így ezek nem befolyásolják a vizsgált mintákat. Kutatásaim során modern jelölésmentes módszereket alkalmaztam az EGCg vizsgálatára, hogy megfigyeljem a hatásait élő sejtekre (HeLa sejtvonal), és kopolimer bevonatokra, mindezt valós időben. Különös figyelmet fordítottam a szakirodalomban eddig meglehetősen hiányosan taglalt oxidált formájára is. Megvizsgáltam, hogy az oxidált forma hogyan befolyásolja a bevonatokat, illetve a sejtek életfolyamatait, adhézióját, morfológiáját.

PhD munkám során Holomonitor képalkotó technikával bebizonyítottam, hogy az EGCg gátolja a HeLa rákos sejtek mozgását. Epic BT bioszenzorral mért eredmények alapján megállapítottam, hogy az EGCg hozzákötődik az alkalmazott PLL-*g*-PEG (sejttaszító) és PLL-*g*-PEG:PLL-*g*-PEG-RGD (sejtek adhézióját segítő) szintetikus kopolimer bevonatokhoz, és multiréteget alkot. Az EGCg molekulák kötődése a bevonatokhoz elhangolja azok tulajdonságait, és az alkalmazott koncentrációk függvényében befolyásolják a HeLa sejtek adhézióját az említett felületekre. A bioszenzorral rögzített adhéziós kinetikai görbék tekintetében felfedeztem egy határ koncentrációt (27,3 ± 10 μg/ml), mely alatt szigmoid jellegű adhéziós kinetikai görbéket kapunk (élő, aktív folyamatra jellemző), míg ennél nagyobb koncentrációnál adszorpciós görbéket rögzítettem (élettelen folyamat jellemzője). Ezen eredmények egyezést mutatnak a sejtek életképességét vizsgáló MTT teszttel. Megfigyeltem, hogy az oxidált formának még erőteljesebb a hatása; több réteg képződik a bevonatokon, és a sejtadhézióra gyakorolt befolyása is jelentősebb. Az orvostudomány többek között nanoméretű részecskék segítségével igyekszik megoldást nyújtani a hatóanyagok kizárólag a célsejtekbe történő bejuttatására. Ezen irányvonalat felvéve kísérletet tettem olyan ellentétesen töltött, arany nanorészecskékből álló klaszterek (AuMUA és AuTMA) előállítására, melyek a jövőben esetlegesen alkalmassá válhatnak az EGCg célsejtekbe történő szállítására, és így betegségek gyógyítására.

Abstract (English)

Scientists examine the effects of epigallocatechin-gallate (EGCg), one of the active substances of green tea, for a long while. Beneficitial impacts on health are revealed in a lot of cases, for example, it reduces the risk of the formation and metastasis of cancer, it reduces the risk of cardiovascular diseases, blood pressure, level of cholesterol and blood sugar, it intensifies the metabolism and helps to fight against bacteria and viruses. Numerous papers have been published about its positive effects, however, there are contradictory data and results in the literature as well. The reason is probably that the EGCg has small molecular weight and it is a very unstable, sensitive material. Because of these properties, its examinations by labeling techniques can be difficult and problematic. In the literature the authors mostly uses labeling methods in general, thus, examination of this specific material EGCg by label-free techniques may supply the incompletions.

Label-free biosensors and imaging techniques underwent enormous progress in the past years; their utilization in biological basic researches has just begun, the appliances are more and more sensitive, their application may open new ways in biological basic research and biotechnology. The advantages of these methods are that they are real-time, and do not use labels, such as dyes, that may affect the samples. In my experiments, I applied these novel techniques to investigate EGCg and its effects on living cells (HeLa cell line), and on copolymer coatings in a real-time way. I paid attention to the EGCg's oxidized form, which is a pretty untended topic in the literature, and I examined that how can the oxidized EGCg affect the coatings and the action, adhesion, morphology of the cells.

In my PhD work, I proved by Holomonitor M4 imaging technique that EGCg inhibit the movement of the HeLa cervical cancer cells. I revealed by Epic BT biosensor that EGCg binds to the PLL-*g*-PEG (cell repellent) and PLL-*g*-PEG: PLL-*g*-PEG-RGD (cell attractive) synthetic copolymer coatings and the EGCg molecules form multilayers. The EGCg binding modifies the original properties of the coatings and inhibits HeLa cell adhesion to them in a concentration dependent manner. In the case of kinetic curves, I discovered a border concentration (27.3 ± 10 μg/ml μg/ml). At lower concentration of EGCg than this value, I recorded sigmoid type cell adhesion curves (active, living process), and at higher concentrations, adsorption type curves (dead process) were obtained. I verified with MTT assay, that the cell viability of HeLa cells start to decrease at around 27.3 ± 10 μg/ml EGCg concentration, thus I got the same result by MTT as well. The oxidized form has more powerful effect; more layers formed than in the case of freshly created EGCg solutions, and its inhibitory impact on cellular adhesion is more robust as well.

Medical sciences try to cure illnesses by transporting active substances in nanoparticles to reach only the targeted cells. To follow this trend, I attempted to create clusters from oppositely charged gold nanoparticles (AuMUA and AuTMA), which may be able to transport EGCg to targeted cells and thus cure illnesses in the future.

Estratto (Italiano)

Gli scienziati esaminano gli effetti di epigallocatechina gallato (EGCg), uno dei principi attivi del tè verde, per lungo tempo. Effetti caritatevoli sulla salute sono rivelati in molti casi, per esempio riduce il rischio della formazione e la metastasi del cancro, riduce il rischio di malattie cardiovascolari, pressione sanguigna, livelli di colesterolo e di zucchero del sangue, si intensifica il metabolismo e aiuta a combattere contro i batteri e virus. Esso è stato pubblicato numerosi articoli di suoi effetti positivi, tuttavia, ci sono dati ed i risultati opposti nella letteratura. La ragione è probabilmente che EGCg ha piccolo peso molecolare ed è molto instabile. Grazie a queste proprietà, i suoi esami di tecniche di etichettatura può essere difficile e problematico. Nella letteratura gli autori utilizza prevalentemente i metodi di etichettatura in generale, in tal modo, l'esame di questo materiale specifico, EGCg con tecniche senza etichette possono fornire le carenze. Biosensori senza etichette e tecniche di imaging ha subito enormi progressi negli ultimi anni; il loro utilizzo in ricerche di base biologica è appena iniziata, gli apparecchi sono sempre più sensibili, la loro applicazione potrebbe aprire nuove strade nel campo della ricerca di base biologica e biotecnologia. I vantaggi di questi metodi è che sono in tempo reale, e non utilizzano etichette o coloranti che possono influenzare i campioni. Nei miei esperimenti, ho applicato queste nuove tecniche per indagare EGCg e il suo impatto sulle cellule viventi (linea cellulare HeLa), e sui rivestimenti copolimero in un modo in tempo reale. Ho preso in considerazione la forma ossidata della EGCg, che è un argomento incustodito abbondanza nella letteratura, e ho esaminato che come può il EGCg ossidato influenzare i rivestimenti e l'azione, l'adesione, morfologiche delle cellule. Nel mio lavoro di dottorato, ho dimostrato da Holomonitor M4 tecnica di imaging che EGCg inibisce il movimento delle cellule del cancro del collo dell'utero HeLa. Ho studiato da Epic BT biosensore che l'EGCg si lega al PLL-*g*-PEG (repellenti cellulare) e PLL-*g*-PEG: PLL-*g*-PEG-RGD (cellule attraente) rivestimenti copolimeri sintetici e le molecole EGCg formano multistrati su di loro. EGCg vincolante modifica le proprietà originali dei rivestimenti e inibisce l'adesione delle cellule HeLa a loro in un modo dipendente dalla concentrazione. Nel caso di curve cinetiche, ho scoperto una concentrazione confine (27.3 ± 10 μg/ml). A valori inferiori a 27.3 ± 10 μg/ml di EGCg ho ricevuto diffusione curve (attivi, processo vivente), e al di sopra di questo valore, le curve di assorbimento (processo morto). Ho verificato con test MTT, che la vitalità cellulare di cellule HeLa inizia a diminuire a 27.3 μg ± 10 μg/ml concentrazione d'EGCg, quindi ho ottenuto lo stesso risultato MTT pure. La forma ossidata ha un effetto più potente; più strati possono essere formati che nel caso di appena creato EGCg, e il suo impatto inibitorio sulla adesione cellulare è più robusto pure. Scienze mediche cerca di curare le malattie da trasporto di sostanze attive in nanoparticelle di raggiungere solo le cellule bersaglio. Per seguire questa tendenza, ho cercato di creare grappoli da nanoparticelle d'oro di carica opposta (AuMUA e AuTMA), che possono essere in grado di trasportare EGCg alle cellule mirati e quindi curare le malattie in futuro.

1. INTRODUCTION

Herbs and traditional medicines have been applied for thousands of years, but researchers started to study their mode of action at the molecular, cellular and tissue levels only recently. Nowadays, just like in the ancient ages, natural compounds are still determining factors in remedy. To support this statement, the recently won Nobel Prize in 2015 could be mentioned for an anti-malaria agent from the plant sweet wormwood which had been used to effectively treat the disease. Among natural compounds and traditional Chinese medicines, the green tea polyphenol epigallocatechin gallate (EGCg) is one of the most studied active substance. However, in general scientists apply labeling techniques to investigate its effects on cell adhesion, migration, motility, apoptosis, etc. However, label-free biosensors can be emerging platforms to investigate the mode of action of small molecules and are highly relevant for EGCg research and development [1]. My first authored "Biophysical characteristics of proteins and living cells exposed to the green tea polyphenol epigallocatecin-3-gallate (EGCg): Review of recent advances from molecular mechanisms to nanomedicine and clinical trials" titled review paper was mainly used for the introduction of EGCg (chapters 1.1-1.6) [1].

1.1. Epigallocatechin-gallate (EGCg), the green tea polyphenol

Drinking tea is an ancient habit; legends from India and China indicate that it started about 5000 years ago [2]. Traditionally, it was drunk to eliminate toxins and improve blood flow and resistance to illnesses [2], so its habitual consumption has long been associated with health benefits [3]. Infusion of the unfermented leaves of *Camellia sinensis* (L.) Kuntze, known as green tea, is a very popular drink worldwide nowadays as well. Green tea beverage contains polyphenolic compounds, including phenolic acids, flavanols, flavonoids and flavandiols [4]. In a typical green tea infusion, prepared in a portion of 1 g leaves to 100 ml water in a few minutes brew, most of the polyphenols are flavanols, known as catechins, and account for about 30–42 % of the dry weight of the solids [4][5]. Among green tea catechins, epigallocatechin gallate (EGCg) is the most abundant, around 16.5 wt% of the water extractable fraction of green tea leaves [5]. This component is regarded as a constituent characterizing green tea, because it is not found in any plants except *C. sinensis* (L.) Kuntze [5]. Tea catechins, especially EGCg, have been shown and reviewed to have various health benefits, for example, anti-metastasis, anti-cardiovascular, anti-cancer, antiinflammatory and antioxidant effects [4][6][7].
EGCg is one of the most studied active substance, and a lot of studies observed its effects on several cancer and normal cell lines and on animal models (Fig.1.1) [1][6][8].

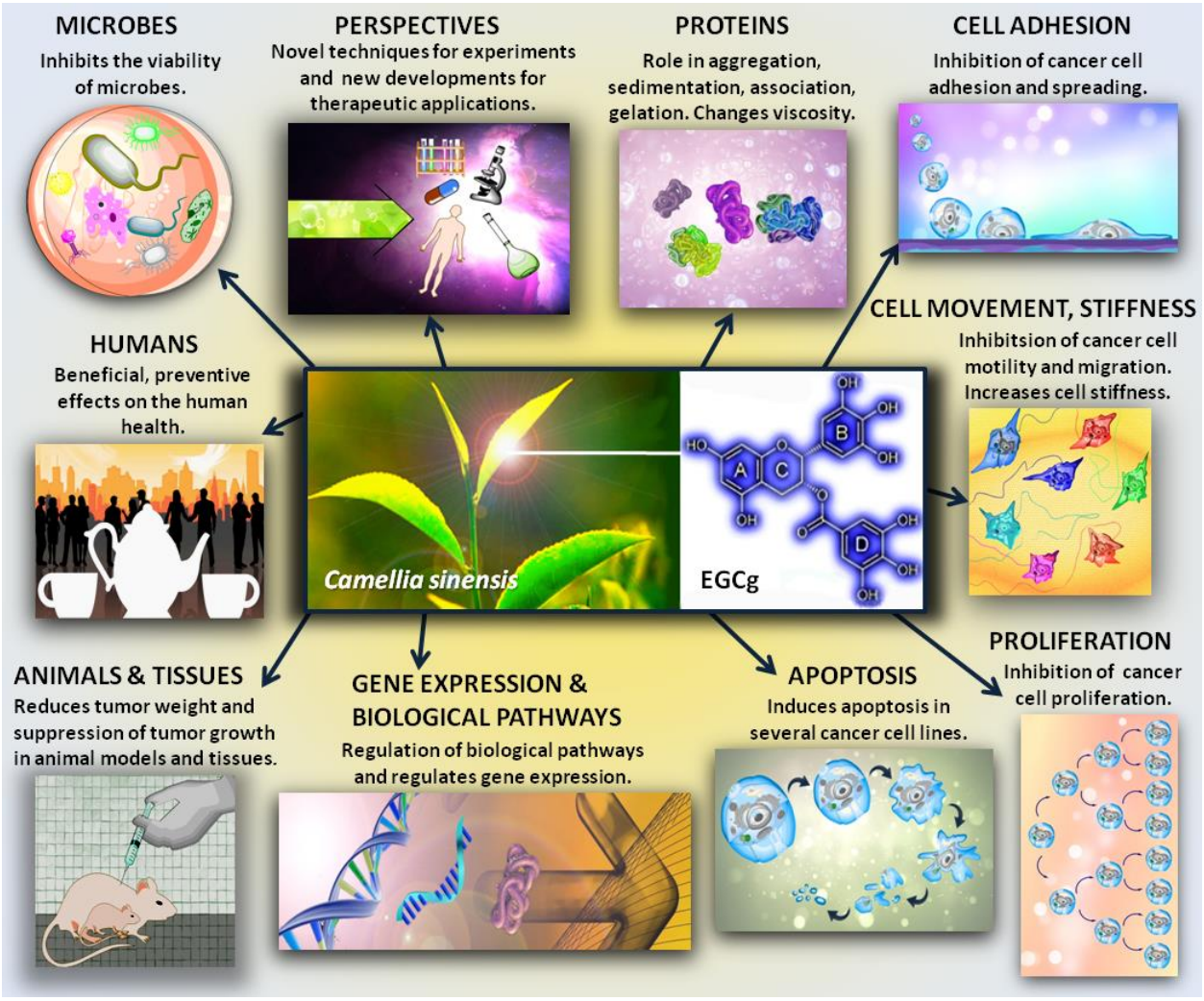

Fig.1.1 Diversified effects of EGCg. This polyphenol affect proteins: EGCg causes aggregation, association, sedimentation, precipitation and gelation, furthermore, increases viscosity, and act as a cross-linker in the case of mucins. It is suggested that EGCg interacts with phospholipids and plasma membrane proteins. It inhibits the amyloid-fibril formation of α-synuclein, amyloid-β and huntingtin. Cancer cell adhesion, movement, proliferation are decreased, while apoptosis is increased in the presence of EGCg *via* gene expression and biological pathways in *in vitro* tests. *In vivo* studies also showed reduced tumor weight and suppression of tumor growth in animal models and tissues, as well as clinical trials also showed its beneficial effects on the human health. Experiments proved that it inhibited the viability of microbes as well. Due to EGCg's special properties, curing and other utilizations, experiments can be put in perspective [1].

1.2. Molecular scale properties and interactions of EGCg

Epigallocatechin gallate (EGCg)[1], is the ester of epigallocatechin and gallic acid. EGCg is an odorless white, (sometimes faint pink) crystals (or powder). It is soluble in ethanol, dimethyl-formamide, dimethyl sulfoxide (DMSO) and water[2]. This compound ([(2R,3R)-5,7-dihydroxy-2-(3,4,5-trihydroxyphenyl)-3,4-dihydro-2H-chromen-3-yl] 3,4,5-trihydroxybenzoate*) consists of a meta-5,7-dihydroxyl substituted A ring and trihydroxy phenol structures on both the B and D rings. The polyphenolic structure of tea polyphenols makes them good donors for hydrogen bonding [8]. For instance, hydrogen bonding of water molecules to EGCg forms a big hydration shell, which reduces the absorption of EGCg [8].The hydrogen bonding capacity enables these compounds to bind strongly to nucleic acids and proteins [1][8].

Bioavailability of EGCg

Poor bioavailability of tea catechin compounds needs to be considered when we extrapolate in vitro results to in vivo situations [5][7][9]. Cool and dry storage, fasting conditions, vitamin C, fish oil, albumin, piperine and soft water enhance the bioavailability of EGCg, while air contact oxidation, gastrointestinal inactivation, glucuronidation, metal ions (e.g., Ca^{2+}, Mg^{2+}), sulfation and COMT polymorphisms decrease its bioavailability [7]. In living organisms, EGCg absorption takes places mostly in the small intestine, and it passes to the large intestine where it is broken down to phenolic acids by the action of colonic microflora [7]. EGCg is principally excreted through the bile to the colon [5]. In human volunteers, the time to reach the maximal concentration (326 ng/ml (=0.326 μg/ml)) in the plasma was between 1.5 and 2.5 h after consumption of decaffeinated green tea solids (4.5 g dissolved in 500 ml water) [5][10]. According to publications, its level in blood after consuming the equivalent of 2-3 cups of green

[1] (CAS Registry number: 989-51-5, PubChem CID: 65064; IUPAC Name*: [(2R,3R)-5,7-dihydroxy-2-(3,4,5-trihydroxyphenyl)-3,4-dihydro-2H-chromen-3-yl] 3,4,5-trihydroxybenzoate; alternative and trade names: (−)-cis-3,3',4',5,5',7-Hexahydroxy-flavane-3-gallate, (−)-cis-2-(3,4,5-Trihydroxyphenyl)-3,4-dihydro-1(2H)-benzopyran-3,5,7-triol 3-gallate (Sigma-Aldrich) (2R,3R)-2-(3,4,5-Trihydroxyphenyl)-3,4-dihydro-1[2H]-benzopyran-3,5,7-triol-3-(3,4,5-trihydroxybenzoate), DNA Methyltransferase Inhibitor IV, HAT Inhibitor X, Histone Acetyltransferase Inhibitor X, p300/CBP Inhibitor VIII, PCAF Inhibitor V, DNA MTase Inhibitor IV (Merck), (2R,3R)-2-(3,4,5-Trihydroxyphenyl)-3,4-dihydro-1[2H]-benzopyran-3,5,7-triol 3-(3,4,5-trihydroxybenzoate), inhibitor of NOS, telomerase and Dnmt (Enzo Life Sciences), molecular Formula: $C_{22}H_{18}O_{11}$, molecular weight: 458.40 Da)

[2] according to substance records available from Sigma-Aldrich; Merck and Alexis Biochemicals (now fully integrated into Enzo Life Sciences)

tea was 0.1-0.6 μM and for an equivalent of 7-9 cups was still lower than 1 μM (=0,458 μg/ml) [5].The catechin levels were not detectable by 24 h, and the half-life of EGCg was 5.0–5.5 h [5][10].

Antioxidant activity and stability

Tea polyphenols are well known for their antioxidant activities [11]. Among them, EGCg is the most effective in reacting with the reactive oxygen species (ROS) [5]. Thus, some studies have reported that EGCg is an antioxidant; however, on the other hand, Kim et. al reviewed that it exerts pro-oxidant actions as well [12]. Its antioxidant activities are due to the presence of phenolic groups that are sensitive to oxidation and can generate quinone, an oxidized derivative of aromatic compounds [3]. The antioxidant potential of EGCg is reported to be greater than those of vitamin C and E [13]. Tea polyphenols are also strong chelators [5]. They have a significant interaction with transition metal ions and form insoluble complexes with iron [2]. Thus, this binding in the gastrointestinal tract inhibits iron absorption; however, it only affects non-heme iron and can be overcome by the presence of ascorbic acid [2]. As pointed out by Tachibana, the chelation of free metal ions prevents the formation of ROS from auto-oxidation of many components [5]. It has been reported by several authors that EGCg and other catechins are unstable at high temperature and under alkaline as well as neutral conditions, at pH above 7, EGCg dimerizes and oxidizes easily [11][14]. It changes from non-colored at around pH 7 to yellow at higher pH regions in aqueous solution, and the absorption is in the UV range [15]. This observation indicated that the oxidation is an irreversible reaction, and Mizooku et al. reported that the oxidation species was found to correspond to *M*w + 14 (where *M*w is the molecular weight of EGCg), which has two hydrogen atoms removed and addition of one oxygen atom to the gallyl moiety in the B-ring of EGCg [15]. EGCg is stable in saline or Ringer's solutions at low temperature, unless there are particular metal ion contaminants present [16]. According to a study of Zhou and co-workers, there are clear advantages to stabilizing EGCg solutions by using an antioxidant (ascorbic acid), metal scavenger (EDTA), keeping the pH somewhat below neutral and keeping the temperature low during storage and sampling of EGCg [16]. EGCg is known to be unstable under cell culture conditions, and both autooxidation and H_2O_2 generation are induced [15][17][18]; however, formation of H_2O_2 was observed in aqueous solutions as well [15]. According to a proposed mechanism by Hou and co-workers, the reaction in cell culture medium is probably catalyzed by metal ions such as Cu^{2+} and produces EGCg radicals and superoxide [19]. The unpaired electron may delocalize around the B ring [19]. The superoxide radical can further react with another EGCg molecule to produce EGCg radical and H_2O_2 [19]. Two EGCg radical molecules probably collide to form a dimer, or it can be possible that the EGCg radical may attack the B ring of another EGCg molecule, which is more abundant, to form a dimer radical [19]. It can react with molecular oxygen to form the EGCg dimer and regenerate the superoxide radical [see Fig. 2(a)] [19]. An alternative mechanism by the same authors is that

the EGCg radical is oxidized by an oxygen molecule to form $\cdot O_2^-$ and EGCg quinone (oxidized derivative), and the quinone reacts with another molecule of EGCg to form the dimer [see Fig. 2(b)] [19]. In both cases, the process is propagated by the reaction of superoxide with EGCg, generating H_2O_2 and EGCg dimers [19]. Then these dimers can be further transformed to other compounds, supposedly polymers, in a similar manner of oxidation (see Fig. 1.2) [19].

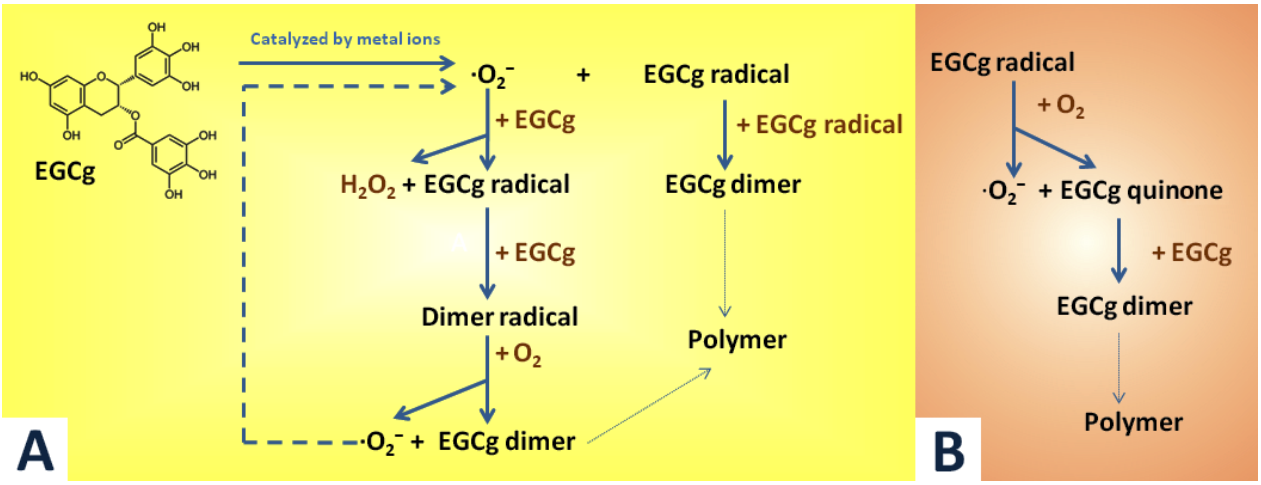

Fig.1.2 Proposed mechanisms of EGCg auto-oxidation under cell culture conditions by Hou and co-workers [1][19]. (a) The reaction in cell culture medium is probably catalyzed by metal ions such as Cu^{2+}, and produces EGCg radicals and superoxide radicals [19]. The unpaired electron may delocalize around the B ring [19]. The superoxide radical can further react with another EGCg molecule to produce EGCg radical and H_2O_2 [19]. Two EGCg radical molecules probably collide to form a dimer, or it can be possible that the EGCg radical may attack the B ring of another EGCg molecule, which is more abundant, to form a dimer radical [19]. It can react with oxygen molecule to form the EGCg dimer and regenerate the superoxide radical [19]. (b) An alternative mechanism by the same authors is that the EGCg radical is oxidized by an oxygen molecule to form $\cdot O_2^-$ and EGCg quinone (oxidized derivative), and the quinone mayreact with another molecule of EGCg to form the dimer [19].

The major oxidation products are theasinensin A (molecular weight 914 Da) and another dimer with a molecular weight of 884 Da [11][19]. Both are dimers of EGCg, which have been reported to be formed in mild alkaline fluids or after radical reaction with 1,1-diphenyl-2-picryl-hydrazyl radical, and show a brown-yellow color (Fig.1.3) [11].

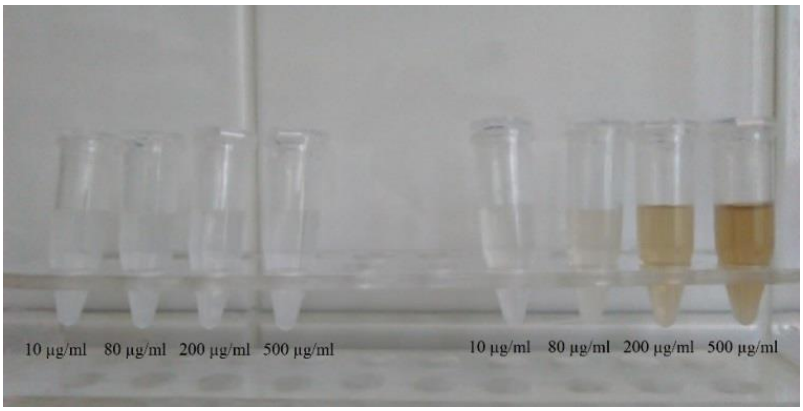

Fig.1.3 Freshly created EGCg suspensions on the left, and their oxidized form on the right. The solutions became brown in a concentration dependent manner when left at ambient temperatures.

It remains to be determined whether the auto-oxidation of EGCg occurs in vivo, but there is no evidence for auto-oxidation in the mouse: the EGCg is rather stable, and dimers have not been detected in the blood [19]. Furthermore, the *O*-methylated form of EGCg, the (−)-epigallocatechin 3-*O*-(3-*O*-methyl) gallate (EGCg3″Me), is more stable than EGCg in animal and human plasma [18]. However, in a previous study of Hong et al., EGCg was unstable in McCoy's 5A culture media with a half-life of <30 min, and it increased to 130 min in the presence of cells: addition of 50 µM (= 22.9 µg/ml) EGCg to the culture media caused the production of H_2O_2, but the amount was lower and decreased in the presence of cells [11]. Addition of superoxide dismutase (SOD) and catalase is proposed to avoid artifacts and stabilize itself. Since EGCg degradation is intensified by the higher temperature and humidity, capsules should be stored in dry, cool and hermetically closed places as well, to avoid enhanced oxidation with air contact [7]. However, human serum albumin participates in the stabilization of EGCg in the blood circulation (as an in vivo carrier) [20]. According to a study of Ishii and co-workers, EGCg is stable in human plasma or in aqueous solutions with human serum albumin [20]. The authors suggest that the reversible covalent modification of EGCg via a Schiff base formation and immobilization of the polyphenol to human serum albumin through the formation of a stable complex prevent its decomposition and polymerization [20].

Role of EGCg in protein layer structures and its effect on protein misfolding associated conditions

Saliva is the human and animal organism's first line of defense against ingested insults [21]. Aberrant saliva can result in signs of xerostomia ("dry mouth") and it can interfere with oral defense too [21].The cure of some of these symptoms by treatment with mucin-based saliva substitutes highlights the significance of the mucin-rich network in saliva [21]. Among tea polyphenols, EGCg has the highest affinity to interact with mucins, causing gelation and

precipitation, whereas epicatechin and non-galloylated epicatechins do not [22]. Thus, it is suggested that the presence of the galloyl moiety [D-ring (gallyl)] in the EGCg molecule allows it to bind to mucin, which leads to association and aggregation [22]. EGCg-mucin mixtures indicate that discrete particles are formed whose size increases with the ratio of EGCg to mucin [23]. A study of Zhao et al. suggests that the EGCg-mucin binding process happens by single and/or clusters of EGCg molecules driven to the surface of the mucin's hydrophobic globules by the hydrophobic interaction followed by hydrogen bonding between mucin and EGCg [24]. Multilayer formation by the adsorbing EGCg molecules onto already bound EGCg molecules can occur as well [24]. The adsorption properties of EGCg-mucin mixtures on metal-oxide and biomimetic surfaces were also investigated [23]. In the experiment by optical waveguide lightmode spectroscopy (OWLS), the authors proved that the EGCg triggers a massive adsorption-desorption hysteresis, reflecting a complicated structurally sequential adsorption-desorption behavior [23]. Furthermore, the enhancement of this phenomena with an increasing excess of EGCg mimics the increase of mucin concentration in an EGCg-free system as well [23][25]. Furthermore, it is suggested that EGCg directly interacts with phospholipids and plasma membrane proteins which stimulates intracellular signaling pathways as well [12].EGCg can bind to fibronectin and histidinerich glycoprotein and to the α, β and γ subunit chains of fibrinogen [6][26]. Furthermore, it can bind to keratin as well, and the process is governed by both hydrophobic interactions and hydrogen bonding [27].

Protein-misfolding diseases associated with the failure of a specific peptide/polypeptide or protein to adopt or remain in their native functional form cause diseases such as cataract, type II diabetes, Alzheimer's and Parkinson's diseases [28]. The majority of misfolding diseases are associated with amyloidosis, which involves the aggregation of specific polypeptides into highly stable and cytotoxic amyloid fibrils [28]. Recent studies indicate that EGCg has the ability to inhibit protein aggregation and efficiently inhibits the amyloid-fibril formation of α-synuclein, amyloid-β and huntingtin, the amyloidogenic proteins involved in Parkinson's, Alzheimer's and Huntington's diseases [28][29]. The current understanding of the non-covalent interactions between amyloidogenic polypeptides and EGCg (or other polyphenols) is based on the physicochemical properties and structural similarities of polyphenols [28]. It is conjectured that EGCg and similar polyphenols interact with fibril-forming proteins with aromatic π–π interactions between the polyphenolic rings and the aromatic residues common to most fibril-forming sequences and hydrogen bonding to the polypeptide main chain via the phenolic hydroxyls [28]. In vitro data and results on in vivo animal models suggest that tea consumption may decrease the incidence of dementia [29]. In particular, EGCg showed neuroprotective/ neurorescue activities in various cellular and animal models of neurological disorders [29].

Interaction with laminin, laminin receptor and regulation of signaling

A receptor for the extracellular matrix glycoprotein laminin was isolated and identified by three different laboratories in 1983 [30]. Isolation of the protein from either normal or cancerous cells results in a product with an approximate molecular mass of 67 kDa [30]. The so-called 67LR (67-kDa laminin receptor) is a cell surface receptor with high affinity for its primary ligand [30]. Its role as a laminin receptor makes it an important molecule in both cell adhesion and signal transduction following this binding event [30]. At the cell surface, the laminin receptor exists as both a monomer (37 kDa) and a dimer (67 kDa), and the association with the cell surface is mediated by fatty acid acylation [31]. The 67LR receptor has been implicated in laminin-induced tumor cell migration, attachment, metastasis, angiogenesis, and invasion, too [5]. It is possible that the receptor plays a role in the regulation of cell adherence via the basement membrane laminin [5]. The biological activities of EGCg are mediated through the binding to the cell surface 67LR [32]. Experiments of Tachibana and co-workers using surface plasmon resonance demonstrated the binding of EGCg to the 67LR with a 39.9 nM *K*d value [33]. Furthermore, affinity chromatography revealed the affinity between laminin and EGCg [34]. In an experiment of Suzuki and Isemura, spreading of the cells was markedly inhibited on laminin pretreated with EGCg at 6.25 μM compared to the untreated laminin [34]. These results also suggest the direct binding of EGCg to laminin [34]. Furthermore, it was demonstrated by the authors that gallatecontaining catechins inhibit the adhesion of B16 melanoma cells to laminin [34]. 67LR is a cancer metastasis-associated protein expressed in of tumor cells [31]. The anticancer action of EGCg is due to the lipid raft-associated laminin receptor, which hijacks EGCg from the surface of the cell [31]. According to a study of Fujimura et al., the ten-amino-acid sequence IPCNNKGAHS might be a functional domain responsible for the EGCg's anticancer activity [32]. Expression of the 67-kDa laminin receptor confers EGCg responsiveness to cancer cells at physiologically relevant concentrations (0.1–1 μM (=0.0458-0.458 μg/ml)) [33]. Through 67LR, EGCg can activate myosin phosphatase by reducing MYPT1 phosphorylation and can be involved in EGCg-induced cell growth inhibition [35].

Eukaryotic translation elongation factor 1A (eEF1A) is identified as a component responsible for the anticancer activity of EGCg, through both eEF1A and 67LR; EGCg induces the dephosphorylation of myosin phosphatase-targeting subunit 1 (MYPT1) at Thr-696 and activates myosin phosphatase and silencing of 67LR, eEF1A or MYPT1 in tumor cells, which results in abrogation of EGCg-induced tumor growth inhibition in vivo [35]. eEF1A is upregulated by EGCg through 67LR [35]. These findings of Umeda et al. implicate both eEF1A and MYPT1 in EGCg signaling for cancer prevention through 67LR [36]. 67LR is a critical sensor molecule to respond to EGCg and mediate the beneficial activities of this polyphenol [5]. MYPT1 and eEF1A are EGCg-sensing molecules for EGCg-elicited tumor prevention at physiological concentrations [5]. According to Byun and co-workers, silencing of signaling of Toll-interacting protein (Tollip), a negative regulator of the Toll-like receptor (TLR), impaired the TLR2 (one of the TLRs) signaling inhibitory activity of EGCg, suggesting that TLR2 response can be inhibited by EGCg

via Tollip and 67LR [37]. Thus, EGCg action through the cell surface 67LR can negatively regulate TLR2 signaling [37]. The obstructive effect of EGCg on tumor cell proliferation is exerted through its binding to the 67LR as a cell surface receptor [37]. This green tea polyphenol inhibits cell growth by reducing the myosin regulatory light chain phosphorylation mediated through 67LR [37]. As pointed out by the study of Byun et al., Tollip is a mediator responsible for the anti-TLR2 signaling action of EGCg and provides new perspective into the understanding of negative regulatory mechanisms for the TLR2 signaling pathway [37]. Silencing of 67LR or anti- 67LR antibody treatment resulted in repeal of the inhibitory action of EGCg on peptidoglycan (PGN)-induced output of proinflammatory mediators and activation of mitogen-activated protein kinases [37]. Downregulation of 67LR expression induced a reduction in activity of galloylated catechins [38]. The B-ring hydroxylation pattern and galloyl moiety also participate in the exertion of biological activities of tea catechins and their 67LR-dependencies [38]. 67LR not only mediates the anticancer action of EGCg, but it has also been shown to be responsible for the antiallergic effects of EGCg [38]. Fujimura and co-workers found that the binding of catechins to the cell surface 67LR is responsible for the inhibition of histamine release [38]. 67LR mediated the EGCG3″Me-induced suppression of the high-affinity IgE receptor FcεRI expression by decreasing ERK1/2 (MAP kinases) phosphorylation [18]. According to these findings, the anti-allergic effects of EGCG3″Me may be generated by the inhibition of ERK1/2 or myosin regulatory light chain (MRLC) phosphorylation mediated through the cell surface 67LR [18]. EGCg suppresses the expression of FcεRI and histamine release by binding to 67LR [37].

1.3. Impacts of EGCg at cellular level

Much of the information on the biological activities of green tea polyphenols originated from in vitro studies on cell cultures. The cellular uptake of EGCg is concentration dependent and does not reach a plateau, suggesting a passive diffusion process [11][39]. It is metabolized in the cell, and the metabolites and ECGg are pumped out by multidrug-resistant proteins (MRPs) or Pgp [9][11]. The temperature is important in the uptake process [11]. For example, in the case of HT-29 cells, EGCg accumulation is significantly higher at 4 °C than at 37 °C by over 40 % [11]. In the studied cell lines, this compound has a significant effect on cell adhesion and movement, apoptosis and proliferation generally by altering gene expression [13][40][41][42][43][44][45].

Inhibition of cellular adhesion and spreading in the presence of EGCg

Monitoring of the cellular adhesion and spreading procedures are substantial because these processes take part in maintaining the multicellular structure of the cells, migration, survival, proliferation, differentiation, gene expression, cell-cell communication and immunity, and in cancer metastasis as well. Tea polyphenols, especially EGCg, have become more popular in cell adhesion studies, and many experiments have proved its inhibitory effect [26][34][40][41][46][47][48][49]. EGCg blocks retinal pigment epithelium (RPE) cell adhesion to fibronectin, and it changes the actin cytoskeleton organization during the adhesion process [47]. Fibroblast cell adhesion is greatly reduced on mucin-coated substrata when compared with PLL, but the reduction can be countered by incorporating EGCg into the layer [46]. It is possible that the substratum's viscoelastic properties are the leading influence on initial cell spreading [46]. Tea polyphenols inhibited the expression of CD44 and CD54 adhesion molecules in PG cells (highly metastatic lung carcinoma cell lines) in a dose-dependent manner and significantly blocked the adhesion of these cells to endothelial cells not only in a state of rest but also when active [40]. EGCg influenced CD44 and CD54 expression during the adhesion process of PG cells to endothelial cells [40]. Lo and co-workers reported that EGCg and also epicatechin gallate (ECG) were able to inhibit smooth muscle cell (SMC) adhesion on laminin and collagen (ECM proteins) expressed in physiological and pathological conditions, and the authors found that EGCg can bind more strongly to laminin than collagen [41]. EGCg could inhibit smooth muscle cell adhesion to integrin β1 Ab and affect their β1 integrin expression; proposing it also affects the cellular components [41]. Suzuki and Isemura reported that EGCg in the culture medium was found to inhibit B16 melanoma cell adhesion, furthermore, approximately 50 % adhesion inhibition occurred when the laminin coating was incubated with 4.8 μM (= 2.19 μg/ml) EGCg [34] Table 1.1 summarizes the results and details of the listed references [1].

Table 1.1 Summary of the listed references about the experiments of cellular adhesion and spreading[3]. Cancerous and normal cell cultures were examined by different methods and techniques to reveal the effect of EGCg (concentration between 0 and 200 μM) on adhesion and spreading. EGCg inhibited the cell adhesion and down-regulated the genes evolved in the stimulation of proliferation, adhesion, motility, and invasion processes [1].

CELL LINE	METHOD	OBSERVED EFFECTS	CONCENTRATION OF EGC_g	REFERENCE
B16 (ATCC No.CRL-6322,murine C57BL/6J, mouse melanoma, derived from skin)	Trypan blue dye exclusion assay (cell viability) Affinity chromatography Alamar blue assay (cell viability)	Inhibition of cell adhesion to laminin EGCg binds to laminin	1-200 μM (0.458-91.6 μg/ml)	Suzuki and Isemura 2001
McCoy (ATCC No.CRL-1696,murine, mouse fibroblast)	OWLS110 Staining and confocal microscopy Dynamic Light Scattering HPLC	Cell attachment and spreading is reduced on mucin coated substrata but the reduction can be countered by incorporating EGCg into the layer	no data	McColl et al. 2009
PG (highly metastatic lung carcinoma) **EC** (endothelial cells)	Flow cytometer Laser scanning confocal microscope LPS activating EC cell test	Inhibition of the expression of CD44 and CD54 adhesion molecules Cell adhesion blocking	100, 200, 400, 800 μg/ml (tea polyphenols)	Zheng et al. 2012
A10 (ATCC No.CRL-1476, rat thoracic aorta smooth muscle cells, derivedfrom aorta, thoracic/medial layer)	Dot binding assay Western blot Flow cytometer Cell migration assay (Boyden chamber) Phase-contrast microscope	Inhibition of A10 cell adhesion on collagen and laminin EGCg binds laminin more than collagen Inhibition of A10 cell adhesion to integrin β1 Ab Affection of β1 integrin expression Inhibition of migration	10, 20, 50 μM (4.58, 9.16, 22.9 μg/ml)	Lo et al. 2007
ARPE19 (ATCC No.CRL-2302,human, retinal pigment epithelial cells, derived from eye retina)	Electric cell-subtrate impedance sensing (ECIS) Dot binding assay Immunofluorescence microscopy Western blotting Boyden chamber (migration assay)	Inhibition of PDGF-BB induced RPE cell migration Inhibition of RPE cell adhesion to fibronectin	0,1,3,10 μg/ml	Chan et al. 2010
THP-1 (ATCC No.TIB-202, human, monocytic leukemia, derived from peripheral blood)	Flow cytometry, Annexin V-PE apoptosis kit FRET-based competition assay MCP-1 Human Biotrak Easy ELISA kit Adhesion assay Chemotaxis transwell system (migration assay)	Decreased MCP-1 and CCR2 gene expression Inhibited β1 integrin activation EGCg-induced inhibition of THP-1 migration Inhibited adhesion to fibronectin treatment of inflammation-dependent deseases	100 μM (45.8 μg/ml)	Melgarejo et al. 2009
HeLa (ATCC No. CCL-2, human, cervix epithelial adenocarcinoma derived from cervix)	RNAeasy Mini Kit (total RNA isolation) PCR ELISA MTT assay (cell viability) Attachment assay Spreading assay Adhesion to endothelium assay Transwell migration assay (Boyden chamber)	Down-regulation of genes involved in the stimulation of proliferation, adhesion, motility, invasion processes Up-regulation of several genes known to have antagonist effects	10 μM (4.58 μg/ml)	Tudoran et al. 2012

[3] (ATCC: American Type Culture Collection, CCR2: chemokine (C-C Motif) receptor 2, CD54: cluster of differentiation protein 54 (also known as ICAM-1, intercellular adhesion molecule 1), ELISA: enzyme-linked immunosorbent assay, FRET: fluorescence resonance energy transfer, HPLC: high performance liquid chromatography, LPS: lipopolysaccharide, MCP-1: monocyte chemoattractant protein-1, MTT: 3-(4,5-dimethylthiazol-2-yl)-2,5-diphenyltetrazolium bromide, OWLS: optical waveguide lightmode spectroscopy, PCR: polimerase chain reaction, PDGF: platelet-derivated growth Factor, RPE: retinal pigment epithelium).

Impact on cell motility, migration and stiffness

Observation of the movement of the tumor cells is an important topic: the formation of tumors and metastasis arises when cells are moving [50]. Highly tumorigenic cells move faster than non-tumorigenic cells [51]. Developing drugs that inhibit migration are the focus of many research projects [50]. Traditional herbal extracts have become increasingly popular in the cure of these illnesses. Some studies showed that EGCg is effective against many cancer cell lines [2][3][4][52]. The action of EGCg on cell motility and migration is an actively researched topic today [42][49][52][53][54]. Cell stiffness and motility are related to metastatic activity in tumor cells [42]. An earlier experiment of Takahashi and co-workers also showed that EGCg treatment dose dependently inhibited cell motility and increased cell stiffness in human lung cancer cells and inhibited the expression of vimentin protein and Slug transcription factor as well [42]. EGCg has inhibitory effects on chemoattractant- and hypoxia-stimulated migration of HeLa cells [52] and blocks plateletderived growth factor-BB-induced (PDGF-BB) RPE cell migration [47]. EGCg inhibits the migration of 4T1 cells through the inhibition of nitric oxide production, reduces the levels of cGMP, and inhibits mammary cancer cell migration through the inhibition of NO/NOS and guanylate cyclase [43]. EGCg dose dependently inhibits cell motility and induces rigid elasticity of cell membranes [42]. According to a study of Takahashi et al., treatment with 50 and 100 μM (= 22.9 and 45.8 μg/ml) EGCg can block H1299 cell migration from 100 to 67.5 and 43.7 % [42]. Furthermore, addition of 10, 50 and 100 μM (= 4.58, 22.9 and 45.8 μg/ml) EGCg inhibited Lu99 cell migration to 81.3, 71.7 and 31.5 % as well [42]. In an experiment of Tudoran et al., EGCg caused an average of 48 and 68 % reduction of migration capability after 24 and 48 h [49]. In a novel study, the inhibitory effect on HeLa cell migration, motility and motility speed was also monitored by an incubator proof miniaturized Holomonitor [54]. Table 1.2 summarizes the results and details of the listed references.

Table 1.2 Summary of the listed references about the experiments of motility and migration[4]. Different cancer cell cultures were examined by different methods and techniques to reveal the effect of EGCg (concentration between 0 and 500 μM) on migration, motility and stiffness. EGCg reduced cell movement (migration, motility), increased stiffness and affected the genes evolved in the stimulation of movement of the cells [1].

CELL LINE	METHOD	OBSERVED EFFECTS	CONCENTRATION OF EGCg	REFERENCE
H1299 (ATCC No. CRL-5803, human, non-small cell lung cancer, derived from lymph node) Lu99 (human non-small cell lung cancer)	Wound healing assay (migration assay) Western blot AFM	Reduction of cell motility Increase in cell stiffness Inhibition of expression of vimentin and Slug Inhibition of epithelial -mesenchymal transition phenotypes	5,10, 50,100 μM (2.29, 4.58, 22.9, 45.8 μg/ml)	Takahashi et al. 2014
4T1 (ATCC No. CRL-2539, murine BALB/cfC3H, animal stage Iv human breast cancer)	MTT assay (cell viability) Boyden chamber (migration assay) Immunofluorescent detection Nitric Oxide Assay Kit Western blot	Suppression of the elevated levels of endogenous NO/NOS in 4T1 cell Blocked the migration promoting capacity of l-arginine Reduction of the elevated levels of cGMP in cancer cells Blocked the migration restoring activity of 8-Br cGMP (cGMP analogue) Inhibition of 4T1 migration through the inhibition of NO/NOS and guanylate cyclase	0,10,20,40,60 μg/ml	Punathil et al. 2008
ARPE19 (ATCC No.CRL-2302,human, retinal pigment epithelial cells, derived from eye retina)	Electric cell-subtrate impedance sensing (ECIS) Dot binding assay Immunofluorescence microscopy Western blotting Transwell migration assay (Boyden chamber)	Inhibition of PDGF-BB induced RPE cell migration Inhibition of RPE cell adhesion to fibronectin	0,1,3,10 μg/ml	Chan et al. 2010
HeLa (ATCC No. CCL-2, human, cervix epithelial adenocarcinoma derived from cervix)	RNAeasy Mini Kit (total RNA isolation) PCR ELISA MTT assay (cell viability) Attachment assay Spreading assay Adhesion to endothelium assay Transwell migration assay (Boyden chamber)	Down-regulation of genes involved in the stimulation of proliferation, adhesion, motility, invasion processes. Up-regulation of several genes known to have antagonist effects	10 μM (4.58 μg/ml)	Tudoran et al. 2012
HeLa (ATCC No. CCL-2, human, cervix epithelial adenocarcinoma derived from cervix) HepG2 (ATCC No. HB-8065, human, hepatocellular carcinoma, derived from liver)	Hypoxic chamber with an auto-purge airlock Transient Transfection and Luciferase Reporter Assays Western blot RT-PCR ELISA Cell migration kit (migration assay) Cell viability assay	Inhibition of hypoxia- and serum-induced HIF-1α protein accumulation EGCg abolishes both chemottractant- and hypoxia- stimulated HeLa cell migration	50, 100 μmol/L (22.9, 45.8 μg/ml)	Zhang et al. 2006
HeLa (ATCC No. CCL-2, human, cervix epithelial adenocarcinoma derived from cervix)	Holomonitor M4	Reduced migration, motility and motility speed	500 μg/ml	Peter et al. 2015

[4] (AFM: atomic force microscopy, ATCC: American Type Culture Collection, ELISA: enzyme-linked immunosorbent assay, HPLC: high performance liquid chromatography, MTT: 3-(4,5-dimethylthiazol-2-yl)-2,5-diphenyltetrazolium bromide, NO/NOS: nitrogen monoxide, nitrous oxide, PDGF: platelet-derivated growth factor, RT-PCR:reverse transcripton polimerase chain reaction, RPE: retinal pigment epithelium).

Reduced proliferation and induced apoptosis of cancer cells

A study of Hou and co-workers showed that in cell culture conditions, the auto-oxidation of EGCg result in epidermal growth factor receptor (EGFR) inactivation, however, the inhibition of cell growth is due to other mechanisms [19]. EGCg itself induces chromosomal damage in WIL2-NS cells at 100 μmol/l (=45.8 μg/ml), and this damage is due to the production of H_2O_2 [55]. But EGCg at <10 μmol/l (=4.58 μg/ml) does not induce chromosomal damage and does not produce H_2O_2 [55]. Hypothesis of Song et al. presents that EGCg exerts no direct effect on cancer cells in culture; instead, any anticancer effect observed is an indirect result of the generation of H_2O_2 during the oxidation of EGCg [17]. However, it blocked the expression of HSP70 and HSP90 and demonstrated that this effect was not induced by H_2O_2 [17][56]. As pointed out by Hayakawa and co-workers, EGCg elevates the caspase8 activity and its fragmentation in U937 cells [57]. According to this study, DNA ladder formation caused by EGCg treatment was inhibited by the caspase 8 inhibitor [57]. These findings of the authors suggested the involvement of the Fas-mediated cascade in the EGCg-induced apoptosis in U937 cells, and thus EGCg binding to Fas presumably on the surface of the cells, triggers the Fas-mediated apoptosis in these cells [57]. EGCg treatment not only results in the downregulation of genes involved in the stimulation of proliferation, motility, adhesion, and invasion processes, but also leads to the upregulation of several genes known to have antagonist effects [49]. EGCg exposure decreases the HeLa cell proliferation rate and invasion potential; thus, this compound might be an important anti-angiogenic therapeutic approach in cervical cancers [49]. EGCg treatment resulted in a dose-dependent inhibition of cell growth, induction of apoptosis, and G0/G1-phase arrest of the cell cycle in human epidermoid carcinoma A431 cells, furthermore, itwas found that 10–80 μM (= 4.58-36.64 μg/ml) EGCg treatment results in loweringof nuclear factor κB NF-κB levels in both the cytoplasm and nucleus in a dose-dependent manner [13]. EGCg exposure was found to result in a dosebased differential inhibition of TNF-α- and LPS-mediated activation of (NF-κB) in the previously mentioned cells in the study of Ahmad and co-workers [13]. EGCg at 50 μg/ml inhibited the activity of NF-κB and hypoxia-inducible factor 1-α (HIF-1α) as well as vascular endothelial growth factor (VEGF) expression in cultured E0771 cells compared to control, thus, EGCg suppresses breast tumor angiogenesis and growth [44]. The hypothesis of Gu et al. is that EGCg directly targets both cancer cells and also their vasculature, thereby reducing tumor growth, proliferation, migration and angiogenesis of breast cancer, which is mediated by the inhibition of NF-κB and HIF-1α activation as well as VEGF expression [44].In a previous study of Weber and co-workers, it was demonstrated that EGCg blocked PDFG-BB isoform-mediated signal transduction pathways and cell proliferation [45]. In the experiments of Siddiqui et al., EGCg decreased the growth and proliferation of prostate cancer cells (PCa), accompanied by the reduction of prostate-specific antigen [58] . EGCg inhibits the activity of the protein phosphatase-1 (PP1) recombinant δ-isoform of the PP1 catalytic subunit (PP1c), and the galloyl group of the polyphenol may play a role in phosphatase inhibition [59] . An experiment by D'Agostino et al. demonstrated that the mucus gel layer on HT29 human colonic adenocarcinoma cells probably

protects the cells against EGCg toxicity [60]. Cytotoxic impacts of high polyphenol levels may be associated with the ability of polyphenolic compounds to interact with cellular mucins and proteins [60]. According to the authors, food-related ingredients also can influence the toxicity of EGCg, for instance, β-casein is effective in protecting cells against the toxicity effect; however, maltodextrin is less efficient [60]. The speculation that certain carcinogenetic processes are initiated and maintained by cancer stem cells (CSCs) has been partially verified [61]. It has been reviewed by Scarpa and Ninfali that phytochemicals and herbal extracts are able to target and kill CSCs, therefore, EGCg and other phytochemicals, for example, β-carotene, genistein curcumin, piperine, sulforaphane and whole extracts of some plants can inhibit CSCs [61]. Most of these active substances act by interfering with the canonical Wnt [β-catenin/T cell factorlymphoid enhancer factor (TCF–LEF)] pathway implicated in the pathogenesis of some tumors [61]. Table 1.3 summarizes the results and details of the listed references.

Table 1.3 Summary of the listed references about the experiments of apoptosis and proliferation[5]. Different cancer cell lines were examined by different methods and techniques to reveal the effect of EGCg (concentration between 0 and 4000 μM) on migration, motility and stiffness. EGCg reduced proliferation and induced apoptosis via different signaling pathways [1].

[5] (ATCC: American Type Culture Collection, CBMN: cytokinesis-block micronucleus, EGFR: epidermal growth factor receptor, FLICE: FADD-like interleukin-1 beta-converting enzyme, ERK: extracellelar-signal regulated kinases, FRET: *fluorescence resonance energy transfer,* HPLC: high performance liquid chromatography, HSP: heat shock protein, MTT: 3-(4,5-dimethylthiazol-2-yl)-2,5-diphenyltetrazolium bromide, NK: natural killer cells, *NMR:* Nuclear Magnetic Resonance, RT-PCR:reverse transcripton polimerase chain reaction, *SPR: surface plasmon resonance,* TEM: transmission electron microscopy, TNF: tumor necrosis factor).

CELL LINE	METHOD	OBSERVED EFFECTS	CONCENTRATION OF EGC_g	REFERENCE
A431 (human epidermoid carcinoma) NHEK (human epidermial keratinocyte)	Gel electrophoresis Electrophoretic mobility shift assay Immunoblot analysis	Apoptosis in A431 cells but not in NHEk Inhibition of TNF-α-and LPS mediated expression Differential dose-based NF-κB inhibitory response in cancer cells vs normal cells	0,10,20,40,80, 100 μM (0, 4.58, 9.16, 18.32, 36.64, 45.8 μg/ml)	Ahmad et al. 2000
Jurkat (ATCC No. TIB-152, human, acute T cell leukemia, derived from peripherial blood) 293T (ATCC No. CRL-3216, human, embryonic kidney)	Western blot HPLC Hydrogen peroxide quantitative assay kit	Activation of ERK1/2 ERK1/2 phosphorylation was caused by auto-oxidation of EGCg	12.5, 50 μg/ml	Song et al. 2014
KYSE150 (human esophageal squamous cell carcinoma) A431 (ATCC No. CRL-1555,human, epidermoid carcinoma, derived from skin) OE19 (esophageal adenocarcinoma)	Western blot HPLC Colony formation assay Amplex Red Hydrogen Peroxide assay kit	Decreased EGFR protein level Decreased signals of HER-2/neu in OE19 cells The effects of EGCG were prevented/diminished by addition of SOD or SOD+catalase EGCg was unstable in the media Formation of dimers and other oxidative products Auto-oxidation of EGCG leads to EGFR inactivation the inhibition of cell growth is due to other mechanisms	5,10,20,50 μM (2.29, 4.58, 22.9, 45.8 μg/ml)	Hou et al. 2005
WIL2-NS (ATCC No.CRL-8155, human B lymphoblastoid, derived from spleen)	CBMN-assay (chromosomal damage) HPLC with electrochemical detector (ECD) Phenol red method	Chromosomal damage Production of H2O2 EGCg under 10 μmol/L prevented chromosomal damage induced by H_2O_2	0, 0.3, 1, 10, 30, 100 μmol/l (0, 0.13, 0.458, 4.58, 13.74, 45.8 μg/ml)	Sugisawa et al. 2002
MCF-7 (ATCC No. HTB-22, human, breast adenocarcinoma) 4T1 (ATCC No. CRL-2539, murine BALB/cfC3H, animal stage Iv human breast cancer) CT26 (ATCC No. CRL-2638, murine BALB/c, colon carcinoma)	MTT assay (cell viability) Flow cytometry Cell colony formation assay (soft agar assay) Western blot Luciferase riporter assay EGCg pull-down assay Immunohistochemistry assay	Inhibition of the expression of HSP70 and HSP90 by inhibiting the promoter activity of HSP70 Increased stress sensitivity of MCF-7 cells Decreased cell proliferation and colony formation of MCF-7 cells	0-200 μg/ml	Tran et al. 2010
U937 (ATCC No. CRL-1593.2, human, histiocytic lymphoma)	DNA fragmentation analysis (electrophoresis) FLICE/caspase 8 fluorometric assay kit Western blot Affinity cromatography (EGCG-sepharose 4B column) Flow cytometry	EGCg binds to Fas Fas-mediated apoptosis	50,100,200,400 μM (22.9, 45.8, 91.6, 183.2 μg/ml)	Hayakawa et al. 2001
LNCaP (ATCC No. CRL-1740, human, prostate carcinoma, derived from left supraclavicular lymph node) 22Rv1 (ATCC No. CRL-2505, human, prostate carcinoma)	In silico molecular modeling study MTT assay (cell viability) Transient transfection and reporter assays FRET-based competition assay AR protein stability assay Immunohisttochemical analysis Immunofluorescence images RT- PCR	EGCg is a direct antagonist of androgen action Interaction with the ligand-binding domain of androgen receptor by replacing a high-affinity labeled ligand Inhibition of androgen receptor nuclear translocation and protein expression Repression of R1881-induced PCa cell growth Functionally antagonizes androgen action at multiple levels	10-60 μM (4.58-27.48 μg/ml)	Siddiqui et al. 2011
HeLa (ATCC No. CCL-2, human, cervix epithelial adenocarcinoma derived from cervix)	SPR NMR Assay of protein phosphatases MTT assay (cell viability) Molecular docking	Docking at the hydrophobic groove close to the catalytic center of PP1c protein phosphatase protein. Supression the viability of HeLa cells by PP1c-inhibitory potencies. Phosphatase-inhibitory features of these polyphenols may be implicated in the wide spectrum of their physiological influence.	0-100 μM (0-45.8 μg/ml)	Kiss et al. 2013
HT29 (ATCC No. HTB-38, human, colorectal adenocarcinoma) HT29-MTX-E12 (human colon adenocarcinoma subclone)	TEM Alcian blue staining Trypan blue exculsion method (cell viability)	The mucus gel layer on the cells can protect the cells against EGCg toxicity Proteins in the mucus layer may bind to the galloyl ring of EGCg β-casein was very effective in protecting the cells against the toxicity effect of EGCG Maltodextrin was less effective in protecting against this toxicity	400, 1000, 4000 μM (183.2, 458, 1832 μg/ml)	D'Agostino et al. 2012

Differences in effects on healthy (normal) and cancer cells

It is very important to know the effects of a prospective anticancer agent on healthy cells as well. In an experiment by Tao and co-workers, EGCg induced mitochondrialocalized ROS in human oral squamous carcinoma cells (SCC-9, SCC-25) and in premalignant leukoplakia cells (MSK-Leuk-1) as well, but not in normal human gingivalfibroblast cells (HGF-1) [62]. EGCg suppressed mitochondrial redox modulator SIRT3 in SCC-25 cells, whereas it increased SIRT3 activity in HGF-1 cells [62]. The polyphenol selectively decreased the nuclear localization of the estrogen-related receptor α (ERRα), the transcription factor regulating SIRT3 expression in SCC-25 cells, and this indicates that EGCg may regulate SIRT3 transcription in oral tumor cells via ERRα [62]. In the mentioned cells, SIRT3 activity and expression are inhibited by EGCg, resulting in the accumulation of mtROS, as well as mitochondrial dysfunction and death [62]. In normal oral cells, EGCg activates SIRT3 and related downstream antioxidant responsive genes (AOX genes); thus, this process protects them cells from oxidative injuries [62]. In another study, EGCg exposure resulted in a dose-dependent inhibition of cell growth, G0/G1-phase arrest of the cell cycle and induction of apoptosis as well human epidermoid carcinoma A431 cells, but not in normal human epidermal keratinocytes (NHEK) [13]. The inhibition of NF-κB expression and activation in NHEK was monitored only at high concentrations [13]. The authors found that EGCg imparts differential dose-based NF-κB inhibitory responses in tumor cells versus normal cells [13]. EGCg caused inhibition of NF-κB expression, and activation was found to happen at much higher doses of the polyphenol in NHEK as compared to A431 cells [13]. However, another result showed that EGCg is much more toxic against normal cells, while at low concentrations (<100 μM=45.8 μg/ml) increased the lung cancer cell viability slightly [63]. EGCg induced DNA double-strand breaks and apoptosis in normal cells and intensified their mutation frequency, too [63]. EGCg did not induce chromosomal damage at <10 μmol/l (=4.58 μg/ml) concentrations; however, 100 μmol/l EGCg triggered chromosomal injury in WIL2-NS cells (human B lymphoblastoid cell line) [55]. EGCg at physiological concentrations (<1 μmol/l= 0.458 μg/ml) are not genotoxic, but rather can anticipate ROS-induced chromosomal damage [55]. Experiments showed that EGCg inhibited the growth and proliferation of various prostate cancer cells through multiple mechanisms, with minimal impacts on normal human prostate epithelial cells [58].

Inhibitory properties on microbes

EGCg has a broad antimicrobial (antifungal, antibacterial, antiviral) spectrum as reviewed earlier [64]. EGCg and ECG showed inhibitory effects on the growth and adherence of carcinogenic bacteria on the tooth surface and on the glucan synthesis of streptococci [2]. EGCg also blocks the adherence and growth of bacterium *Porphyromonas gingivalis*, responsible for periodontal disease [2]. Furthermore, other compounds of tea, delta-cadinene and indole have a synergistic effect on the inhibition of the growth of *Streptococcus mutans* [2]. It has been reviewed that tea extracts have inhibitory effects against several other bacteria, for example, *Vibrio cholerae*, *Salmonella typhi*, *Helicobacter pylori*, *Campylobacter coli*, *Salmonella*, *Shigella*, *Clostridium*, *Pseudomonas* and *Candida* as well [2]. Tea can exhibit a beneficial effect against viral infections, too: tea polyphenols significantly inhibit influenza A virus in animal cell culture and rotavirus in monkey cell culture [2][64]. Recent studies showed that tea polyphenols inhibit the survival of *Mycobacterium tuberculosis* in macrophages [65]. EGCg blocks the NADH-dependent enoyl-ACP reductase encoded by the *Mycobacterium* gene inhA with an IC50 of 17.4 μM (= 7.96 μg/ml) and interferes with the binding of NADH [66]. The enoyl acyl carrier protein reductase (ACP, ENR) is one of the most important enzymes involved in the type II fatty acid biosynthesis pathway of the intracellular pathogen and a relevant factor for their survival within host cells [66]. EGCg has anti-inflammatory and antioxidant effects on infected host cells by suppressing the augmented expression of MTB 85B and proinflammatory TNF-α of human monocytes [67]. A study of Hellmann et al. also showed that EGCg inhibits even the motility of the *Plasmodium* sporozoite, the causative agent of malaria [53]. It happens because the EGCg may bind to the adhesion of molecules of the parasite surface, for example circumsporozoite protein (CSP) and thrombospondin- related adhesive protein (TRAP), which are important for their motility [53]. The surface antigen PfEMP of *Plasmodium falciparum* is involved in the cytoadherence of the pathogen-infected erythrocytes to a range of receptors on the host endothelium, e.g., ICAM-1, which is related to cerebral malaria [68]. EGCg can be an effective inhibitor of ICAM-1-based cytoadherence of *P. falciparum*-infected erythrocytes [68]. EGCg is able to inhibit the formation of merozoite surface protein 2 (MSP2) fibrils and can alter the β-sheet-like structure of the fibril and disaggregate pre-formed fibrils of MSP2 into soluble oligomers as well [69] . The summary of the results and details of the listed references is shown in Table 1.4.

Table 1.4 Summary of the listed references about the experiments with microbes[6]**.** Protozoons and bacteria and human cells were examined by different methods and techniques. The treatment inhibited the viability of the microbes. Measurements with *Mycobacterium tuberculosis* showed that EGCg maybe can be used in tuberculosis infection or prevention in the future [1].

CELL LINE	METHOD	OBSERVED EFFECTS	CONCENTRATION OF EGC_g	REFERENCE
Plasmodium berghei (strain NK65) (produced in Anopheles stephensi mosquitoes)	Cytotoxicity assay (with fluorescent dyes) Zeiss microscopy (GFP filter set), ImageJ	Inhibited motility and viability Digitonin increases the cytotoxic of EGC_g	12.5-1000 μg/ml	Hellmann et al. 2010
Mycobacterium tubercolosis (H37Rv) THP-1 (ATCC No.TIB-202, human, monocytic leukemia, derived fromperipheral blood) Jurkat (ATCC No. TIB-152, human, acute T cell leukemia, derived from peripherial blood)	HPLC RT-PCR PCR Transfection and reporter plasmid assay *M. tubercolosis* invasion assay Immunofluorescent labeling Flow cytometry	Inherent capacity to down regulate TACO gene transcription within human macrophages Inhibition of Sp1 transcription factor Inhibition of survival of *M. tubercolosis* within macrophages prevention of tubercolosis infection	0-60 μg/ml	Anand et al. 2006
Mycobacterium tubercolosis	Direct binding assay Jobin-Yvon Horiba fluorimeter (Fluorescence titration assay) PCR Ni-NTA affinity chromatography	Inhibition of InhA, the enoyl-ACP reductase of *M. tubercolosis* EGCg increased the inhibitory activity of triclosan towards InhA and vice-versa Tea cateechins and triclosan based drugs for treating tubercolosis	100 nM-20 μM (0.04-9.16 μg/ml)	Sharma et al. 2008
Mycobacterium tubercolosis (H37Rv) PBMC (ATCC No. PCS-800-011, human, peripherial blood mononuclear cells)	MTT assay (cell viability) Trypan blue excursion assay (cell viability) Quantitative RT-PCR Assay for GPx activity and GHS levels (GSH kit) ELISA	Augmented expression of 85B in *M. tubercolosis* Suppression of TNF-λ at the gene and protein levels in infected monocytes Antiinflammatory mechanism was mediated by inhibition of NF-κB pathway Ameliorates the sIFN- γ and glutathione levels, and glutathion peroxidase activity in infected monocytes Infected monocytes were suppressed Anti-inflammatory and antioxidant effects can be exploited in tubercolosis management	0-25 μg/ml	Fatima et al. 2012

1.4. Observed action of EGCg using tissues and animal models and results of clinical trials

Drug pharmacokinetic profile determines the onset, duration, and intensity of a compound's effect. Understanding the pharmacokinetics (the uptake of the compound into, through, and out of the human body, the time course of its absorption, bioavailability, distribution, metabolism, excretion, receptor binding, postreceptor effects, and chemical interactions) of EGCg is urgently needed to interpret epidemiological, experimental data and to extrapolate *in vitro* or *in vivo* animal data to humans [1].

[6] (ATCC: American Type Culture Collection, ELISA: enzyme-linked immunosorbent assay, HPLC: high performance liquid chromatography, GFP: green fluorescent protein, MTT: 3-(4,5-dimethylthiazol-2-yl)-2,5-diphenyltetrazolium bromide, Ni-NTA: nickel-charged affinity resin (nitrilotriaceticacid), NK: ntural killer cells, PMBC: peripheral blood mononuclear cell, RT-PCR:reverse transcripton polimerase chain reaction, TNF: tumor necrosis factor).

Experiments with tissues and animal models

In CF-1 mice, EGCg exhibited a linear dose relationship in their plasma, prostate and liver [70]. In the colon and small intestine the levels of EGCg plateaued between 500 and 2,000 mg/kg [70]. These results of Lambert and co-workers suggest that absorption of EGCg from small intestine is largely via passive diffusion; however, at higher concentrations, the colonic and small intestinal tissues become saturated [70]. EGCg treatment reduced tumor weight in mice; nevertheless, it had no effects on body weight, heart weight, angiogenesis and VEGF expression in the heart and skeletal muscle of these animals [44]. Another study also showed that administration of EGCg caused a 70 % decrease in tumor volume in BALB/c mice, and the cure did not alter body weight compared with PBS-treated controls [56]. Furthermore, the expression levels of HSP70 and HSP90 stress-inducible proteins were decreased in EGCg-treated mice [56]. In rats, epicatechin (EC) and epigallocatechin (EGC) in plasma increased over time and reached peak values [71]. Among tea catechins, the plasma concentrations of EGCg were much lower than those of EC and EGC [71]. Kim and co-workers found high levels of EC and EGC in urine, while high levels of EGCg were found in feces [71]. When purified EGCg or green tea were administrated to mice in drinking water, traversed angiogenesis in vivo and restrained Kaposi's sarcoma tumor growth [31]. Consumption of tea by rodents could induce adaptive responses influencing tissue and blood levels of catechins with time, and an investigation of a similar phenomenon in humans can be predicted [71]. In an experiment of Li and co-authors, it has been suggested that EGCg inhibits high-mobility group box 1 protein (HMGB1, late proinflammatory mediator of lethal sepsis) release by stimulating its aggregation and autophagic ("self-eating") degradation [72]. EGCg blocked bacterial endotoxin-induced HMGB1 release in vitro and saved mice from lethal sepsis when EGCg was given to them intraperitoneally, even when the first dose was given orally at 24 hours after onset of the illness [72]. The authors validated the therapeutic potential of EGCg in animal models of sepsis by administering it through a clinically practicable process [72]. The summary of the results and details of the listed references are presented in Table 1.5.

Table 1.5 Summary of the listed references about the experiments with animal models[7]. Male and female mice and rats were treated by EGCg for days (oral administration or injection). The tumor growth was suppressed and the treatment reduced tumor size in the animals [1].

ORGANISM	METHOD	OBSERVED EFFECTS	CONCENTRATION OF EGC_g	REFERENCE
C57BL/6 mice female, 8 week old	ELISA Bio-Rad Protein Assay 3H-thymidine incorporation assay BD BioCoat Matrigel Invasion Chamber (migration assay) Motif binding assay Morphometric analysis Immunohistochemistry	Decrease in tumor angiogenesis Down-regulation of VEGF Reduced tumor weight A relative high oral dose significantly inhibits the progression of breast cancer growth	50-100 mg/kg/d in drinking water for 4 weeks	Gu et al. 2013
Balb/C mice male, 6 week old	MTT assay (cell viaability) Flow cytometry Cell colony formation assay (soft agar assay) Western blot Luciferase riporter assay EGCg pull-down assay Immunohistochemistry assay	Inhibition of the expression of HSP70 and HSP90 by inhibiting the promoter activity of HSP70 and HSP90 Delayed tumor incidence and reduced tumor size Supression of tumor growth	10 mg/kg for 7 days injection	Tran et al. 2010
A/J mice (female, 6 week sold) (female, 6 week old) Sprague-Dawley rats (male, 10 weeks old)	HPLC	Catechin levels was observed in plasma, lung and liver EGCg levels where higher than in the rats	0,1 and 0,6% (wt/vol) EGCG as drinking fluid	Kim et al. 2000
Balb/C mice male, 7-8 week old	Western blot Fluorescence immunostaining TEM Nitroblue tetrazolium staining Cytokine antibody array RNA interference array	Induction of HMGB1 aggregation Stimulation of LC3-II production and autophagosome formation Inhibition of LPS-induced HMGB1-up-regulation and extracellular release Inhibition of HMGB1release by stimulating its autophagic degradation Protection against lethal sepsis	4 mg/kg daily for three days oral administration	Li et al. 2011

Clinical trials and beneficial influences of EGCg

The effects of tea consumption on the risk of human cancer have been investigated in many studies; however, the results have been inconclusive. Tachibana reviewed in 2011, that some experiments suggested a cancer-preventive effect of tea, while other studies did not show an association [5]. The inconsistent results of the studies were probably due to, for example, different disturbing factors, difficulties in quantifying tea consumption, population heterogeneity and varied cancer etiology in different populations [5]. Traditional cancer drugs often destroy some healthy cells along with tumor cells, but EGCg appears to target functions unique to tumor cells, thus, this green tea compound has a very acceptable safety profile [3]. For example, in previous a clinical trial reviewed by Singh et al, EGCg capsules (200 mg p.o.) for 12 weeks was reported to be effective in human papilloma virus-infected persons [3]. Epidemiological studies identified an inverse association between tea consumption and the frequency of rectal and colon cancer as well as esophageal and gastric tumors [9]. Other epidemiological data also show that

[7] (ATCC: American Type Culture Collection, ELISA: enzyme-linked immunosorbent assay, HMGB: high-mobility group box proteins, HPLC: high performance liquid chromatography, MTT: 3-(4,5-dimethylthiazol-2-yl)-2,5-diphenyltetrazolium bromide, LC3: microtubule-associated protein light chain 3, LPS: lipopolysaccharide, TEM: transmission electron microscopy, VEGF: vascular endothelial growth factor).

prostate cancer is sharply rising in the west, but its incidence has been especially low in East Asian countries where green tea is a popular drink [58]. Fujiki and co authors reviewed that ten Japanese-size cups of green tea daily, supplemented with tablets of green tea extract, reduced the recurrence of colorectal adenoma by 51.6 % in persons after polypectomy according to a trial in 2008 [73]. Furthermore, a study also revealed that green tea most significantly prevented lung cancer (the relative risk of 0.33 with at least 10 cups of green tea per/day), and at high consumption prevented tumors of liver, colorectum, and stomach as well [73]. Unfortunately, the antimicrobial activity of tea in humans is not well documented and should be investigated in a multidimensional way because certain mechanisms are implicated, for example, the immune system, heredity, microbial ecology, etc. [2]. Mereles and Hunstein summarized in their review article that providing EGCg is a pharmacon, side effects should also be expected, for example, effects on the anxiolytic and hypoglycemic activity, hypochromic anemia, and liver and kidney failure [7]. However, 800 mg caffeine-free EGCg per day for 4 weeks was shown to be well tolerated and safe in healthy persons [7].

1.5. Perspectives: Investigation and application possibilities in the near future

Recently, several novel directions appeared concerning the research and development and future applications of EGCg.
Nanocarriers and nanocomposite systems for targeted drug delivery are also emerging and may involve the application of EGCg.

Combination of EGCg and anticancer compounds

As reviwed by Fujiki and co-authors, some studies showed that the combination of green tea catechins and anticancer drugs has the potential to enhance the efficacy of the drugs [73]. The combination of these components induced similar synergistic anticancer effects for both in vivo and in vitro experiments and showed an average reduction in tumor volume of 70.3 % [73]. Furthermore, among others, in in vivo mouse xenograft models, the combinations of paclitaxel and EGCg as well as docetaxel and EGCg completely eliminated tumors of human prostate cancer cell line PC-3ML, but other combinations also reduced the tumor volumes in the case of various cancer cell lines [73]. The amount of EGCg for the elimination of tumors in mice varied from 4.56 to 6.84 mg/day/mouse [73].Converted these numbers to humans, it would be 1.37–2.05 g/day/ person (6–9 Japanese-size cups of green tea) [73]. The results suggest that the combinations of nonsteroidal anti-inflammatory drugs and EGCg activate the GADD153-DR5-TRAIL apoptotic pathway [73]. There are also experiments involving EGCg alone or in

combination with oxaliplatin and cisplatin because of EGCg's ability to synergistically increase the efficacy of these drugs against colorectal and prostate tumors [61][74]. According to Fujiki et al., the combination of anticancer compounds and green tea catechins can be a new cancer therapeutic strategy [73].

Enhancing stability and bioavailability of EGCg employing polymeric carrier systems with controlled release: nanoparticles, liposomes and micelles

In the field of therapeutics, nanoparticles may serve as carriers in targeted therapy because of EGCg's poor stability and bioavailability [75] (see Fig. 1.4). Nanoparticles can increase the stability and solubility of active compounds, enhance their absorption, protect them from premature degradation in the organism and prolong their circulation time as well [76]. Furthermore, nanoparticles can show high differential uptake efficiency in the target cells/tissue over normal cells/tissue and protect them from prematurely interacting with the biological environment, enhanced retention and permeation impact in disease tissues [76]. Thus, nanoparticle interactions with a biological system may determine its targeting effects and therapeutic effectiveness [39]. For example, in a novel development of Ding et al., the multiple core-shell functionalized colloidal mesoporous silica nanoparticle system (CMS) was shown to be a good platform for prolonging the half-life of unstable active substances and thus enhancing their pharmacodynamic action [77]. CMS is capable of entering easily into the cells and mostly located around the nuclei [77]. These nanoparticles exert no visible cytotoxic effects on HeLa cells, and it is an illustrious carrier for inhibiting the collision of EGCg radicals to form dimers and polymers [77]. Furthermore, it improves the formation of certain compounds, for instance H_2O_2 for inducing cell apoptosis [77]. Active substances can then be released into the tumor cells; thus, it may be an improved, better treatment with fewer side effects [77]. In another study, EGCg enhanced the interaction and/or internalization of dextrancoated magnetic nanoparticles (composed of an iron oxide core and a polymer coating) by glioma cells, but not vascular endothelial cells [39]. The enhancing effects are depending on the concentration and time, too [39]. This is a novel interaction of a nanocarrier system and nutriment component, which may be potentially amenable to cell labeling, magnetofection, and targeted therapeutics [39]. The niosome is a kind of recent vesicular system with a bilayer that contains cholesterol and nonionic surfactants [75]. Niosomal formulation significantly enhanced drug absorption, compared with the free drugs [75]. Furthermore, drug-loaded niosomes showed lower toxicity and stronger stability, too [75]. EGCg can be loaded into liposomes and chitosan-coated liposomes as well to reach its higher stability [76][78]. Nanoliposomes can be used as carriers prepared by reverse-phase evaporation method, and it has been showed that prepared EGCg nanoliposomes are stable and suitable for more widespread application [79]. EGCg at lower and physiologically relevant concentrations by oral intake has little or very limited effect, thus improving its bioavailability is very important, and the nanotechnology can help in this need [76]. For instance, chitosan

nanoparticles can significantly enhance its bioavailability [80]. Chitosan is a biocompatible polysaccharide, which confers a positive charge to the surface of nanoparticles, thus it can be used as an absorption enhancer [76][80] [81]. Encapsulation of the green tea compound enhances its inhibitory effect on cancer cell viability at higher concentrations [79]. These results showed that the oral absorption of tea polyphenols could be improved by applying drug delivery systems [75]. In the case of prostate tumors, a study of Shukla and co-workers showed that the formulation of biocompatible radioactive gold nanoparticles (198AuNPs) uses the redox chemistry of prostate tumor-specific EGCg [82]. It alters gold salt into gold nanoparticles and selectively binds with good affinity to 67LR receptors, which are overexpressed in prostate cancer cells [82]. This intratumorally injectable 198AuNP-EGCg nanotherapeutic active substance may provide notable advances in oncology for use as a potent cure for prostate or other tumors [82]. As reviewed earlier by Landis-Piwowar et al., micellar nanocomplexes can be used as well. The coupling of excess EGCg with acetaldehyde in water/ethanol/acetic acid or DMSO result is oligomeric epigallocatechin gallate (OEGCg) [83]. Aldehyde-terminated polyethylene glycol (PEG-CHO) can be coupled with EGCg to give PEG-EGCg, furthermore, PEG-OEGCg can be obtained from the conjugation of PEG-CHO with OEGCg [83]. A two-step conjugation (similar to PEG-OEGCG) results in a micellar nanocomplex with the flavonoid-rich OEGCg in the central core, and the PEG on the external core [83]. These micellar nanocomplexes can be used to deliver high doses of EGCg, potentially combined with other bioactive agents [83]. OEGCg can be coupled to an anticancer agent to create a micellar nanocomplex with PEG-EGCg as an external core [83]. The anticancer agent conjugated to OEGCg is assembled in the micellar nanocomplex [83]. For example, in a recent study of Chung et al., this system was obtained by the complexation of oligomerized EGCg with the Herceptin anticancer protein Herceptin to form the core, followed by the complexation of PEG-EGCg to form the shell [84]. In mice, the Herceptin-loaded micellar nanocomplex exhibited better growth reduction, tumor selectivity and a longer blood half-life than free Herceptin [84]. The complexes demonstrated good stability in the presence of serum for 15 days at 37 °C for 15 days, without any change in their size, additionally, they did not undergo any size reduction following a 1,000-fold dilution [84].

In another work by Haratifar and coworkers, the authors supposed that due to the binding of caseins with EGCg casein micelles can be a good platform for the delivery of this agent and that the binding would not affect the bioaccessibility of the green tea polyphenol [85].

In their publication they proved that EGCg-casein complexes were able to reduce the proliferation of HT-29 cancer cells, demonstrating that bioavailability may not be decreased by the encapsulation [85]. Thus, these mixed systems may ensure better stability of the tea polyphenols both in storage and during digestion [85].

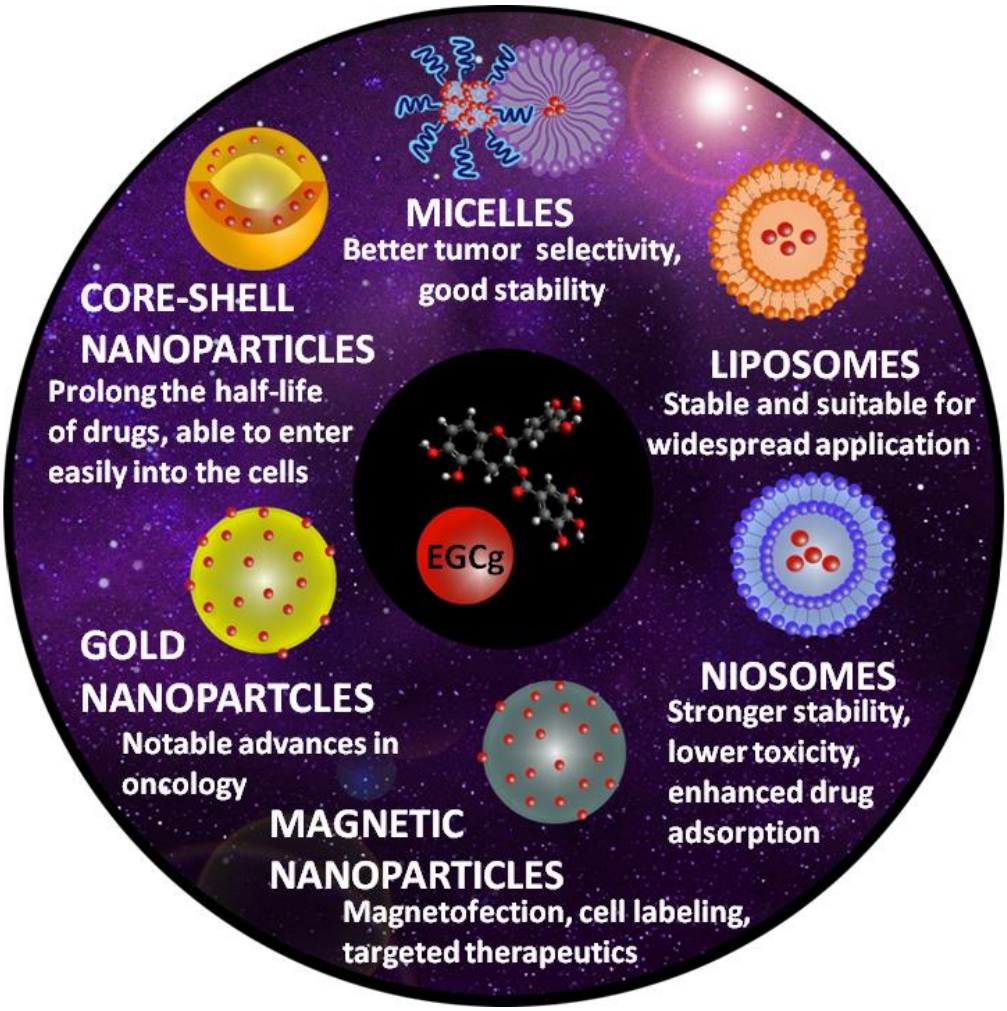

Fig.1.4 Schematic representation of the carrier systems of EGCg: micelles, liposomes, niosomes, gold nanoparticles, magnetic nanoparticles, and core-shell nanoparticles. These nanoobjects can serve as carriers in targeted therapy, because of EGCg's poor stability and poor bioavailability [1].

Nanocluster carriers

It has been published in certain studies, that gold nanoparticles have been applied succesfully to carry EGCg and to cure tumors [86][82].
The fact, that not just nanoparticles, but also clusters can be applied in carrying EGCg and curing illnesses, is just a possibility at this moment. Nobody studied nanoparticle clusters and EGCg together yet.
However, polysaccharide-gold nanocluster supramolecular conjugates (HACD-AuNPs) have been used to carry other anticancer compounds, for example doxorubicin-hidrochloride, paclitaxel, campothecin, irinotechan-hidrochloride, topotecan-hidrochloride [87]. The experiment was successful, and its main advantage was that the toxicity of compounds was less harmful compared to their free form [87].

In a study of Croissant et al. protein-gold clusters-capped mesoporous silica nanoparticles were used for co-delivery gemcitabine and doxorubicin [88]. The advantage of this system is that the co-delivery of these compounds was achieved for the first time via an inorganic nanocarrier, possessing a zero-premature leakage behavior and drug loading capacities seven times higher than what was obtained for polymersome nanoparticles [88].
Not just active substances can be delivered by nanoparticle clusters. For instance, in a study of McIntosh and co-workers, cationic mixed monolayer protected gold clusters were used to deliver DNA/vector to mammalian cells [89].
From these publications, it seems to be a promising trend to apply nanoclusters and not just nanoparticles to carry EGCg molecules in the future. In my PhD work, I started basic researhes to create gold nanoparticle clusters and observe their formation in real time.

1.6. Emerging label-free techniques in polyphenol research

Label-free biosensors are emerging platforms to investigate the mode of action of small molecules and are highly relevant for EGCg research and development. The significant chemical variety encompassed by natural products continues to be of relevancy to drug discovery [90]. In the field of EGCg research (or in research on other active compounds in traditional Chinese medicines) novel methods, for example, optical waveguide lightmode spectroscopy (OWLS), resonant waveguide grating (RWG), holographic microscopy can be applied without using any dyes or other labels [91][54][46][92]. These label-free devices are more and more important to systematically study special properties of active substances on cell behavior, and to investigate various biological coatings and living cells in a high-throughput format. The above-mentioned techniques do not require any labels which may disturb cells or the chemicals used in the measurements, making them ideal for investigating the biological roles of small molecules. Adhesion assays and migration tests can be also achieved in a completely label-free way. For example, our recent study using Holomonitor M4 holographic microscopy showed that EGCg reduced the migration, motility and motility speed of the HeLa cells [54]. Furthermore, the instrument was able to create 3D images of the exposed cells and the changes in cell morphology could be observed in real-time [54].

The above techniques, especially the highly sensitive waveguide based methods [46][91][92], represent one of the promising phenotypic assays for drug discovery, owing to their capacity to provide a holistic view of receptor-ligand interactions in living cells and show the complexity of drug actions. Due to the recent technological development of label-free biosensors, these devices became more and more popular in the field of drug discovery and in other areas focusing on the biological roles of small molecules [1].

In the following subsection I survey the imaging techniques and evanescent field based methods.

Label-free imaging optical techniques

Imaging techniques underwent a grandiose progress through the decades from the beginning of the last century. *Bright-field microscopy* can be mentioned as the simplest of all the label-free imaging optical techniques. The visualization is due to the absorbance of some of the transmitted white light in dense areas of the observed biological object [93]. In general, the appearance of the image is a darker biological object on a bright background [93]. It is a popular tool, but its main disadvantage is that it has low contrast, thus transparent objects are difficult to see (Fig.1.5) [I1][93].

Then Fritz Zernike invented the *phase contrast microscope*, which became an everyday tool for all cell biologists (Fig.1.6) [I1][93].

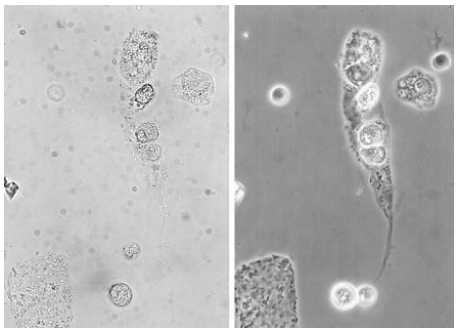

Fig.1.5 The bright-field technique has low contrast (left). Zernike's phase contrast utilizes specific optical elements (e.g. phase-shift rings) to enhance the contrast of an image and visualize unstained cells. (This image is from www.phiab.se. Scalebar is not shown) [I1].

Conventional phase contrast microscopy utilizes specific optical elements (e.g. phase-shift rings) to enhance the contrast of an image and visualize unstained cells. He won Nobel Prize in 1953 for this invention [I1].

Two years later Georges Nomarski invented the *differential interference contrast (DIC) microscopy*. This technique also enhances the contrast of transparent objects [I1][93].

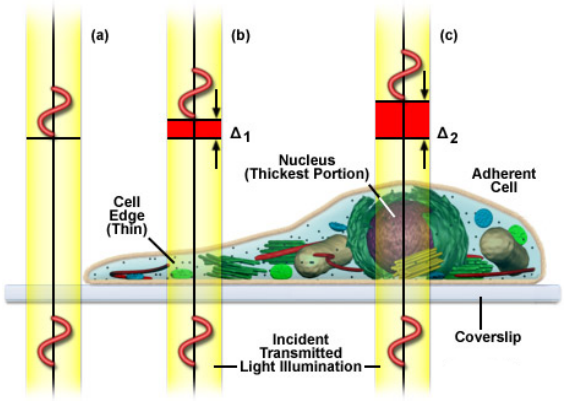

Fig.1.6 Phase contrast imaging oftransparent thin objects [I2].

Later, appearance of the quantitative phase contrast microscopy was possible due to the development of high resolution digital image sensors [I1]. By computer processing image information, *quantitative phase contrast* measures differences in optical distance (Fig.1.7) [I1]. These measurements can either be used to calculate the optical thickness of the sample or to create a topographic image of it [I1].

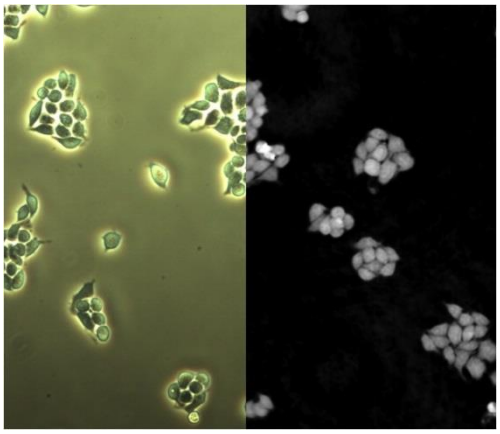

Fig.1.7 The difference between the two imaging principles. On the left the image is taken by phase contrast microscope, and by quantitave phase contrast on the right side. (This image is from www.phiab.se. Scalebar is not shown) [I1].

Dennis Gabor (Gábor Dénes) won the Nobel Prize in 1971 for his invention and development of the holographic method. This idea and the appearance of fast computers enabled the *digital holographic microscopy* to be developed.
This is a relatively novel, label-free, non-phototoxic non-invasive and nondestructive method [94]. It records all available diffraction information in a hologram, from which any particular image in the observed volume can be reconstructed subsequently by numeric simulation of wave

propagation with high precision [94]. Digital holograms can be obtained using single or multiple light sources of different wavelengths, with or without an objective (lens) and possibly enhanced by interferometry, for example Mach-Zehnder interferometry, when the illuminating light (for instance HeNe laser at 633 nm wavelength) is split into an object beam and a reference beam [94]. The object beam upon illumination of the sample is then re-joined and interfered with the reference beam producing a hologram [94]. This technique can be used for refractometry of different microscopic objects, including living cells, allowing both quantitative and qualitative experiments of living cells over time, visualization of cell integrity, and observation of ongoing cell-morphological changes (Fig.1.8) [94].

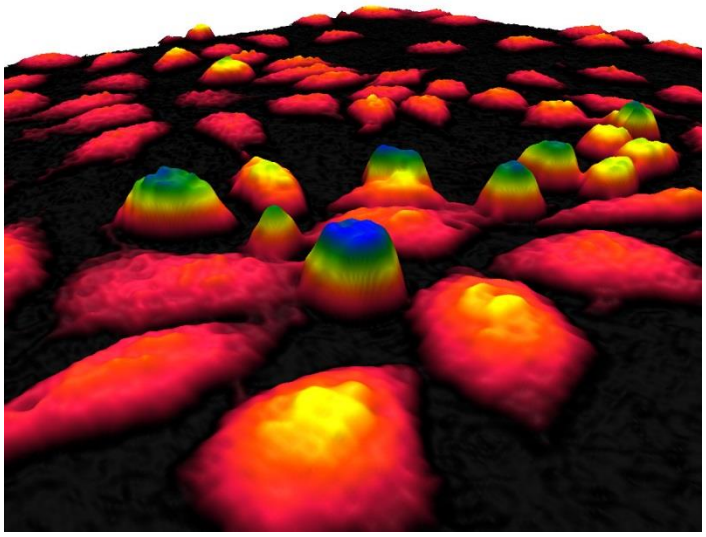

Fig.1.8 3-D image of L929 cells in culture. (This image is from www.commons.wikimedia.org. Scalebar is not shown) [I3].

A commercial digital holographic microscope, Holomonitor M4 allows cytometric time-lapse microscopy created from image sequences of cultured cells recorded over long time periods [94].

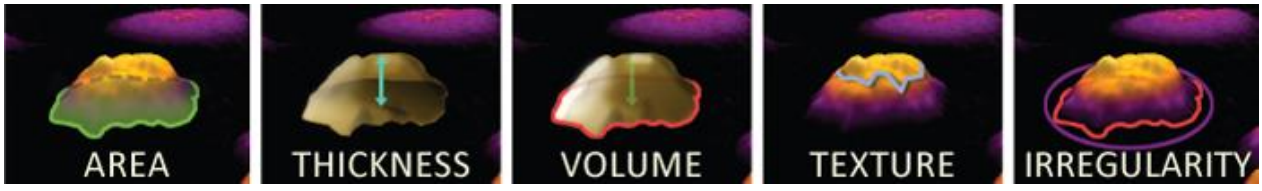

Fig.1.9 Holomonitor M4's software is capable to calculate the parameters of the monitored cells. (This image is from www.phiab.se. Scalebar is not shown) [I4].

Holomonitor M4 is capable of monitoring cell movement (Fig.1.9). This type of investigation is more and more important today [51][54]. Several other techniques exist to study cellular movements, but they have been mainly directed at migration studies and they have their drawbacks. For example, filter assays measure the cell migration over a membrane in response to chemoattractants (Boyden chamber, Zigmond and Dunn chambers) [54]. The disadvantage is that

they are very specialized, requiring cells to migrate through both a matrix and the pores of the filter [51]. Very few cell lines can migrate through both of them. Single cell movements can be studied by using time-lapse imaging, often with fluorescent markers [51][54].
Fluorescent imaging also has disadvantages [93]. It may disturb the cells and the imaging time is limited by the bleaching of the fluorescent marker [51]. In contrast with fluorescent imaging, holographic microscopy is a label-free technique [50][51][54], however, for investigating exact processes in molecular levels, the dyes and labels are yet necessary.
Another application example beyond monitoring cell movement is the cytotoxicity study [95], where holographic transmission microscopy was successfully applied to measure cell morphology parameters as cell viability descriptors [94]. It was shown to be applicable to quantitatively determine the effect of several agrochemicals (glyphosate, polyethoxylated tallowamine) on a neuroectodermal cell line [94][95]. A similar study was published on the effects of edaravone and methylglyoxal on brain endothelial cells, essential components of the the blood-brain barrier [94][96].

Evanescent field based surface sensitive optical biosensors

Evanescent optical field based sensorics is capable of monitoring cellular and biomolecular events localized at the solid-liquid interface using surface bound optical waves, the so-called evanescent waves [94]. The advantage of these waves is their strong localization at the solid-liquid interface [94]. Cellular and molecular events taking place in the 100–200 nm thick surface layers are detected and changes happening further away from the interface are excluded, they are not contributing to the biosensor signal [94]. When optical evanescent waves are used for monitoring, the biosensor signal is mostly affected by local refractive index variations at the interface [94]. Molecular binding, mass redistribution and adsorption can cause local refractive index changes and therefore contribute to the monitored signal [94]. Prisms or nanosized gratings can be used to generate these modes when the interface is illuminated by a laser beam [94]. Refractive index variations within the evanescent fields are changing the resonant condition and affecting the resonant wavelength or angle [94]. Thus, the application of evanescent optical waves can discover molecular interactions at the interface in real time with high sensitivities [94]. Biosensors can provide direct sensing of cell integrity and viability, can differentiate between dead and living cells, and can provide label-free, real time methods to investigate the impacts of cytotoxic agents [94].
The optical evanescent field effect, enhancing sensitivity, can be created by several ways, for example plasmon generation on metal (in general gold) surfaces, as in surface plasmon resonance (SPR) sensors, or by electromagnetic wave incoupling into suitable fabricated thin film waveguides [94].

Surface plasmon resonance

Surface plasmons are mostly generated when the incident light interacts with delocalized electrons of a metal surface [94]. When the surface momentum of the incident light matches the surface momentum of the electron oscillations of the conductive metal layer, the *surface plasmon resonance* (SPR) condition is achieved, and the plasmon created is the quasi particle of the collective oscillation of the free electrons [94]. A surface plasmon is confined to the surface and interacts with light [94][97]. In SPR, the guiding layer is the metal surface, where light can be coupled into these propagating surface plasmons through a prism or grating (Fig.1.10) [94]. SPR is a frequently applied technique for label-free biological and chemical sensing (including cellular characterization), allowing real-time analysis with high sensitivity [94][97].

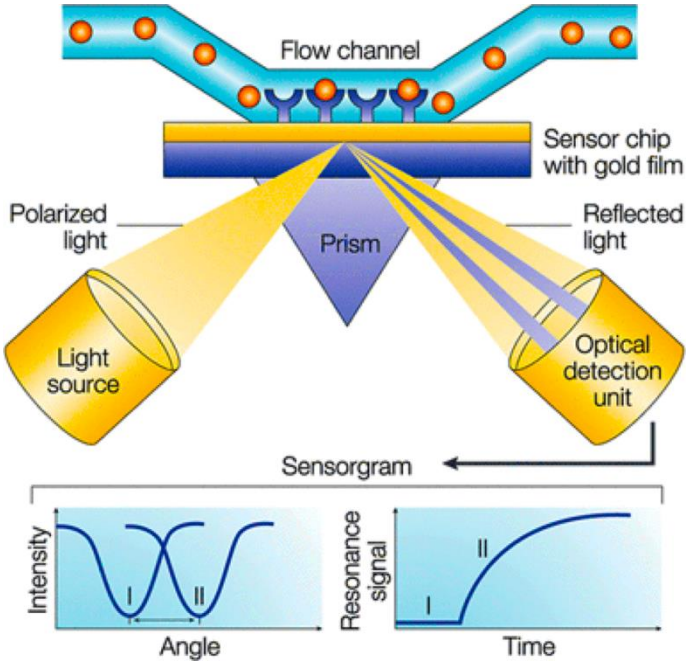

Fig.1.10 A schematic illustration for SPR biosensing [97].

Optical waveguide based biosensors

Optical waveguides are structures with high refractive index capable of guiding the propagation of electromagnetic waves by total internal reflection [94]. Thus, waveguide sensors are based on the phenomenon of incident light incoupling into a dielectric layer by using a diffraction grating [94]. Optical waveguide signals are affected by an adlayer built up on the waveguide layer, where it comes to contact with the analyte medium [94]. Molecular processes going on in this adlayer may modify various characteristics (phase, intensity, polarization state or its incoupling resonance angle) of light propagating in the waveguide, thus, all these optical characteristics can serve as signal transducing elements [94]. Most important measurement setups include various optical waveguides, interferometer based sensors, total internal reflection fluorescence (TIRF),

ring resonator, total internal reflection ellipsometry (TIRE), reflectometric interference spectroscopy (RIfS), etc [94]. Thus, a lot of optical methods have been developed for biosensing by evanescent wave optical appliances in real time, without using labels [94][98], and gained importance in environmental and food safety, as well as in biomedical and pharmaceutical research [94][99].

Sensing principle of *optical waveguide lightmode spectroscopy (OWLS)* is based on the evanescent electromagnetic field of guided light, which extends a few hundred nanometers above the waveguide [100]. A grating serves to incouple light into a planar optical waveguide in which the light then propagates, generating an evanescent field, which is used to probe the optical properties of the solution in the vicinity of the surface [100]. This is the basis for the sensitivity of the method; refractive index changes when deposition of macromolecules occurs [100]. OWLS devices are equipped with flow-through cuvettes to introduce the liquid sample solution to the grating part of the sensor surface [100][101][102].
An early exploration of the utility of this method in cell biology studies [103] revealed the cellular processes of utmost importance on the surface of the sensor [94]. When the cells were seeded onto the surface, they initially attached, subsequently flattened in shape, underwent reorganization and spreading over the sensor surface [94]. Thus, small and growing flat regions were formed at the initial points of contact, and only the cell shape modified, their number remained constant [94]. The change in the signal measured by the OWLS sensor resulted from the flattening and spreading of the cells on the surface of the sensor (Fig.1.11) [94]. This observation has been the basis of several later applications [94][104].

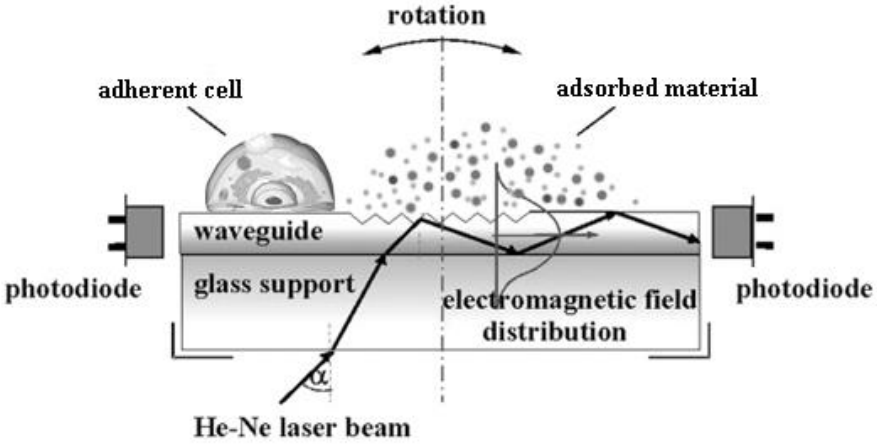

Fig.1.11 OWLS is capable of measuring small molecule adsorption and cell adhesion as well [105].

OWLS technique is an applicable tool for monitoring the adsorption of proteins and other biological samples, for example EGCg polyphenol.
The adsorption properties of EGCg-mucin mixtures on solid oxide, biomimetic surfaces was also investigated by this device [23]. It has been studied that the EGCg engenders a massive adsorption-desorption hysteresis, reflecting a complicated structurally sequential adsorption-

desorption behavior [23][25]. Furthermore, the intensification of the phenomena with increasing excess of EGCg mimics the increase of mucin concentration in an EGCg-free system [23][25]. Cell attachment was also investigated with OWLS, when fibroblast cell attachment and spreading was decreased on mucin-coated substrata when compared with PLL, however, the reduction could be countered by mixing EGCg into the layer [46]. The disadvantage of this technique that this is not high-throughput method, we can not do parallel measurements simultaneously, and it may take a long time (weeks, months) to do the whole experimentalsession.

Other evanescent field based optical biosensors, for example *photonic crystal biosensors* [106], *grating coupling interferometry (GCI)* [107] and resonant waveguide grating biosensors [108] are particularly capable of monitoring surface adhesion processes as these techniques detect molecular interactions on the surface of the in a 100–200 nm thick layer [94].

In a *resonant waveguide grating (RWG) biosensor*, the binding signals represent the averaged response of the binding at a defined area, as predetermined by the size of illumination light as well as the distance of the propagation length of the coupled light traveling within the waveguide [108]. The propagation length is in the range of several micrometers to hundreds of micrometers, it depends on the detection system and sensor design [108]. RWG biosensors have been used in biomedical analysis to probe cancer signaling [109], and biosensor systems have been applied to receptor assays as well [94].
The Epic BenchTop (BT) system (Corning Inc.) is a next-generation RWG imager biosensor allowing high-throughput label-free detection [91][110][111]. The RWG imager accepts 96- or 384-well standard format biosensor microplates (Fig.1.12) [91].

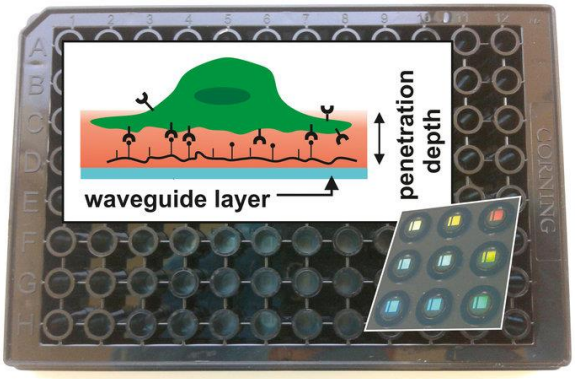

Fig.1.12 Epic BenchTop (BT) accepts 96- or 384-well microplates with biosensors in each well (colorful bottom). With this setup, a lot of parallel measurements can be done simultaneously and quickly, thus this is a high-throughput system [91].

The bottom of the microplate is a planar optical waveguide, a thin, high refractive-index, transparent dielectric layer (waveguide layer, made of the biocompatible niobium pentoxide)

deposited on a glass substratum [91]. Epic Benchtop has been used mostly for signaling experiments [110][111]. Our research group has started to measure cellular adhesion with this appliance for the first time. Orgovan et al. published the first article in 2014 [91] in this topic. Since then, it is evident that this technique is capable of measuring adhesion process, not just only cell signaling. Its main advantage is that we can do a lot of parallel measurements (because of the microplate wells) simultaneously, and thus, we can get a lot of responsible results during few hours, in contrast with for example using OWLS. We can do only maximum 3-4 experiments per day by applying OWLS device (depending on the experimental time).

Finally, it has to be mentioned, that not just label-free evanescent field based techniques exist. *Waveguide evanescent field fluorescence microscopy* [93][112] was applied to examine plasma membranes of living osteoblast cells, imaging plasma membranes with high axial resolution, and allowing time-lapse imaging to investigate the effect of membrane disrupters and cell morphology [94].

2. MOTIVATION AND OBJECTIVES

In general, scientists apply labelling techniques to investigate the impacts of EGCg on cell adhesion, migration, motility, apoptosis, etc. They are grandiose and popular techniques, but they may have few drawbacks. For example, labeling techniques use dyes/fluorescent markers that may disturb the cells, and the imaging time is often limited by the bleaching of the marker [54]. Furthermore, dyes may interact with the sample material itself. Some techniques are not high-throughput and/or not real-time. Contralily, label-free methods are untapped and unexplored in the EGCg experiments. It is well known, that EGCg oxidizes easily, but scientific literature usually neglects the EGCg's oxidized form; its properties and effects.
In my PhD work my aims were to:

- improve Holomonitor set-up to investigate the movement of HeLa celIs exposed to the green tea polyphenol
- investigate EGCg's impacts on cells and polymers and prove that label-free techniques are suitable to measure natural compounds and draw conclusions as well
- map the differences between EGCg and its oxidized form by label-free biosensors
- record the kinetic curves of cell adhesion when the polymer substrate is treated by EGCg at different concentrations, and to observe the kinetic parameter changes during alterating conditions, furthermore to compare these results with MTT viability tests
- create a basic nanoparticle system, that perhaps can be used in the future to carry EGCg molecules to targeted cells.

3. MATERIALS AND METHODS

3.1. Employed solutions and their prepartions

Synthetic polymer solutions

The synthetic copolymers, poly(L-lysine)-*graft*-poly(ethylene glycol) (PLL-*g*-PEG, [PLL(20)-g(3.5)-PEG(2)]) (hereafter PP) and its RGD functionalized counterpart, PLL-*g*-PEG/PEG-GGGGYGRGDSP (PLL-*g*-PEG-RGD, [PLL (20)-g(3.5)-PEG(2.3)/PEG(3.4)-RGD]) (hereafter PPR) were obtained as powders from SuSoS AG, Dübendorf, Switzerland. The materials were stored at -20 °C until use. Each powder was then dissolved in 10 mM 4-(2-hydroxyethyl)-1-piperazineethanesulfonic acid (HEPES, from Sigma-Aldrich Chemie GmbH, Munich, Germany) at pH 7.4 to make stock solutions with a concentration of 1.0 mg/ml. Coating solution with RGD-motifs and PLL-*g*-PEG were created by mixing the two 1 mg/ml stock solutions (hereafter PP:PPR) [91].

Assay buffer was prepared by adding 20 mM HEPES to Hank's balanced salt solution (HBSS, from Sigma-Aldrich) and adjusted to pH 7.0 with 1 mM NaOH (hereafter HBSS-HEPES) [91].

Preparation of EGCg and oxidized EGCg solutions

The EGCg powder (from Sigma-Aldrich Chemie GmbH, Munich, Germany) was solved in 10 mM HEPES at pH 7.4, or in assay buffer (20 mM HEPES in HBSS, pH 7). Oxidation process happens if simply the created EGCg solutions are exposed to light and higher temperature (for example room temperature), and as a result, we get brown, oxidized liquids [11][14][15]. To increase the speed of the process, the freshly created solutions were underwent heat treatment at 70°C for 1-1.5 hours.

Oppositly charged gold nanoparticle solutions

I used oppositely charged gold nanoparticles (average metal core diameter 5.5 nm and standard deviation σ = 15%) stabilized with self-assembled monolayers of N,N,N-trimethyl(11-mercaptoundecyl)ammonium chloride (TMA, positively charged) and mercaptoundecanoic acid (MUA; negatively charged and fully deprotonated at pH ~ 11). The zeta potentials of positively and negatively charged nanoparticles are 45 mV and -45 mV, respectively. The concentration of the AuMUA and AuTMA NPs used in experiments were 2.5×10^{-6} mM (refractive index: 1.33141) and 1.58×10^{-6} mM (refractive index: 1.33146), respectively, and the pH was adjusted to 10 prior to the experiments. The used buffer during the alternating deposition was tetramethylammonium hydroxide solution (TMAOH, Sigma-Aldrich) pH = 10 (refractive index: 1.33143) [113].

3.2. Cell culture, cell fixation and staining

Cell lines and chemicals of reagent grade were obtained from Sigma-Aldrich (Hungary), unless stated otherwise. The cervical cancer cell line HeLa cells (ATCC® number: CCL-2) were routinely cultured in tissue culture polystyrene Petri dishes (Greiner) placed in a humidified incubator (37°C, 5% CO_2).
The cells were maintained in Dulbecco's modified Eagle's medium (DMEM), supplemented with 10% fetal bovine serum (Biowest SAS, France), 4 mM L-glutamine, 0.25 μg⁄ml amphotericin B, 100 U⁄ml penicillin and 100 μg⁄ml streptomycin solution. On reaching 80% confluence, cells were detached every 3-5 days using 0.05% (w/v) trypsin, 0.02% (w/v) EDTA solution and were not used beyond passage 20 [54].

During the fixation and cell staning procedure 55000 cell/well HeLa cells were seeded into a 96-well, cell imaging, membrane bottom plate (Eppendorf, Cat. no.: 0030741013). The final concentration of freshly created EGCg solutions were 0, 0.5, 5, 10, 20, 40, 50,100, 250 μg/ml.

The following steps were procecuted in the experiments. I created the PP:PPR (1:1) coating (30 μl/well for 30 minutes), then I washed it with HBSS-HEPES buffer for 3 times. After that I prepared the cell suspension and the cell number was counted (55000 cell/well). Then the cells were seeded into the wells of the plate. The same volume of EGCg solutions (in different concentrations) was pipetted into the wells to treat the cells. There was a waiting period for 2 hours. Then cell fixation was procecuted; I washed the wells with PBS buffer. After that I pipetted PBS, and the same amount of 4% PFA very carefully, and I waited for 20 minutes. Then, there was a washing step again with PBS for 3 times.

Millipore's Actin Cytoskeleton and Focal Adhesion Staining Kit (Catalog Number FAK100) was used to stain actin filaments and focal contacts of the EGCg treated HeLa cells. The kit contains DAPI ((Part No. 90229. One vial containing 100 μl at 0.1mg/ml). Vinculin Monoclonal Antibody, (purified clone 7F9 (Part No. 90227. One vial containing 100 μl at 1 mg/ml), TRITC-conjugated Phalloidin (Part No. 90228. One vial containing 15 μg lyophilized TRITC-conjugated Phalloidin). To prepare a stock solution, I resuspended one vial of TRITC-conjugated Phalloidin (15 μg) into 250 μL of methanol. I stored at -20°C upon reconstitution).
Further required materials for the staining were the fixative (4% paraformaldehyde), permeabilizing reagent, (0.1% Triton X-100), blocking solution (1% BSA in 1x PBS), fluorescent-labeled anti-mouse secondary antibody (Millipore Cat. No. AP124F), 1x wash buffer (1x PBS containing 0.05% Tween-20), antifade mounting solution (Millipore Cat. No. 5013), glass slides and coverslips.
The steps of cell staining is the following according to the manufacturer's protocol [114].
After the fixation procedure, they were washed twice with 1x wash buffer. I permeabilized cells with 0.1% Triton X-100 in 1x PBS for 1-5 minutes at room temperature, then I washed again twice with 1x wash buffer. Blocking solution was applied for 30 minutes at room temperature.

After that, I diluted the primary antibody (Anti-Vinculin) to a working concentration in blocking solution, and I incubated the cells for 1 hour at room temperature. (Recommended dilution for anti-Vinculin was 1:100-1:500), then I washed them three times (5-10 minutes each) with 1x wash buffer. The secondary antibody (Gt x Ms, FITC-conjugated, for example Millipore Cat. No. AP124F) was diluted in 1x PBS just before use and I incubated it for 30-60 minutes at room temperature. For double labeling TRITC conjugated Phalloidin could be incubated simultaneously with the secondary antibody for 30-60 minutes at room temperature. (Optimal dilution for TRITC-conjugated Phalloidin is 1:100 -1:1000). After that I washed three times (5-10 minutes each) with 1x wash buffer. Following this washing step, nuclei counterstaining was performed by incubating cells with DAPI for 1-5 minutes at room temperature, followed by washing cells three times (5-10 minutes each) with 1x wash buffer. (Recommended starting dilution was 1:1000). The cells were covered with 1x PBS prior to visualization to prevent cells from dryingout. Fluorescence images were visualized with a fluorescence microscope.

3.3. MTT cell viability assay

3-(4,5-Dimethylthiazol-2-yl)-2,5-diphenyltetrazolium bromide (MTT) reduction is one of the most frequently used methods for measuring neural cytotoxicity and cell proliferation [115]. Tetrazolium salts accept electrons from oxidized substrates or appropriate enzymes, for instance NADH and NADPH [116]. MTT is reduced at the ubiquinone and cytochrome b and c sites of the mitochondrial electron transport system and as the result of succinate dehydrogenase activity of the cells [116][117][118]. This reaction converts the yellow salts to blue-colored formazan crystals that can be dissolved in an organic solvent (for example in dimethyl sulfoxide, DMSO) whose concentration can be spectrophotometrically determined (Fig. 3.1) [116][117][118]. It has been suggested that MTT is taken up by cells through endocytosis and the reduced MTT formazan accumulates in the lysosomal/endosomal compartment and then transported to the surface of the cell through exocytosis [115].

HeLa cells were plated into 96-well plate with initial cell number of 12500 per well. After 24 h incubation at 37^{o}C, cells were treated with the compound EGCg in 200 μL serum free medium or in 200 μl HBSS-HEPES buffer. Cells were incubated with the compounds at 0.064 to 500 or 1000 μg/ml concentration range for 2 hrs. Control cells were treated with serum free medium only or with HBSS-HEPES buffer at 37^{o}C for 2 hrs. After washing the cells three times with serum free medium or HBSS-HEPES buffer the viability was determined by 3-(4,5-dimethylthiazol-2-yl)-2,5-diphenyltetrazolium bromide (MTT)-assay [119][120]. 45 μl MTT-solution (2 mg/ml) was added to each well. The respiratory chain [15] and other electron transport systems reduce MTT and thereby form non-water-soluble violet formazan crystals within the cell [121]. The amount of these crystals can be determined spectrophotometrically

[122]. After 3 hrs of incubation cells were centrifuged for 5 min (2000 RPM) and supernatant was removed. The obtained formazan crystals were dissolved in DMSO and optical density (OD) of the samples was measured at λ = 540 and 620 nm using ELISA Reader (iEMS Reader, Labsystems, Finland). OD_{620} values were substracted from OD_{540} values [123].

In the case of cytostatic effect determination, cells were cultivated for further 72 h DMEM medium containing 10% fetal calf serum (FCS), 2 mM L-glutamine, 160 μg/ml gentamycin at 37°C after the washing steps. After 72 h, viability was determined by the MTT assay (Fig.3.1).

The percent of cytotoxicity and cytostatic effect was calculated using the following equation:

$$\text{cytotoxicity/cytostasis \%} = [1 - (OD_{treated}/OD_{control})] \times 100, \quad (3.1)$$

where $OD_{treated}$ and $OD_{control}$ correspond to the optical densities of the treated and the control cells, respectively. In each case two independent experiments were carried out with 4 parallel measurements. The 50% inhibitory concentration (IC_{50}) values were determined from the dose-response curves. The curves were defined using MicrocalTM Origin1 (version 8.6) software.

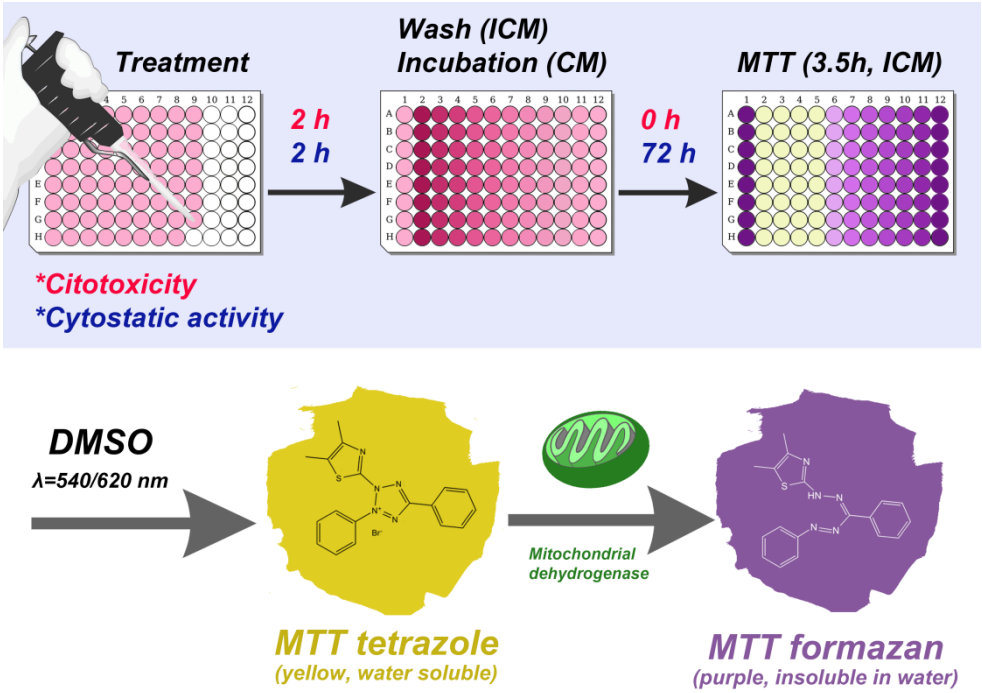

Fig.3.1 Determination of *in vitro* cytotoxic (red) and cytostatic (blue) effect. The basis of the tetrazolium-based colorimetric MTT assay is that the yellow, water soluble tetrazole become purple, insoluble formazan by the mitochondrial dehydrogenase of the living cells. The cytostatic and cytostatic activity can be calculated by the optical density of the treated and control cells. (ICM: incomplete medium, CM: complete medium).

3.3. Holomonitor M4

The applied instrument was an M4 Holomonitor (Phase Holographic Imaging AB, Lund, Sweden) put into a Panasonic MCO-5AC-PE humidified incubator.
Digital holographic microscopy is a high-resolution imaging technique that offers real-time imaging and quantitative measurements of cell morphological and physiological parameters without labeling the observed cells [50][54][51]. This technique explores the phase shift of the probing laser light that has been reflected or transmitted through the monitored object. The amount of phase shift is determined by the optical thickness of the sample, which depends on the index of refraction inside the object and its physical thickness (Fig.3.2). The optical thickness can be measured with a precision down to the nanometer scale [50][54][51].

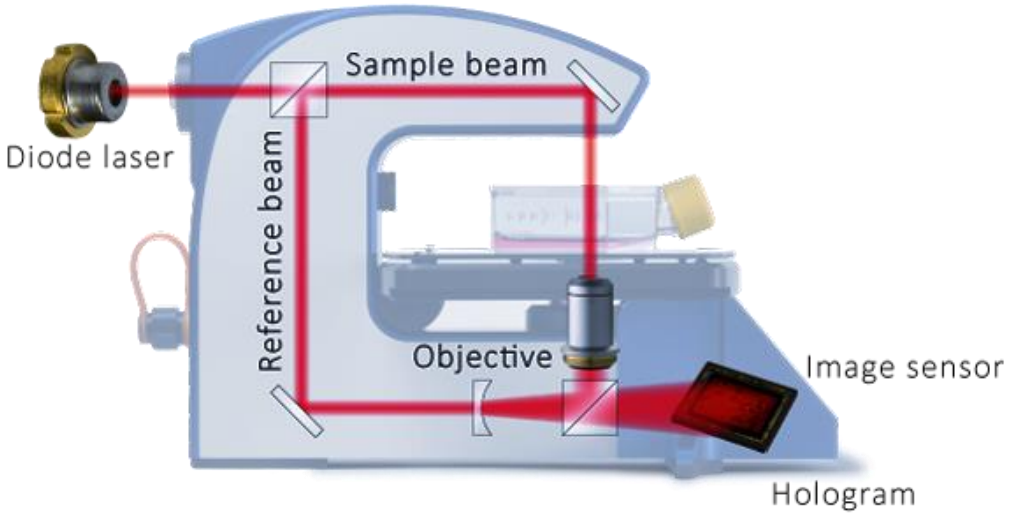

Fig.3.2 The mode of action of the Holomonitor M4. The diode laser is devided into a sample beam and a reference beam. The sample beam get across the sample and the objective, then it become one with the reference beam again. Image sensor senses the signals and than hologram can be formed [I5].

Technical parameters of the Holomonitor M4 instrument (according to the manufacturer):

Light source: external laser unit, 635 nm

Sample illumination: 635 nm, 0.2 mW/cm^2

Objective: 20×

Lateral and vertical resolution: 1 μm

Field of view: 0.25 mm^2

Working distance: 0.5 – 2 mm

Autofocusing range: 1.5 mm

Maximum image rate: 1 image/s

Image size: 1024×1024 pixel

Dimensions (L× W×H) of Holomonitor: 250×160×180 mm

Weight of Holomonitor (incl. fixed stage): 3.9 kg

Cell culture vessels: T25, 6-well, Petri, IBIDI

Cells: Monolayer of adherent

Computer: Windows 7/8 64-bit, 8GB RAM

Incubator: access port for cabling

Operating temperature: 10 – 40° C

Operating humidity: Max. 95%

3.4. Optical Waveguide Lightmode Spectroscopy (OWLS)

Optical waveguide Lightmode Spectroscopy (OWLS210, Microvacuum Ltd., Hungary) is a label-free surface sensitive technique employing evanescent optical waves. The OWLS method uses an optical grating to excite the guided modes of a planar optical waveguide senor chip [100]. During the experiment, linearly polarized light is coupled into the waveguide sensor (Type OW2400, Microvacuum Ltd., Hungary) through a coupling grating. The incident plane-polarized laser is diffracted from the grating and starts to propagate via total internal reflections within the high refractive index waveguide film (Fig.3.3) [100]. Thousands of internal reflections under the illuminated area interfere and excite a guided mode if the phase shift during one complete reflection cycle (total internal reflection at the film-cover and at the film-substrate boundaries) compared to the phase of the original exciting light is equals zero (zeroth order waveguide mode) [100]. This only happens at two distinct incident angles for the employed mono-mode waveguides (represented by the two effective refractive indices, one for the transverse electric (N_{TE}) and one for the transverse magnetic (N_{TM}) mode) according to the mode equations [100][124]. A computer-controlled stepping motor rotates the sensor holder with high reproducibility and accuracy [100].

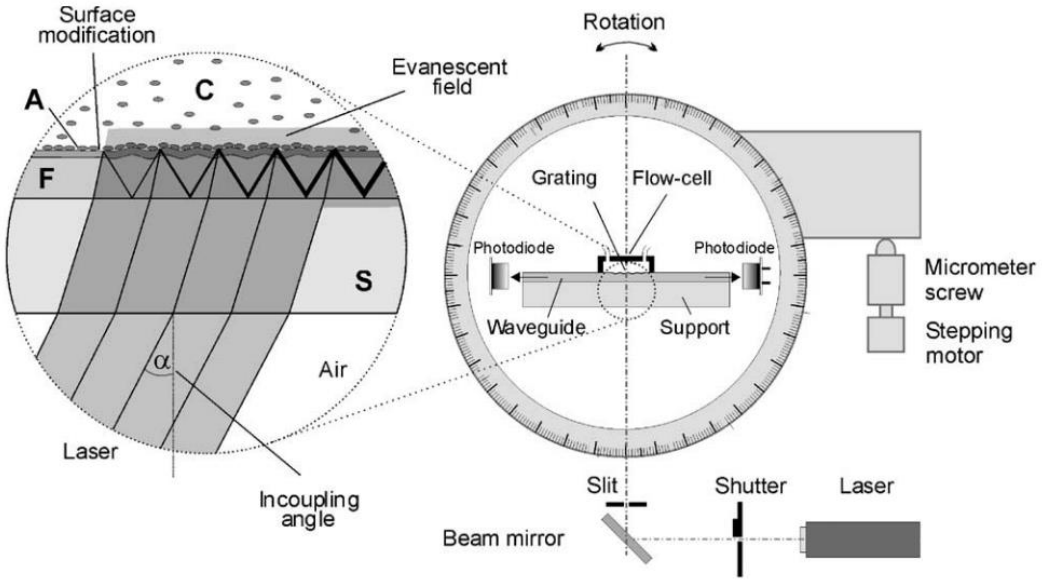

Fig.3.3 Schematic illustration of the optical setup of an OWLS device of Vörös et al. [100]. He–Ne laser beam is diffracted by an optical grating at the surface and starts to propagate via total internal reflection within the waveguiding film (F). At a well-defined incident angle (α) the phase shift during one internal reflection equals zero and a guided mode is excited, which generates an evanescent field penetrating into the bulk solution (C) up to a distance of about 100–200 nm. Changes in the refractive index at the surface (for example formation of an adlayer (A) of adsorbed biomolecules) can then be monitored by precise measurement of the incoupling angle (α) as a function of time [100].

When the incoupling conditions are fulfilled, the waveguide guides the incoupled light of the *TEo* or *TMo* mode to the photodetectors [100]. To determine the direction normal to the waveguide, which is needed to calculate the absolute values of the incoupling angles, the OWLS instrument scans from -7 to +7 degrees and measures the incoupling angles in both directions [100]. The absolute values correspond to the means of the angles monitored in the two directions [100]. Typical anglular resolution is better than 10^{-4} degrees, and in the continuous effective refractive index measurement mode, when only one incoupling angle change is monitored [100].

The effective refractive index (N) of the waveguide mode is calculated from the equation of the incoupling condition:

$$N = n_{\text{air}} \sin(\alpha) + \frac{l\lambda}{\Lambda}, \qquad (3.2)$$

where α is the measured incoupling angle. n_{air} is the refractive index of air, l is the order of the diffraction on the grating (equals 1 for the above mentioned chips), λ is the wavelength of the laser light (nm), Λ is the grating periodicity (nm) [125].
The incoupling angles α_{TE}, α_{TM} for electric and magnetic modes are evaluated from the measured lightmode spectra [125]. The effective refractive indices N_{TE}, N_{TM} of the waveguided modes are calculated on the basis of incoupling condition. Supposing that N_{TE}, N_{TM} has been calculated and

the optical parameters of the waveguide layer (n_F,d_F), the glass substrate (n_S), and the covering medium (n_C) are known, the refractive index (n_A) and the thickness (d_A) of the added layer can be determined [125]. Using a model that the refractive index in the adsorbed layer depends linearly on the concentration of the adsorbed material [125], the mass per unit area (M) of the adsorbed material can be calculated from the de Feijter's formula:

$$M = d_A \frac{n_A - n_C}{dn/dc}, \tag{3.3}$$

where d_A is the thickness of the added layer (nm), n_A is the refractive index of the added layer, n_C is the refractive index of the covering medium [125]. A refractive index increment (dn/dc) value of 0.18 cm^3/g can be used for most of the protein solutions [100][126].
The final surface mass sensitivity of the OWLS device is ~1 ng/cm^2 [I7].

The sensor chip cleaning procedure before each experiment was as follows. The chip was immersed in chromosulfuric acid, ultrapure water, potassium hydroxide and ultrapure water to purify its surface. The plastic cuvette and the fluidic system were treated by oxigen plasma (SPI Supplies Plasma Prep II^{TM}) that removes possible materials remained from the previous experiment [113].

3.5. The Epic Benchtop resonant waveguide grating biosensor

In my experiments Epic BenchTop (BT) system (Corning Incorporated, Corning, NY, USA) next-generation RWG imager biosensor was used. It accepts 96- or 384-well *Society for Biomolecular Screening* (SBS) standard format biosensor microplates [91]. In the present work, a 384-well uncoated cell assay Epic® microplate (Corning, 5040) was used. The bottom of the microplate is a planar optical waveguide, a thin, high refractive-index, transparent dielectric layer (waveguide layer, made of the biocompatible material niobium pentoxide) deposited on a thicker glass substratum [91]. At the central position of each well, a 2x2 mm optical grating is embedded into the optical structure to enable the interrogation of the TM_0 waveguide mode using near-infrared electromagnetic radiation [91]. Thus individually addressable biosensors are created in each well of the microplate [91]. All wells of an Epic microplate are simultaneously interrogated every 3 seconds by sweeping the illuminating wavelength through a range of 15000 pm with 0.25 pm precision (in the range of 825-840 nm) [91]. Waveguide mode excitation only happens at a certain wavelength, called the resonant wavelength (λ) [91]. Refractive index variation in an approximately 150 nm thick layer (in the probing depth of the so-called evanescent wave) over the biosensor surface shift the resonant wavelength to λ'. Refractive index variation can be

caused by, for example, bulk RI change, molecular adsorption, cell spreading, or dynamic mass redistribution inside the cells [91]. The primary signal output of the Epic BT system is the shift of the resonant wavelength ($\Delta\lambda = \lambda' - \lambda$) in each well (Fig.3.4) [91][110].

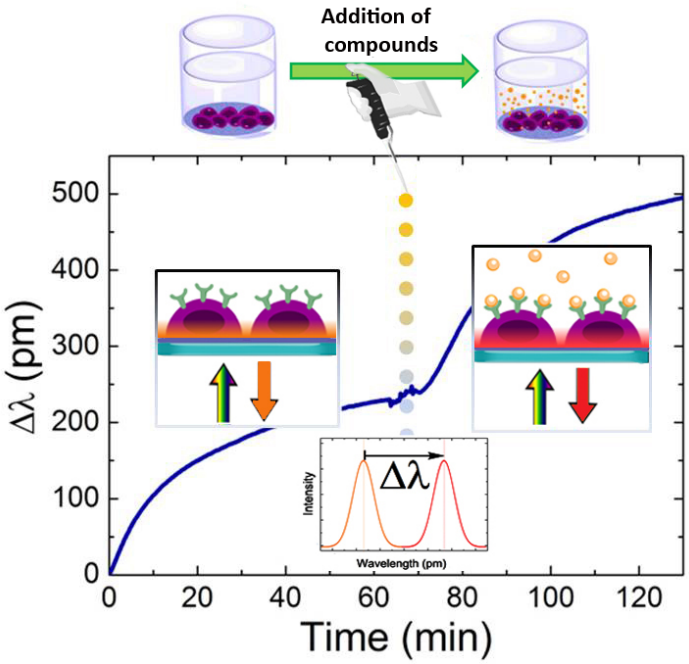

Fig.3.4 Epic BT is capable of measuring the forthcoming changes in the cells (dynamic mass redistribution) influenced by for example compound addition, signaling. Refractive index variation in a ~150 nm thick layer is continually monitored. The primary signal output of the appliance is the shift of the resonant wavelength Δλ in each well.

$\Delta\lambda$ is proportional to the alteration in the effective refractive index N of the TM_0 waveguide mode [127]. The adsorbed mass can be calculated from the Δλ (pm) values by an equation by Orgovan et al., calibrated from OWLS and Epic BT measurements [128].

$$\Delta M = 0.31 \frac{ng}{cm^2} \Delta\lambda \qquad (3.4)$$

where ΔM is the adsorbed mass (ng/cm^2), and Δλ is the wavelength shift (pm) [128].

This equation is regarded to the materials with *dn/dc*=0,182 cm^3/g. If the dn/dc value is different, the calculation need to be corrected.

The device has a limit of detection down to 0.078 ng/cm^2 for the adsorbed mass and 2.2x10^{-6} for refractive index change [128].

3.6. Atomic Force Microsopy (AFM)

Atomic Force Microscopy (AIST-NT, DigiScope1000) in tapping mode with µmasch tips (µmasch, NSC15/AIBS, tip radius < 10 nm, resonant frequency ca. 325 kHz) was used to visualize nanoparticles adsorbed on the sensor's surface.

The scanned areas were 5×5 µm or 2×2 µm. In order to quantitatively evaluate the recorded images a free image analyzing software (Gwyddion 2.3) was used [113]. Scanning speed was 2 Hz, resolution 939x974 pixels.

Technical parameters of the tip (according to the manifacturer):

Typical probe tip radius of uncoated tip: 8 nm

Full tip cone angle: 40°

Total tip height: 12-18 µm

Probe material: n-type silicon

Probe bulk resistivity: 0.01 - 0.025 Ohm*cm

Detector coating: aluminum

Technical parameters of the cantilever (according to the manifacturer):

Resonance frequency: 265-410 Hz (typical 325 Hz)

Force constant: 20-80 N/m (typical 40 N/m)

Length: 125 ± 5 µm

Width: 30 ± 3 µm

Thickness: 4 ± 0.5 µm

4. RESULTS AND DISCUSSION

4.1 Cell morphological changes during EGCg exposure investigated by Holomonitor M4

Digital holographic microscopy offers outstanding potentials in polyphenol research since cell morphological parameters can be monitored in real time without applying any labels. In the following, my results concerning the development and application of holographic microscopy in EGCg research is presented. In short, the findings of a high dose EGCg treatment on single cell motility, motility speed and migration will be summarized. These results were published in the Journal of Biomedical Optics with the title of "Incubator proof miniaturized Holomonitor to *in situ* monitor cancer cells exposed to green tea polyphenol and preosteoblast cells adhering on nanostructured titanate surfaces: validity of the measured parameters and their corrections" [54].

Instrumental developments: new sample stage for precise sample positioning

Previous versions of the Holomonitor (M2 and M3) are too large to be put into a cell culture incubator, which causes serious drawbacks in the observations of the living cells under relevant physiological conditions over long periods of time without any disturbance (Fig.4.1).

Fig.4.1 The difference between the Holomonitor M3 (large, red) and M4 (blue, small). The Holomonitor M4 is tiny enough to put it into the incubator [I6].

For example, to maintain and keep the cells at 37°C environment during the measurements, a heated plate was used, but clearly, this is not as efficient as an incubator (due to the differences in the temperature, humidity, and CO_2 level) [51]. Persson et al. recommended the development of a Holomonitor system with controlled temperature and CO_2 levels [51]. During our experiments, the newly developed remarkably small-sized M4 Holomonitor was inside a cell culture incubator

continuously. The parts of the appliance are specially selected to withstand the harsh climate of the cell incubator.

The Holomonitor creates the image of the cells digitally from the phase information. This process works when the cells are positioned in a certain zone of the optical setup. However, the thickness of the applied petri dishes and Ibidi slides are different. The manufacturer company recommended to use adapter sheets with fixed thicknesses (1, 1.5, 2 or 2.5 mm) between the petri dishes and the Holomonitor's original sample stage. However, our experiments showed that the lifting of the sample by 0.5 mm precision is not enough to get sharp images. To avoid this problem, a special mechanical stage was developed and created by Plósz Engineering Office (Hungary) in order to position the sample into that range of the optical arrangement where digital autofocusing works with high reproducibility and precision. The geometrical constraints of this special aluminum stage guarantee that when the micrometer screw (precision: 15 μm) is rotated, the surface of the table remains horizontal, which does not tilt the sample but moves up or down in a highly precise manner. Due to its formation, we can set the height of the sample and keep it horizontal without bias [see Figs. 4.2(a) and 4.2(b)]. The necessity and importance of this stage is evident. If the sample is positioned too low, only the edge of the field of vision can be seen [see Fig. 4.2(f)], with a similar problem if the sample is positioned too high [see Fig. 4.2(d)]. In focus, we can create clear images [see Fig. 4.2(e)]. This is important, because obtaining sharp images is the main requirement for the further evaluations.

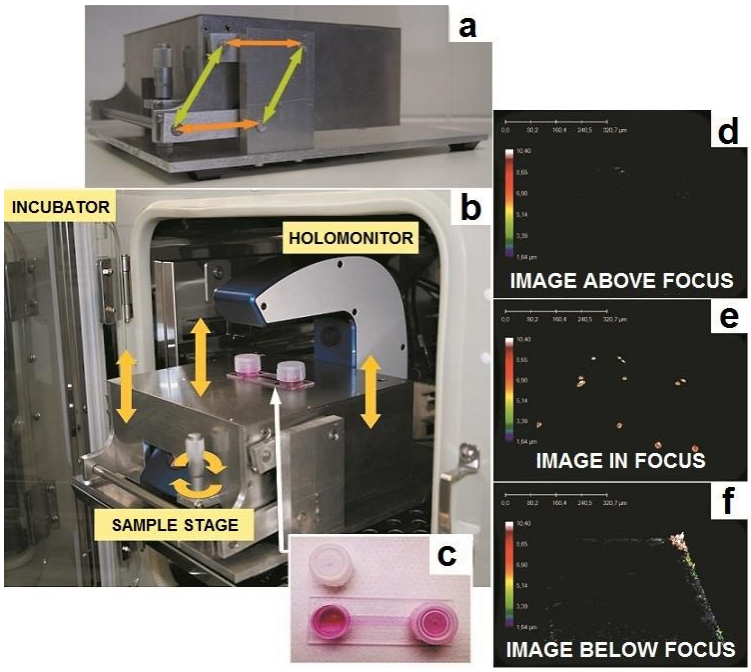

Fig.4.2 Incubator proof Holomonitor M4 and the developed sample stage. (a) Representation of the basics of the working principle of the aluminum sample stage. (b) Appliance in the incubator. The sample stage is moveable upward and downward using the screw. (c) Ibidi μ-Slide filled with cell culture media with adhered cells in the channel of the slide. (d) Image recorded by the Holomonitor above focus (e) in focus and (f) below focus. Note that

the image above and below focus means that the sample stage is positioned above or below that range where the image focus can be found by the Holomonitor digitally [54].

Cell motility, migration and motility speed after EGCg treatment

I used an Ibidi flow chamber (Ibidi, µ-Slide I, hydrophobic, uncoated, sterile) made of the highest optical quality plastic [see Fig. 4.2(c)]. The coating solution, the cell suspension, and later the EGCg solution were pipetted into one of the chambers of the slide.
The 240 µl 1 mg⁄ml PP:PPR (120 µl PP and 120 µl PPR in 1:1 ratio) was pipetted into the chamber for 30 min. Irreversibly adsorbed polymers were removed by an intense washing step with solvent. After that, we filled the channel of the µ-Slide with 100 µl cell suspension in DMEM media (3×105 cells⁄ml). The Ibidi µ-Slide was placed onto the sample stage. The cells were incubated and monitored for 20 h and images were taken every 5 min. During this time, the cells could spread, proliferate, and move. After 20 h, an additional 1 ml 500 µg⁄ml EGCg solution (freshly solved in DMEM media) was added to the cells. From that chamber, the fluids flow into the other chamber through a channel between them. They were incubated and monitored for 20 h and images were again taken every 5 min. The images of the cells were taken at the channel area [see Fig. 4.2(c)].

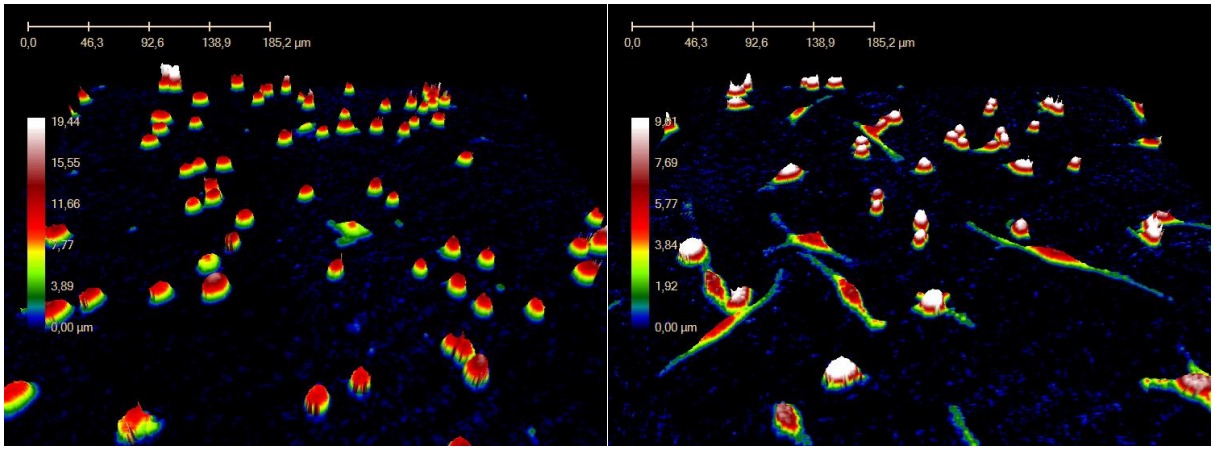

Fig.4.3 Typical 3-D images taken by Holomonitor M4. Left: cells are rounded when they can not adhere to the surface or when they have just started to adhere onto a new surface. Right: The spreading process has begun.

From the captured images, a time-lapse video can be created by combining the images into a continuous film (Fig.4.3). Single cells were tracked in each image sequence to get information about cell movement: migration, motility, and motility speed. Holomonitor software uses 5 min (the sampling time) for the calculations, and the centroid for the cell tracking (Fig.4.4).

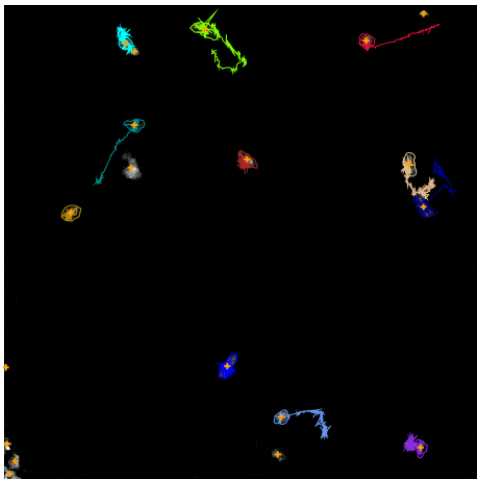

Fig.4.4 Cell tracking. This process is essential to receive informations about the selected cells.

A more detailed profile analysis can be made even of a single cell by the Holomonitor program and by cross-sectional images of the spread cells [see Fig. 4.5(d)].
In the Holomonitor software, motility is calculated as the actual distance the cell has moved from the start to the end of the analysis and migration as the shortest distance from the starting point to the end point. The motility can be very high even if the migration is close to zero. Figures 4.5(a)–4.5(c) show average motility, motility speed, and migration for typical five cells selected from the captured images. My aim was to seed the cells in an optimal concentration, in which they do not disturb each other's movement during the Holomonitor experiment. Because of this reason, a relatively slight cell number was used, and just few of them (25-50 cells) were in the field of vision of the Holomonitor M4. Furthermore, certain cells left, and others got into the field of vision during the 40 h experimental time. Thus, just few cells could be monitored with this Holomonitor settings.

I found that after the addition of EGCg to the cells, mainly the migration, but also the motility (reduction approx. 25%) and motility speed (reduction approx. 35%) of the cells started to reduce or stagnate (see Fig. 4.5).
From the results, it can be seen, that the migrating behavior of the cells almost disappeared after the EGCg treatment, but their movement did not stop completely (motility). With this experiment, I proved that our newly developed sample stage is excellent for monitoring the cells and to observe the effects of active substances. I first demonstrated that the movement of HeLa cells temperately reduced after the addition of the polyphenol EGCg by Holomonitor M4. This effect was monitored in a completely noninvasive and label-free manner under physiologically relevant conditions.

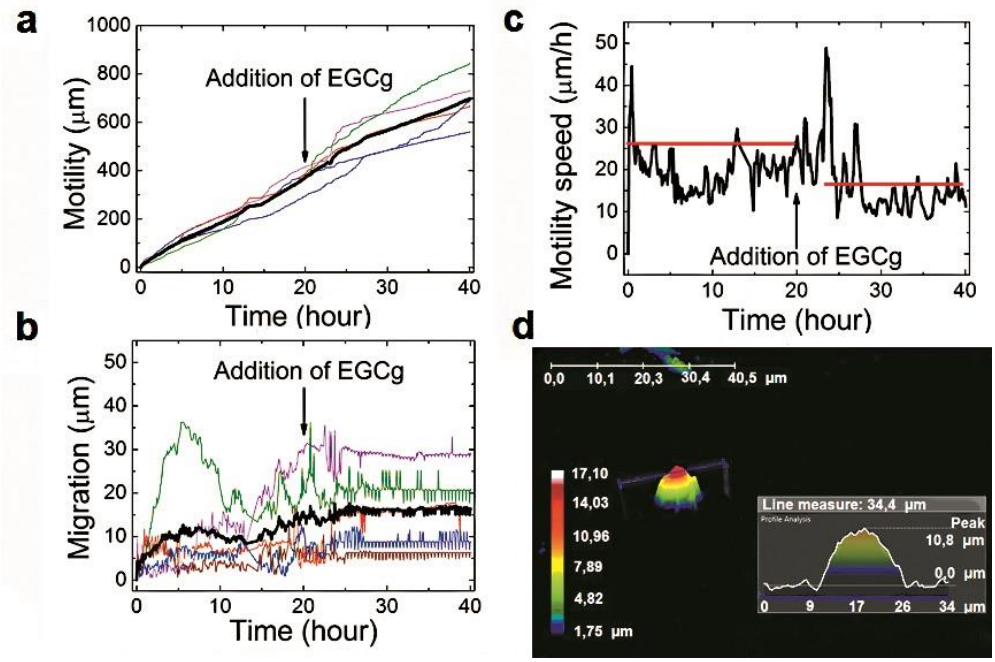

Fig.4.5 Cell movement analysis by Holomonitor M4 when epigallocatechin gallate (EGCg) is added to the HeLa cancer cells. The black lines represent the mean of the values, averaged for five typical cells. (a) Motility, (b) migration, (c) average motility speed, the effect of EGCg is clearly seen, and (d) profile analysis of the spread HeLa cell by Holomonitor M4 [54].

4.2. Cell repellent and cell adhesive polymer coatings exposed to EGCg: multicomponent model systems using biosensors

High dose EGCg treatment resulted in reduction of HeLa cell movement (approximately 25% reduction in motility and 35% reduction in motility speed). In the following, I systhematically analyze the adsorption of EGCg and its oxidized form on the cell repellent PLL-*g*-PEG (PP) and cell adhesive PLL-*g*-PEG: PLL-*g*-PEG-RGD (PP:PPR) coatings and follow the cellular adhesion and spreading on the pre-exposed coatings by using the novel Epic BT biosensor. The results of this chapter is under submission, with the title of "Label-free optical biosensor to real-time study multicomponent model system of cell-surface interactions: a case study on polymer coatings exposed to EGCg and their interactions with living cells" [129].

Real-time EGCg and oxidized EGCg adsorption on PLL-g-PEG (PP) and PLL-g-PEG: PLL-g-PEG-RGD (PP:PPR) coatings followed by OWLS

First, the EGCg adsorption to the coatings was investigated by using OWLS.
In the case of the *PP:PPR measurements* the baseline was recorded with continuous flow of HEPES buffer using peristaltic pump with rate of 1 µl/sec for approximately 40 min. After that 100 µl of PP:PPR was injected onto the sensor surface to create the coating and washed out with HEPES buffer after 20 min incubation. Then the HEPES buffer was changed to HBSS-HEPES buffer and the baseline was recorded for 20 min until the stabilization of the baseline. After that 100 µl of EGCg solution (500 µg/ml, in HBSS-HEPES buffer) was injected to the cuvette and incubated for 20 min, than excess of it was washed out by HBSS-HEPES buffer.

In the case of the *PP measurements* the baseline was fixed with HEPES buffer by using peristaltic pump (1µl/sec) for approximately 40 min. After that PP was injected (100 µl) for 20 min to create the coating, then I washed it with HEPES buffer by peristaltic pump (1µl/sec) for approximately 20 min. After that 100 µl EGCg solution (500 µg/ml, solved in HEPES buffer was injected for 20 minutes. Later, another washing period was performed with HEPES buffer by peristaltic pump (1µl/sec) for approximately 20 minutes.

After performing the mentioned steps described above, the following result was received. Previous studies showed that PP has repellent properties. For instance, Lee at al. have shown that a PP layer on various metal oxide surfaces displays resistance to a nonspecific adsorption of proteins and provides a lubricious surface in an aqueous environment [130], furthermore, a pure PP coating completely blocks cell spreading: all cells remain small and round, observed by Orgovan et.al. [131]. The OWLS measurements showed that although PP layer is a repellent layer, EGCg and oxidized EGCg molecules could bind to this repellent surface.
The degree of nanoscale order of RGD motifs (arginine-glycine-asparagine) on a surface (PLL-*g*-PEG-RGD, here) has been shown to have a serious impact on cell spreading [132][131][133][134]. The PP and its cell adhesive, functionalized counterpart, PPR solutions can be mixed to increase the ligand density and to increase cell spreading [131] .
However, in this work, I proved that EGCg molecules (500 µg/ml) can bind partly irreversibly to the PP coating (Fig.4.6). Moreover, the oxidized EGCg bound in an approximately threefold (375.98 ng/cm^2) amount than the non-oxidized, fresh EGCg (119.31 ng/cm^2). I repeated this measurements on PP:PPR coating as well, and I get almost the same values.

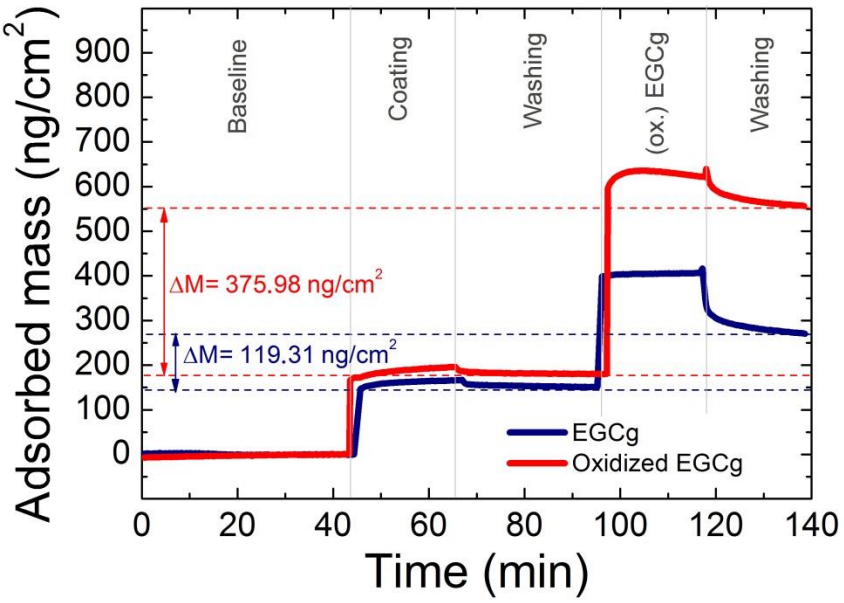

Fig.4.6 Adsorbed mass curves of 500 µg/ml EGCg and oxidized EGCg on PP coating in HEPES buffer.

To do more measurements (for example measurements with more concentrations, observation of cellular adhesion on these coatings, etc.). OWLS is not enough, because it is not a high-throughput appliance. Thus, for further investigations, the Epic BT was used.

EGCg adsorption and subsequent cellular adhesion on the PLL-g-PEG (PP) and PLL-g-PEG: PLL-g-PEG-RGD (PP:PPR) coatings monitored by high-throughput Epic BT

First, the baseline with HBSS-HEPES buffer (30 µl) was taken for approximately 40-60 min. After that the PP:PPR and/or PP were created. Wells were given 30 µl HBBS-HEPES assay buffer to pre-wet the 384-well Epic plate sensors and establish a baseline with the RWG imager [91]. Following the stabilization of the biosensor signal, the measurement was stopped and the buffer was replaced with 30 µl of the desired coating solution and incubated for 30 min while gently shaking at room temperature [91]. The biosensor plate was then replaced into the RWG imager and the signal was recorded [91]. The coating solutions were then removed and the wells were rinsed three times with 30 µl of assay buffer. Wells were then given 30 µl assay buffer for the fourth time to establish a new baseline [91]. Then the EGCg solutions were pipetted (30 µl) into the wells and I measured them for an hour. Then came a wash for 4 times, and after that, new kinetic curves were recorded by the biosensor for 30 minutes with HBSS-HEPES (30 µl). During this time, HeLa cells were brought into suspension by using pre-warmed trypsin-EDTA solution [91]. Trypsin was removed before complete detachment of HeLa cells and its activity arrested by

adding culture medium (containing 10% FBS) [91]. Harvested cells were centrifuged at 2000 rpm for 6 min and the cell pellet was resuspended in assay buffer with intensive pipetting [91]. Cells were then counted in a hemocytometer, and 12000 cells were added to each sensor wells. Wells for buffer control were also coated with the copolymers and treated the same way as the sample wells during the experiment, except that they received assay buffer instead of cell suspension. All measurements were done in triplicate in three different wells at room temperature [91]. Spreading was monitored until saturation of the biosensor signals (2 h). Averaging every 5 subsequent data points, the effective sampling rate was 1/15 s^{-1} [91].

The interaction of the PP and PP:PPR with EGCg was *in situ* monitored and the EGCg exposed coatings were washed with pure buffer. Right after, cellular adhesion on the EGCg treated coatings was recorded in real time. The plate based sensor configuration allowed to follow the mentioned processes with different surface coatings and EGCg/oxidized EGCg concentrations in a single run, on the same biosensor plate. Therefore, the state of the investigated living cells was the same for all experimental conditions. Moreover, the differences between the effects of the freshly prepared and oxidized EGCg solution, often overlooked in literature, could be also revealed. Fig. 4.7 schematically shows the measurement steps.

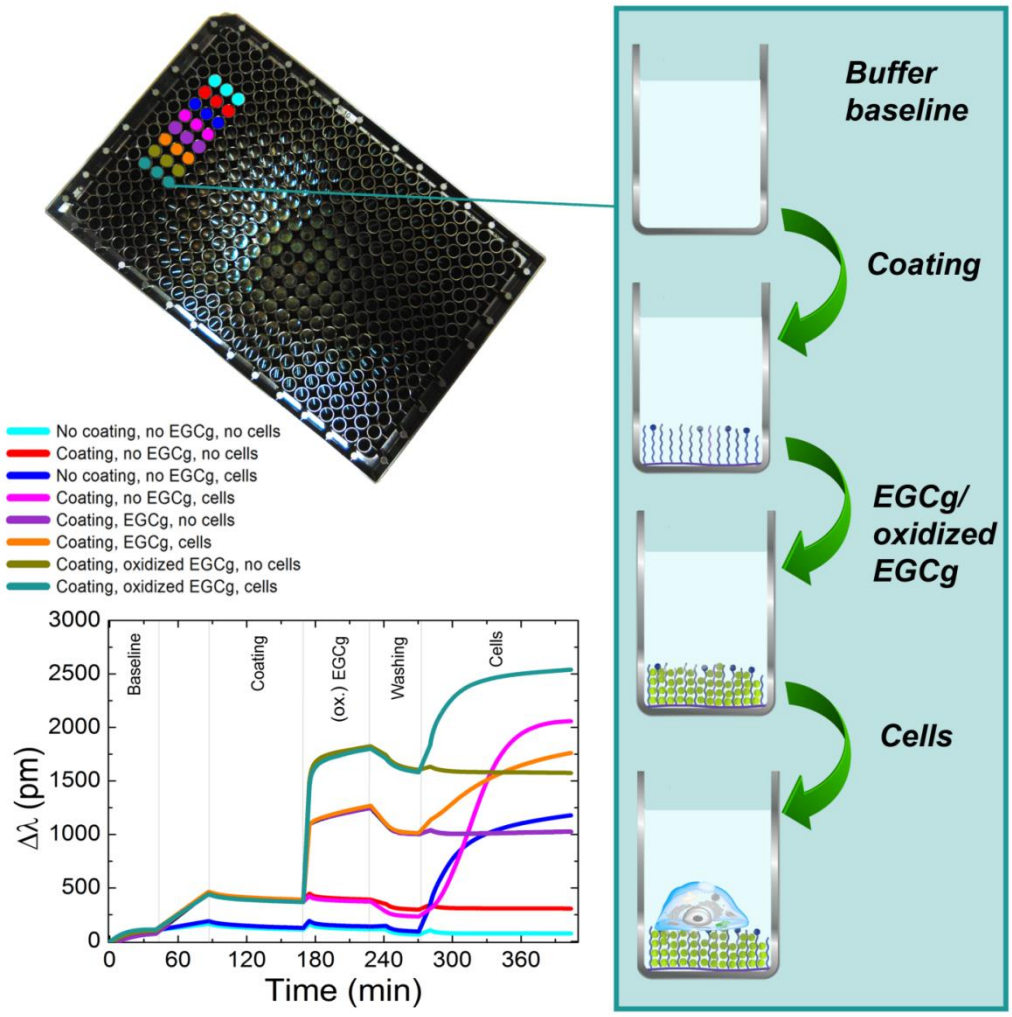

Fig.4.7 384-well plate was used in the experiment. The processes can be observed simultaneously in a lot of wells, so parallel measurements can be easily done. Here, I measured in triplicates, the coating was PP:PPR, and the concentration of the EGCg suspension was 500 µg/ml. The cells cannot adhere to bare biosensor surface (dark blue curve), in this case I get adsorption-like curves. Cells like to spread on PP:PPR coating, I got spreading (sigmoidal) curve (pink). I received adsorption-like curves in the case of treated coatings both by freshly created EGCg suspension (EGCg), and oxidized suspension (oxidized EGCg). This means that the cells could not adhere to this treated surface (orange and dark cyan curves).

PP coating exposed to EGCg and subsequent cellular adhesion

EGCg molecules (added in different concentrations in suspension), adsorbed on the the prepared coatings, and the rest of them remained on the PP chains after the washing procedure [(Fig.4.8 (A),(B),(E),(F)]. No significant cell signal was observed, except for the highest concentration oxidized EGCg. Higher concentrations of EGCg suspension (oxidized form as well) destroys the cell repellent properties of PP [(Fig.4.8 (D),(H)].

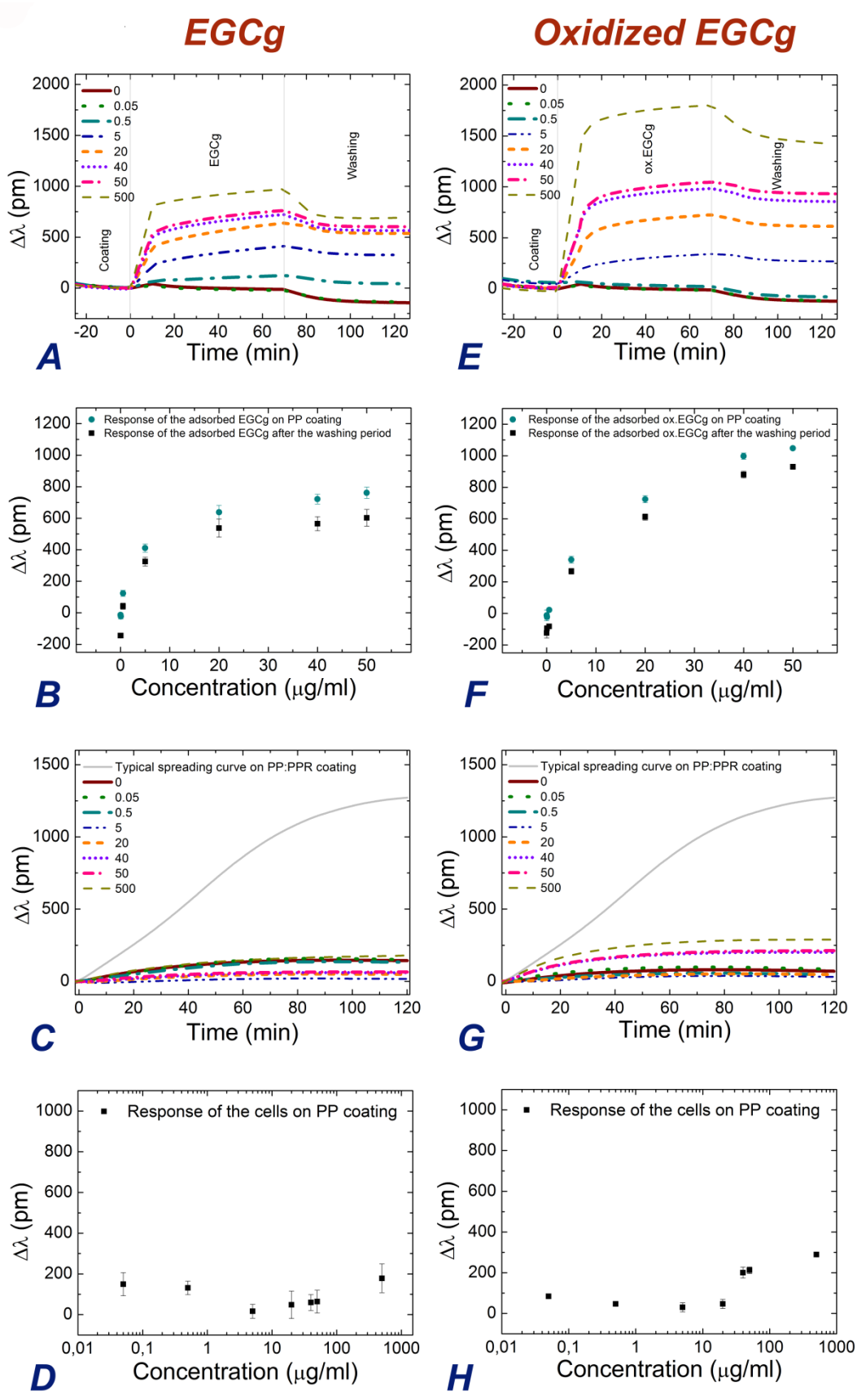
EGCg
Oxidized EGCg
Δλ (pm)
Time (min)
Coating
EGCg
Washing
ox.EGCg
0
0.05
0.5
5
20
40
50
500
A
E
Response of the adsorbed EGCg on PP coating
Response of the adsorbed EGCg after the washing period
Response of the adsorbed ox.EGCg on PP coating
Response of the adsorbed ox.EGCg after the washing period
Concentration (μg/ml)
B
F
Typical spreading curve on PP:PPR coating
C
G
Response of the cells on PP coating
D
H

Fig.4.8 DMR responses of the adsorbed EGCg and oxidized EGCg and cells on EGCg treated PP coating. The used concentrations of EGCg and oxidized EGCg are 0, 0.05, 0.5, 5, 20, 40, 50, 500 μg/ml. (A), (B) shows the response of the adsorbed EGCg. (E), (F) shows the response of the adsorbed oxidized EGCg. (C), (D) shows the response of the cells on the EGCg treated PP coating. (G), (H) shows the response of the cells on the oxidized EGCg treated PP coating.

PP:PPR coating exposed to EGCg and subsequent cellular adhesion

EGCg molecules (added in different concentrations in suspension), adsorbed on the prepared coatings, and the rest of them remained on the PP:PPR chains after the washing procedure [(Fig.4.9 (A), (B), (E), (F)]. At higher EGCg concentrations, decreased cell adhesion signal was observed. The effect is more significant when the oxidized form was used. The cell attractive property of PP:PPR is destroyed by using higher concentrations of EGCg [(Fig.4.9 (D), (H)].

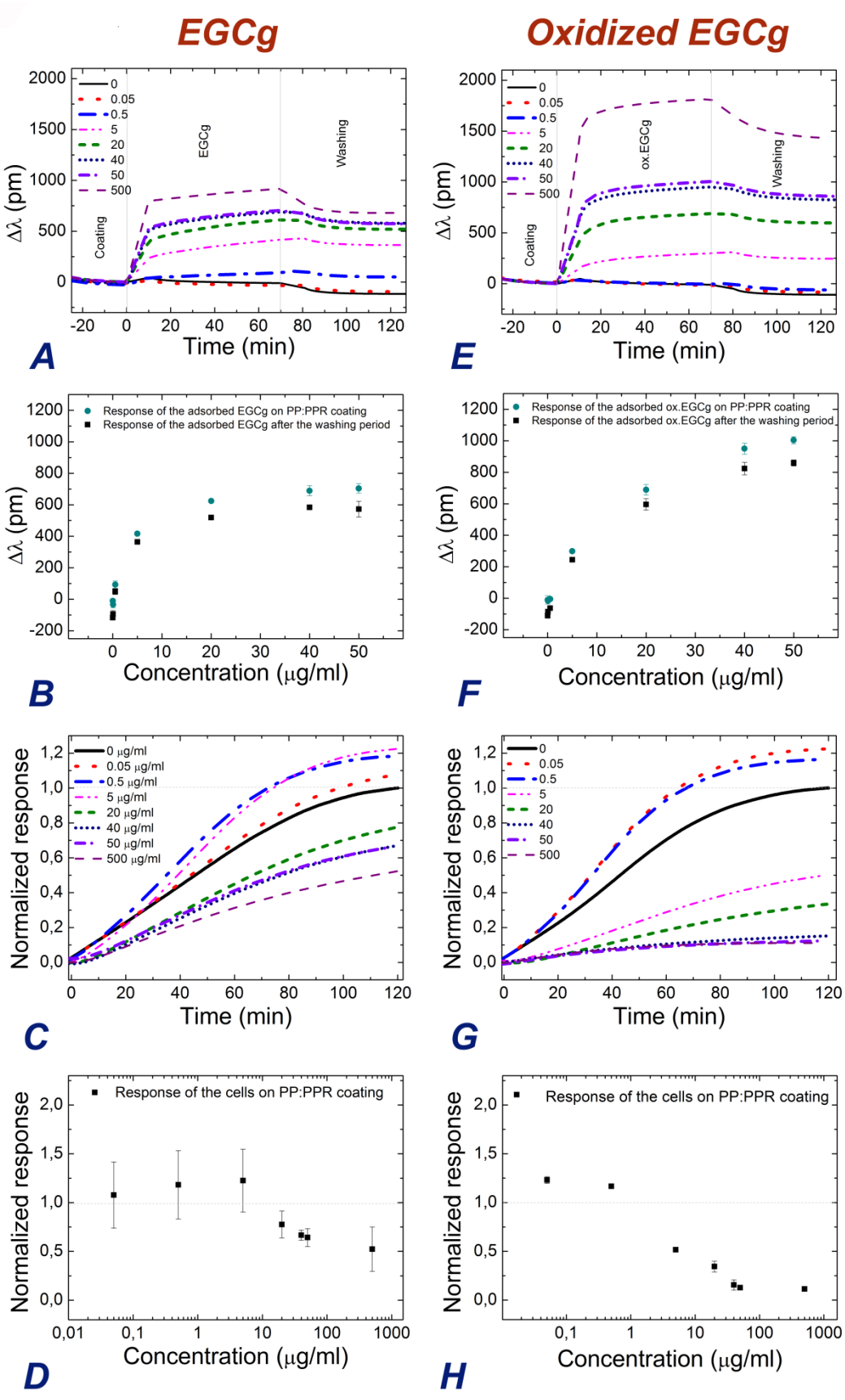
EGCg
Oxidized EGCg
Δλ (pm)
Time (min)
Coating
EGCg
ox.EGCg
Washing
0
0.05
0.5
5
20
40
50
500
A
E
Response of the adsorbed EGCg on PP:PPR coating
Response of the adsorbed EGCg after the washing period
Response of the adsorbed ox.EGCg on PP:PPR coating
Response of the adsorbed ox.EGCg after the washing period
Concentration (μg/ml)
B
F
Normalized response
0 μg/ml
0.05 μg/ml
0.5 μg/ml
5 μg/ml
20 μg/ml
40 μg/ml
50 μg/ml
500 μg/ml
C
G
Response of the cells on PP:PPR coating
D
H

Fig.4.9 DMR responses of the adsorbed EGCg and oxidized EGCg and cells on EGCg treated PP:PPR coating. The used concentrations of EGCg and oxidized EGCg are 0, 0.05, 0.5,5,20,40,50,500 μg/ml. (A), (B) shows the response of the adsorbed EGCg. (E),(F) shows the response of the adsorbed oxidized EGCg. (C),(D) shows the response of the cells on the EGCg treated PP:PPR coating. (G),(H) shows the response of the cells on the oxidized EGCg treated PP:PPR coating.

Taken together, these results showed that OWLS and Epic BT are excellent tools for monitoring EGCg adsorbtion to PP and PP:PPR coatings and gave the same results. However, OWLS is not a high-throughput device, and just the 500 μg/ml fresh and oxidized EGCg solutions were monitored with it. Futher experiments, more concentrations and cellular adhesion to the treated coatings were examined by using Epic BT. EGCg and its oxidized form adsorbed equally to both coatings. The difference is in the case of cell adhesion; although PP:PPR has cell adhesion inducing properties, the EGCg and oxidized EGCg solutions destroyed this feature, and HeLa cells could not adhere to the surface depending on the polyphenol concentration. Cells did not adhered to the originally repellent PP coating either, however, the highest EGCg (500 μg/ml) and oxidized EGCg (50, 500 μg/ml) concentrations seem to increase cellular adhesion. EGCg has a 1.8 times larger inhibitory impact on HeLa cell adhesion in solution, and three times more binds to the copolymer coatings from the oxidized form compared to the EGCg molecules adsorbing from the freshly created EGCg solution.

The bound amount of EGCg and oxidized EGCg

In the case of OWLS measurements, the appliance monitors the *NTE* and *NTM* (transverse electric mode and transverse magnetic mode), and the n_F, d_F (the optogeometric parameters of the film) values. From these data, OWLS calculates the *nA,dA* values, and the adsorbed mass. The mass always must be calculated and corrected by the exact *dn/dc* value of the sample (in this case the *dn/dc* of the EGCg).

The correct adsorbed mass can be calculated from the de Feijter's formula (equation 3.3)

A refractive index increment (*dn/dc*) value of 0.18 cm^3/g can be used for most of the protein adsorption calculations [100].

From this equation, the corrected adsorbed EGCg mass per unit area can be calculated as follows:

$$M_{(EGCg)} = \frac{dn/dc_{(protein)}}{dn/dc_{(EGCg)}} M_{(protein)}, \qquad (4.1)$$

Where the $dn/dc_{(protein)}$ is 0.182 $(g/cm^3)^{-1}$, the dn/dc_{EGCg} is 0.21 $(g/cm^3)^{-1}$. From this formula, the adsorbed mass of the EGCg solutions can be easily calculated. As a result, on the PP coating, the

corrected mass of the EGCg is 119.31 ng/cm^2, while the mass of the oxidized form is 375.98 ng/cm^2 (see Fig.1.). Approximately the same values were obtaine using the PP:PPR coating. The adsorbed mass can be calculated from the Epic BT data. The wavelength shift ($\Delta\lambda$ (pm)) can be transformed to mass (ng/cm^2) from the following equation by Orgovan et al. [128].

$$\Delta M = 0.31 \frac{ng}{cm^2} \Delta\lambda \,, \qquad (4.2)$$

where ΔM is the adsorbed mass (ng/cm^2), and $\Delta\lambda$ is the wavelength shift (pm).

This equation applicable to the materials with *dn/dc*= 0.182 (g/cm^3)$^{-1}$. The *dn/dc* value of the EGCg is 0.21 cm^3/g, so the ΔM value need to be corrected by this value during the calculations.

The number of EGCg and oxidized EGCg layers can be easily calculated with the parameters of the EGCg molecule, for example the molecular size of the EGCg molecule (1.4 nm) and the molecular weight (458.37 g/mol). From these data and Avogadro constant, I could calculate that 37.786 ng EGCg can adsorb on 1cm^2. The number of the layers then can be calculated from ΔM/37.786 ng.

The calculated data are summarized in Table 4.1 (EGCg on PP coating) and Table 4.2 (EGCg on PP:PPR coating).

Table 4.1 The adsorbed mass and the number of created layers of the EGCg and oxidized EGCg solutions (5, 50, 500 µg/ml) on PP coating.

	Conc. (µg/ml)	Δλ (pm)	ΔM (ng/cm²)	Number of layers
	5	324.93 ± 48.97	87.58 ± 13.20	2.31 ± 0.34
EGCg	50	602.51 ± 92.20	162.40 ± 24.85	4.29 ± 0.65
	500	690.09 ± 108.61	186.01 ± 29.26	4.92 ± 0.77
	5	267.51 ± 31.75	72.10 ± 8.55	1.90 ± 0.22
Ox. EGCg	50	930.15 ± 28.21	250.73 ± 7.60	6.63 ± 0.20
	500	1419.29 ± 17.47	382.58 ± 4.7	10.12 ± 0.12

Table 4.2 The adsorbed mass and the number of created layers of the EGCg and oxidized EGCg solutions (5, 50, 500 µg/ml) on PP:PPR coating.

	Conc. (µg/ml)	Δλ (pm)	ΔM (ng/cm²)	Number of layers
	5	364.46 ± 4.81	98.24 ± 1.29	2.59 ± 0.03
EGCg	50	576.52 ± 87.49	154.33 ± 23.58	4.08 ± 0.62
	500	680.91 ± 140.50	183.54 ± 37.86	4.85 ± 1.00
	5	244.51 ± 8.24	65.90 ± 2.21	1.74 ± 0.05
Ox. EGCg	50	859.25 ± 33.55	231.61 ± 9.04	6.12 ± 0.23
	500	1425.75 ± 41.46	384.33 ± 11.17	10.17 ± 0.29

From these data, it can be clearly seen, that the adsorbed mass on the two types of coatings are almost the same. The calculated layers seem to be correct, because the compressible thickness of the PEG polymer layer (z range) is approximately 7 ± 0.5 nm [135] and 4-5 molecules of EGCg (1.4 nm) can be bound to a PEG chain. The spacing between the PEG chains is 1-2 nm [135], so the EGCg molecules fit to the coating.

It is important to note, that the water content of the PP chains is 80 ± 6 wt% [135]. During the polymer adsorption phase, the measured mass data will be the other 20%, since the adsorbed water is not detected by OWLS and Epic BT. Therefore, the polymer bound water molecules might be replaced by EGCg molecules during the interaction of the polymer chains with EGCg and oxidized EGCg, no adsorption on the top of the polymer film is necessary to explain the observed high adsorbed masses.

From the received data of Table 4.1 and 4.2, it can be mentioned that multilayer formation of EGCg molecules on both coatings can also occur. Moreover, after this process, these bound EGCg molecules could inhibit the adhesion of HeLa cells [49] onto PP:PPR surface (Fig.4.10). However, further examinations need to be done to know the exact impacts of EGCg on HeLa cell adhesion without any coatings.

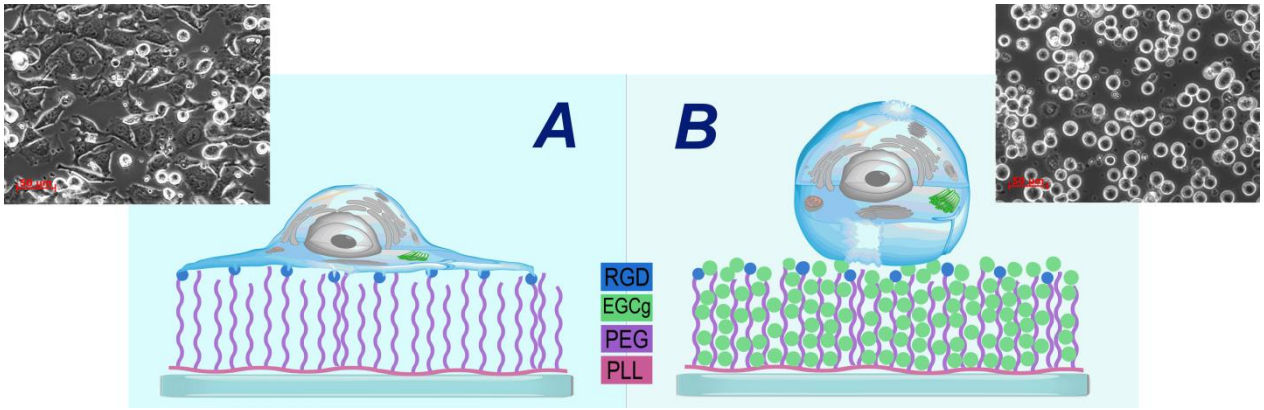

Fig.4.10 Hypothetical schematic illustration of the effects of the bound EGCg molecules on HeLa cell adhesion. A. The cell can easily spread to the PP:PPR coating. B. EGCg molecules bind to the PP:PPR chains, and inhibit cell adhesion. The morphology of the cells can be seen in the images taken by phase contrast microscopy.

4.3. Whole cells exposed to EGCg: comparison of classical cell viability assay with label-free biosensor data and fluorescent imaging of the treated cells

Previously I showed that EGCg strongly affets the cell adhesive properties of PLL-*g*-PEG (PP) and PLL-*g*-PEG: PLL-*g*-PEG-RGD (PP:PPR) in a dose dependent manner. Here, the EGCg was directly added into the cell media. The results are compared with classical MTT tests. Furthermore, fluorescent images were taken of stained cells to obseve the changes in the actin cytoskeleton due to EGCg treatment. The results of this chapter are under publication with a title of "Label-free cytotoxicity assay using the kinetic cell spreading data" [123].

Kinetic curves of the inhibitory impact of EGCg on cellular adhesion monitored by Epic BT

In these measurements, the EGCg solution and the cells are pipetted together to the biosensor surface to observe the effects of EGCg on cell spreading. A typical measurement was the following. After filling the plate wells with HBSS-HEPES, the baseline was taken by the Corning Epic appliance. Then I stopped recording the baseline. PLL-*g*-PEG:PLL-*g*-PEG-RGD coating was created by the already mentioned procedure. After that I removed the PLL-*g*-PEG:PLL-*g*-PEG-RGD from the wells, washed them with HBSS-HEPES (3 times), and I started a new baseline with HBSS-HEPES (pH 7). HeLa cells were trypsinized with 1.0% pre-warmed trypsin-EDTA. Trypsin was removed before complete detachment of HeLa cells and its activity arrested

by adding culture medium containing 10% FBS. Harvested cells were centrifugated at 2000 rpm for 6 min and the cell pellet was resuspended in assay buffer with intensive pipetting. Cells were then counted in a hematocymeter, and ~20000 cells were added to the sensor wells already containing 50 µl assay buffer. The EGCg powder was solved in HBSS-HEPES buffer to get the desired concentrations. EGCg solutions were added to the cells in the wells. We added buffer to the 0 µg/ml EGCg wells. The cells were measured for 2 hours (I let them spread). After a 2 hour period, at the end of the measurement the microplate was placed under Zeiss Observer microscope to visually observe and image the cells.

We can obseve an interesting phenomenon on the kinetic curves measured by Epic BT (Fig.4.11). At lower values than the added 20 µg/ml of EGCg. I received sigmoidal shaped spreading curves (active, living process), and above this value, adsorption curves (dead process). Supposedly, due to the EGCg solution, the cells may emit some compounds from themselves at higher extract concentrations, and that is the reason why I received adsorption curves. This border concentration is approxiamately 20 µg/ml and above it the EGCg has harmful effects on the cancer cells.

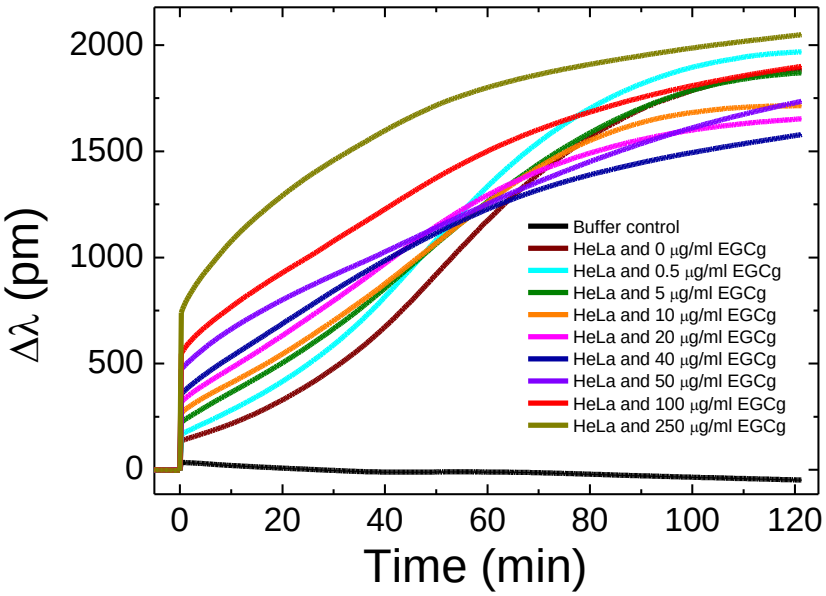

Fig.4.11 Kinetic curves by Epic BT. The cells and the EGCg solutions were pipetted together to the biosensor surface and monitored for 2 hours.

The cells are shrinking, their shape, adhesion and spreading properties are also changing when they are incubated with EGCg solutions. For example, in the microscope images (Fig.4.12) we can clearly see, that at low EGCg concentrations (0-10 µg/ml), the cells could spread together with EGCg, and after the 2 hour period the cells almost spread to the coated biosensor surface. However, at higher concentrations than the added 20 µg/ml of EGCg, the shape of the cells

changed, and they are not as spread as the other cells with lower concentrations or without green tea extract. At higher quantities the cells remained rounded. We can observe the same phenomenon on the measurement curves as mentioned before.

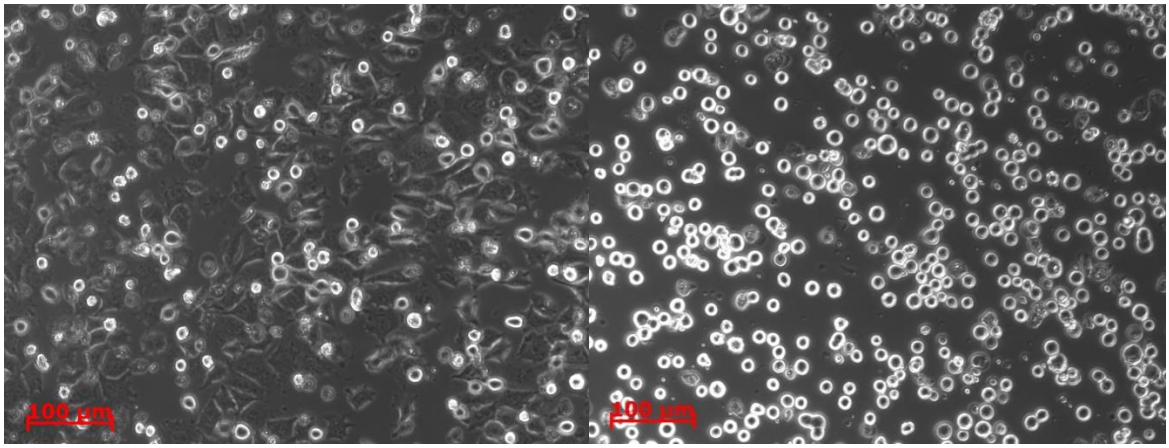

Fig.4.12 Images of the cells after the measurement of the Epic BT microplate wells. Left: cells without EGCg. Cell could spread to the surface. Right: Cells with 250 µg/ml EGCg (highest concentration). Here the cells could not spread and remained rounded. Scalebar: 100 µm.

Cytotoxic and cytostatic activity of the compound EGCg on HeLa cell culture (MTT assay)

3-(4,5-Dimethylthiazol-2-yl)-2,5-diphenyltetrazolium bromide (MTT) reduction is one of the most frequently used methods for measuring neural cytotoxicity and cell proliferation [115]. As the result of the MTT assay, IC_{50} value of a compound can be calculated.

IC_{50} value is the mean of experiments and represents the concentration of the compound which is required for 50% inhibition. In the case of cytotoxicity, this value determines the concentration which destroys the 50% of cell population (direct killing), while in the case of cytostatic activity, it shows the concentration which inhibits the cell growth (proliferation) of 50% of the population.

Note, that negative cytotoxicity values can be occured, if there are higher OD values in several wells, than in control wells. This is most probably due to the inhomogeneous distribution of cell number between the wells and to the low values of signals.

Therefore HeLa cells were treated with EGCg at 0.064 to 500 µg/ml concentration range and the viability of the cells was determined by using MTT-assay. The 50% inhibitory concentration (IC_{50}) values were determined from the dose-response curves (data summarized in Fig.4.13 and 4.14). I found that EGCg exhibited a modest, but not negligible cytotoxic effect on HeLa cells

(IC_{50} > 500 μg/ml). From the cell cytotoxicity curves it can be mentioned that the results with the Epic BT curves are in correlation: the changing concentration is around 20-30 μg/ml in the MTT assay as well. The aim of the scientists is to find an anticancer compound, which has rather cytostatic activity than cytotoxic. The main goal is to inhibit the proliferation of cancer cells. Direct killing compounds are not selective, and destroys not just the abnormal cells. EGCg is rather cytostatic than cytotoxic, thus it can be an optimal substance in curing.

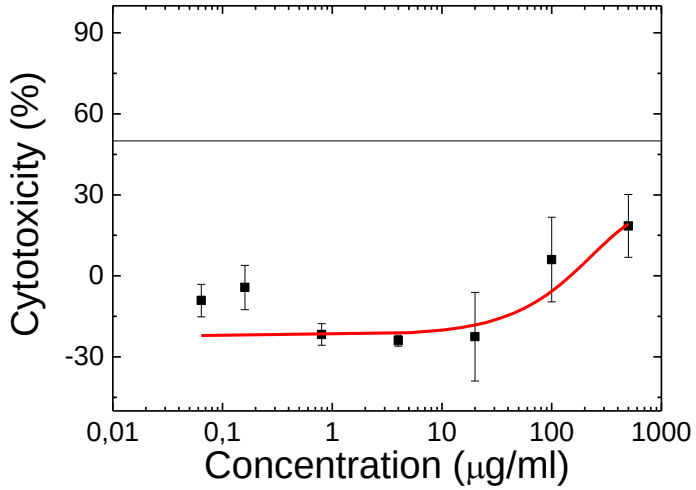

Fig.4.13 Result of the *in vitro* cytotoxic activity assay (MTT-assay). EGCg exhibited a modest, but not negligible cytotoxic effect on HeLa cells (IC_{50} > 500 μg/ml).

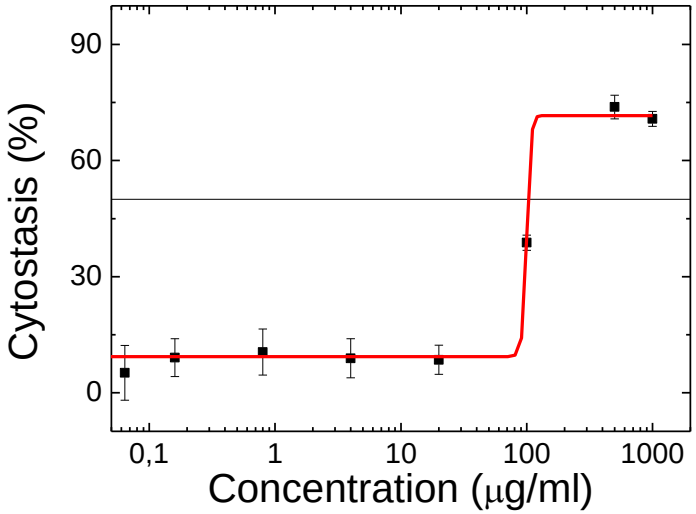

Fig.4.14 Result of the *in vitro* cytostasis activity assay. It shows higher inhibitory concentrations than cytotoxicity test.

Comparison of classical cell viability assay with label-free biosensor data

I tried to analyze the received Epic BT's kinetic curves. First, I derivated the curves (1st derivative), and I recommended an equation:

$$\Delta = \frac{d\Delta\lambda}{dt}\Big|_{max} - \frac{d\Delta\lambda}{dt}\Big|_{t=0} , \qquad (4.3)$$

where Δ (pm/min) is the equivocal value that characterizes the cell adhesion curves monitored by Epic BT, $\frac{d\Delta\lambda}{dt}\Big|_{max}$ is the 1st derivative curve's maximal value (at y-axis), $\frac{d\Delta\lambda}{dt}\Big|_{t=0}$ is the 1st derivative curve's y value at the t=0 timepoint (Fig.4.15). The t=0 definition is very important for the correct calculation. The *dt* was 15 s, because 3 s is the time resolution of the Epic, and the average of 5 datapoints was calculated.

If Δ>0 pm/min, I get sigmoid-like, spreading curves.

In the case of Δ=0 pm/min, I get adsorption-like curves, because the 1st derivative at the t=0 timepoint will be the maxima of 1st derivative for the whole adsoption like curve.

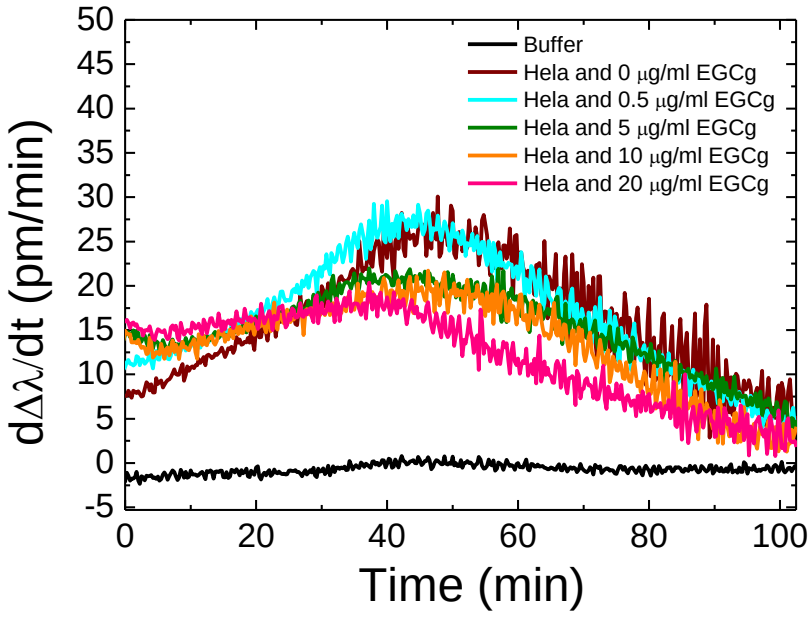

Fig.4.15 1st derivative curves of HeLa cells treated by EGCg from 0 to 20 μg/ml concentrations and a buffer control.

I plotted the Δ values with the concentration data at the x axis and I used logarithmic scale, then I fitted the curve (linear fit) (Fig.4.16).

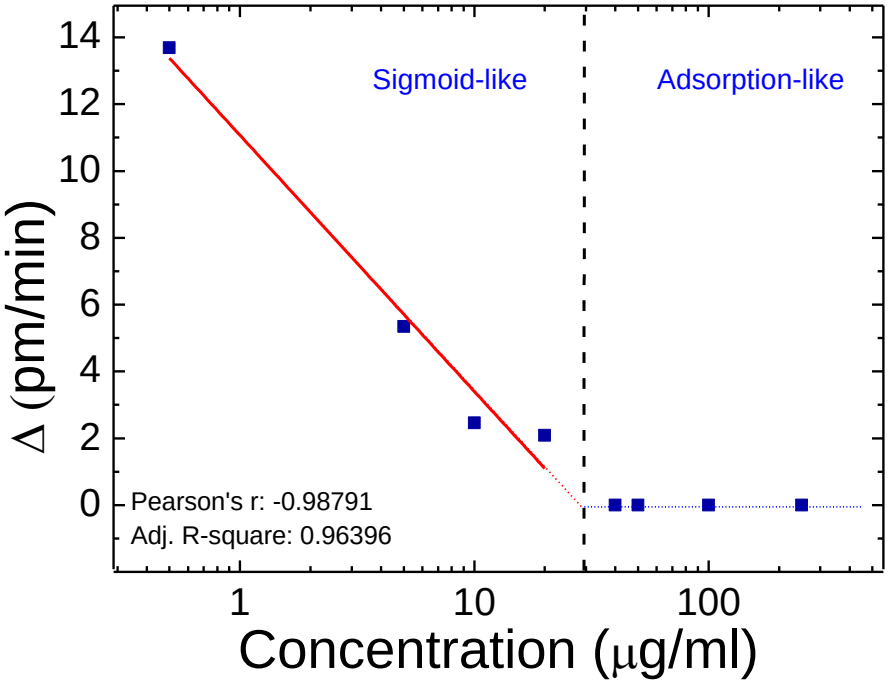

Fig.4.16 On the left the Δ>0 pm/min, indicating a cell spreading process. On the right, Δ values are 0 pm/min, showing an adsorption-like process at higher concentrations. The transition concentration between them is 27.3 ± 10 μg/ml, calculated by linear extrapolation.

At higher concentrations than 20 μg/ml the Δ values are 0 pm/min, and at lower concentrations the Δ values are >0. The exact transition concentration is 27.3 ± 10 μg/ml, calculated by linear extrapolation. The error of the calculation is estimated from the standard errors of the linear fitting.

The calculated transition concentration is compatible with the MTT assay, because this is the point, where the fitted cytostatic activity curve strarts to increase as well.

Therefore, the above protocol might serve as an alternative way to quantitatively characterize cell viability in a completely label-free manner.

Cell staining and fluorescent imaging

I stained the cells to obseve the changes in the morphology of the treated cells by staining the actin filaments and focal contacts.

The actin cytoskeleton is a highly dynamic network composed of actin polymers and associated proteins [114]. Its role is to mediate a variety of essential biological functions in all eukaryotic cells, including structural support and intra- and extra-cellular movement [114]. This dynamic structure rapidly changes shape and organization in response to stimuli and cell cycle progression [114]. Orientational distribution of actin filaments within a cell is, therefore, an important determinant of cellular motility and shape [114][136]. Focal adhesion and adherent junctions are membrane-associated complexes that serve as nucleation sites for actin filaments and as cross-linkers between the cell exterior, plasma membrane and actin cytoskeleton [114][137]. Focal adhesions consist of integrin-type receptors that are attached to the extracellular matrix and are intracellularly associated with protein complexes containing vinculin (universal focal adhesion marker), focal adhesion kinase (FAK), tensin, zyxin, talin, α-actinin and paxillin [114][138][139].

The used staining kit is a very sensitive immunocytochemical tool that contains fluorescent-labeled Phalloidin (TRITC-conjugated Phalloidin) to map the local orientation of actin filaments within cell and a monoclonal antibody to Vinculin that is very specific for the staining of focal contacts in cells. The kit also contains DAPI for the fluorescent labeling of nuclei [114].

As we can see, the cells become rounded when the concentration of EGCg increases. At 0 and low concentrations we can clearly see the actin filaments and filopodia, the cells can spread to the surface. At 40 μg/ml, the cells in general are rounded and smaller, the actin filaments can not be seen very well. The stained cells also showed, that probably the calculated 27.3 ± 10 μg/ml is the border concentration where the inhibitory impact of adhesion evidently begins, and EGCg induces changes in cell adhesion processes and properties (Fig.4.17).

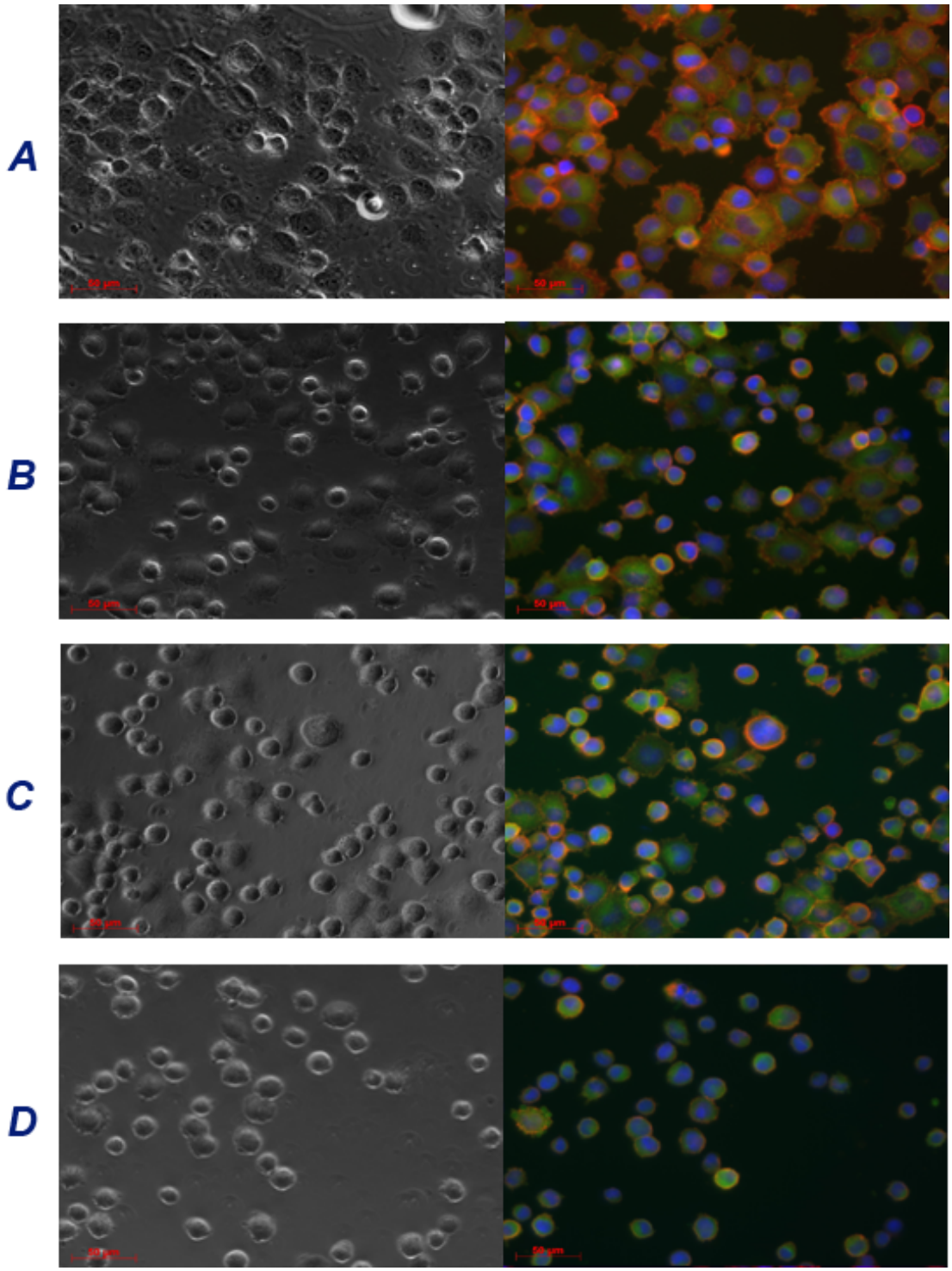

Fig.4.17 Images of the EGCg treated, staining cells by normal and fluorescent mode. Left side: images by normal mode, right side: fluorescent mode. (A) HeLa cells without EGCg treatment. (B) HeLa cells treated by 5 µg/ml EGCg. (C) HeLa cells treated by 10 µg/ml EGCg. (D) HeLa cells treated by 40 µg/ml EGCg. Scalebar: 50 µm.

4.4. Nanoparticle clusters assembled from oppositely charged nanoparticles

Nanoparticles can be used as carrier systems for active substances. In this chapter, I take steps in this direction and I examine the aggregation behavior of oppositely charged gold nanoparticles by optical waveguide lightmode spectroscopy. The formed clusters might be employed to transport EGCg in the future. These results were published in the Langmuir journal with the title of "Label-Free in Situ Optical Monitoring of the Adsorption of Oppositely Charged Metal Nanoparticles" [113].

Alternating deposition of oppositely charged nanoparticles on OWLS chips

During the experiment, nanoparticle adsorption onto the bare waveguide surface was investigated. After the baseline was fixed with TMAOH, the NP solution was allowed to flow and was subsequently flushed with TMAOH. As expected, the negatively charged AuMUA particles did not adsorb at all on the negatively charged surface.
Afterward, I alternately deposited AuTMA and AuMUA on the bare waveguide surface, starting with the positively charged AuTMA nanoparticles. After the baseline was fixed with injected TMAOH (~20 min) {1}, AuTMA solution was injected for 20 min {2}, followed by flushing with TMAOH for 5 min {3}. Then the AuMUA solution was injected for 20 min {4} and was again flushed with TMAOH for 5 min {5}. The entire cycle was repeated four more times. Every deposition cycle clearly increased the deposited amount (see Fig.4.18).

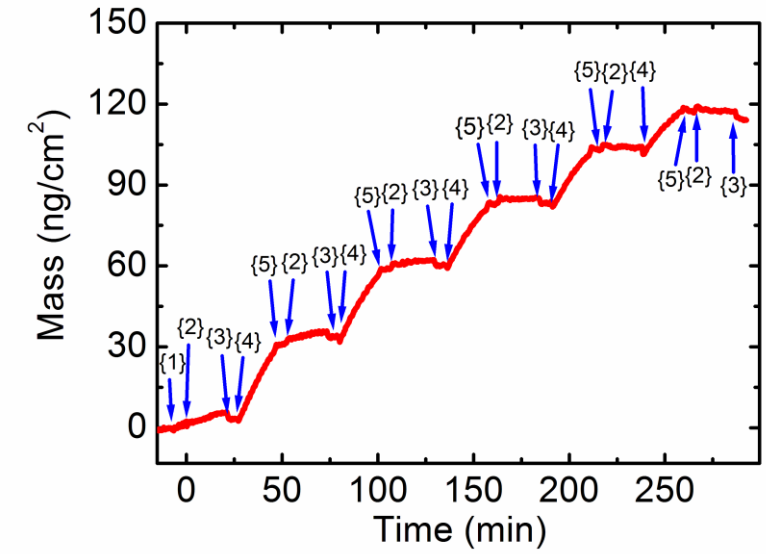

Fig.4.18 Surface adsorbed mass per unit area during the alternating deposition of the AuMUA and AuTMA particles. Baseline with injected TMAOH {1}, AuTMA solution {2}, flushing with TMAOH {3}, AuMUA solution {4}, flushing with TMAOH again {5} [113].

Deposition and characterization experiments were carried out at different dilutions. A serial dilution from stock solutions of AuMUA and AuTMA gold nanoparticles was performed, and a concentration of $\sim 10^{-6}$ mM for both AuMUA and AuTMA nanoparticles was found to be optimal for the deposition experiments. The refractive index of the solutions was measured on a table-top Rudolf Research J157 automatic refractometer. Atomic force microscopy was used to visualize nanoparticles adsorbed on the sensor's surface.

The concentration of the solutions was determined from the absorbance at 520 nm (Agilent 8453 spectrophotometer). Using the measured refractive indices and concentrations of the dilution series, I determined the refractive index increments of the solutions [100][140]. This information was necessary to estimate the mass of the adsorbed particles, which was determined according to de Feijter's formula (equation 3.3) [125].
The averaged refractive index increment of AuMUA and AuTMA was dn/dc = 0.3845 cm^3/g.

Cluster formation of gold nanoparticles

First of all, the most important thing was to determine the nanoparticle concentration where OWLS signal could be detected. If the solution has too high nanoparticle concentration (10^{-5} mM, and 10^{-4} mM order of magnitude), I did not get correct OWLS signals, so I coluld not measure the nanoparticles, since the high densitiy of gold nanoparticles damp the waveguided light and completely eliminate the waveguided mode of OWLS (see Fig. 4.19).

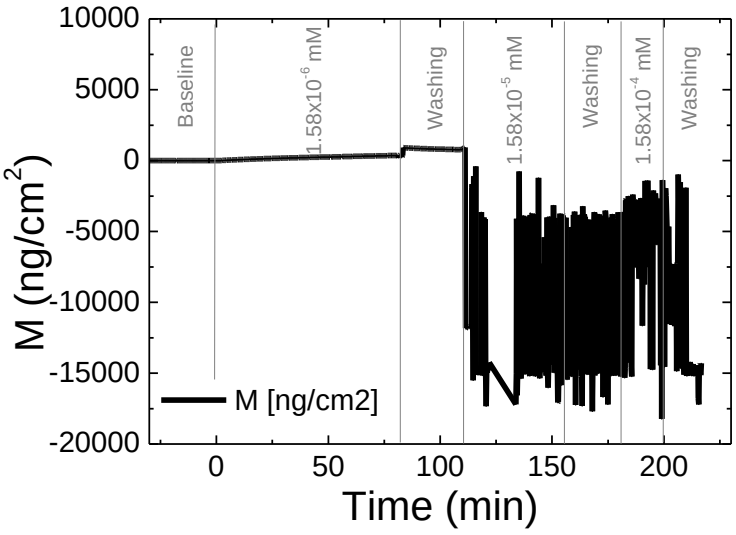

Fig.4.19 AuTMA positively charged gold nanoparticle solutions were injected onto the OWLS biosensor chip in three different concentrations ($1.58x10^{-6}$ mM, $1,58x10^{-5}$ mM, and $1.58x10^{-4}$ mM). Only the lowest, $1.58x10^{-6}$ mM concentration resulted in normal OWLS signal, so this concentration was used for further examinations.

This step was crucial in these experiments. The optimal nanoparticle concentration in the investigations was 1.58 $\times 10^{-6}$ mM in the case of AuTMA and 2.5×10^{-6} mM in the case of AuMUA.

After that, during the alternating deposition, at the beginning of each cycle, the positively charged AuTMAs were allowed to flow over the chip's negatively charged surface. Due to the electrostatic attractions, these nanoparticles deposited onto the substrate, as reflected in the recorded curve in Fig.4.18. After any weakly adsorbed positively charged particles were washed away, negatively charged AuMUAs were introduced to the chip. The already-deposited AuTMA particles facilitated the adsorption of these negatively charged particles. A repeated flush washed away any weakly adsorbed negatively charged particles. These consecutive cycles could be repeated several times, providing alternating deposition of oppositely charged nanoparticles. Interestingly, with increasing deposition cycles, the initial slope of AuMUA adsorption in Fig.4.20 decreases, as the surface is covered with more particles and the number of binding sites available to adsorb negatively charged particles decrease. This behavior contradicts the possible formation of distinct layers of nanoparticles deposited on each other (as in classical layer-by-layer deposition observed for the alternating deposition of oppositely charged polyelectrolytes).

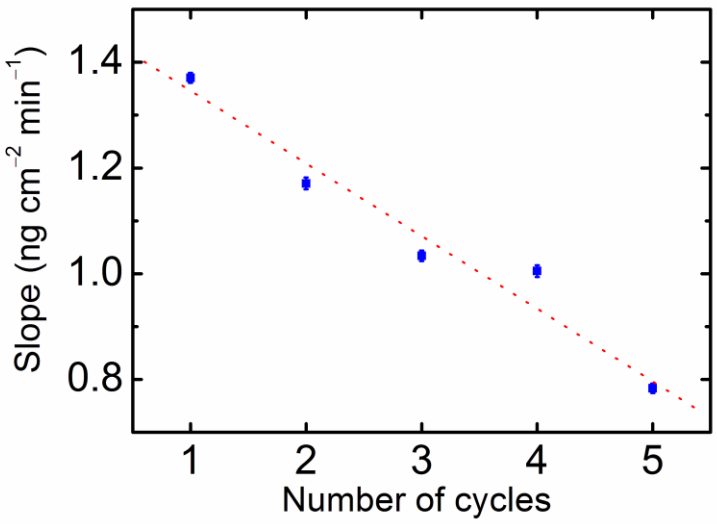

Fig.4.20 Dependence of the relative initial slopes (rate constant for adsorption) of the deposition kinetic curve for AuMUA in each cycle [113].

To investigate the morphology of the nanoparticle films, I examined the surface of the chip after the deposition by AFM microscopy. Fig.4.21 shows the AFM images of the waveguide sensor after the adsorption experiment. The incoupling grating lines and the nanoparticle clusters are clearly seen. These AFM studies revealed that the deposited nanoparticles form distinct patches/clusters rather than a continuous film. I got the cluster sizes and the number of each clusters from the analisys using Gwyddion software. The 5x5 μm image was analyzed for the

calculation. The nanoparticle size (diameter) is approx. 5 nm, the height is approx. 30 nm.The cluster numbers were added together (Fig. 4.22). The total cluster number is 582 on 5x5 μm (=25 μm^2). From this, the density of nanoparticle clusters is 23.3 clusters/μm^2 and the number of clusters decreases approximately exponentially with cluster size (see Fig.4.22). The largest nanoparticle clusters have an area of around 23500 nm^2, corresponding to a mean size of ~ 153 nm, whereas the smallest clusters have an area of around 2350 nm^2 with mean sizes of ~ 48 nm. The height of the clusters is ranging from 5-35 nm depending on the area of the clusters. The volume of the largest and smallest clusters can be easily calculated from the area and height data. Comparing these dimensions with the average diameter of one nanoparticle (~ 5 nm), and their average volume as well, one can conclude the largest clusters contain approximately 5-6000 nanoparticles and even the smallest clusters contain some hundreds of nanoparticles.

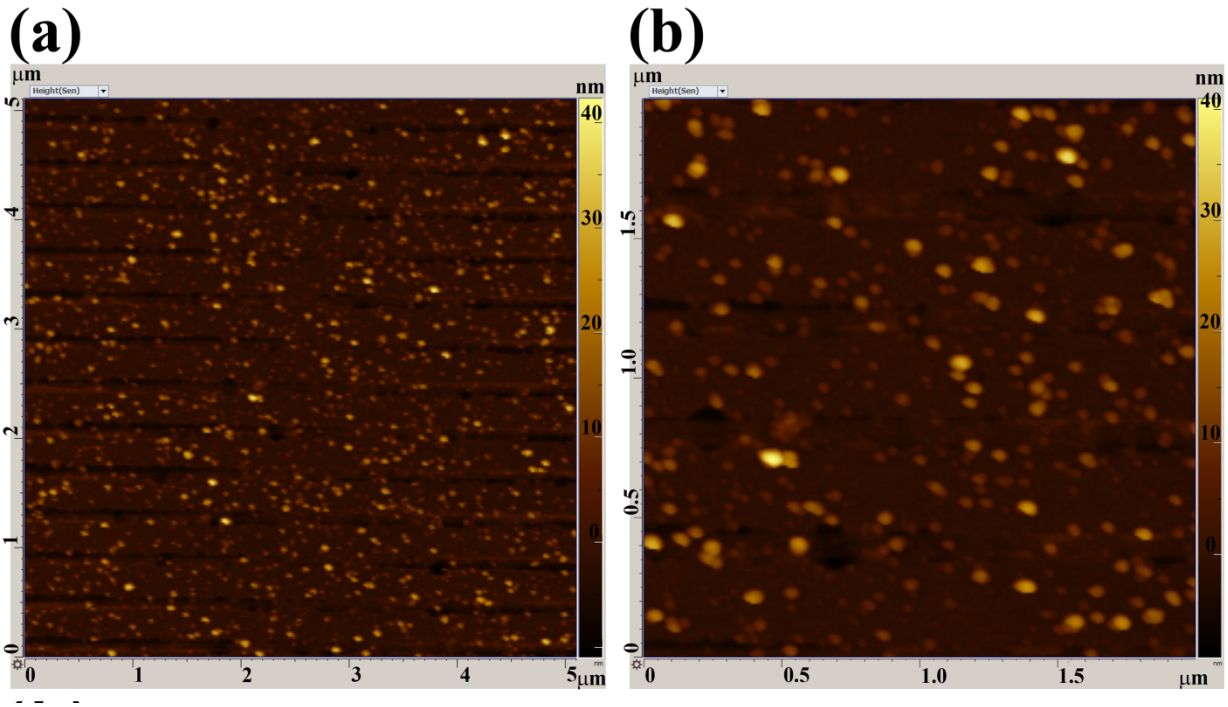

Fig.4.21 AFM image of the sensor surface after five deposition cycles of AuMUA and AuTMA particles. (a) 5μm×5μm imaged area. (b) A magnified 2μm×2μm area [113].

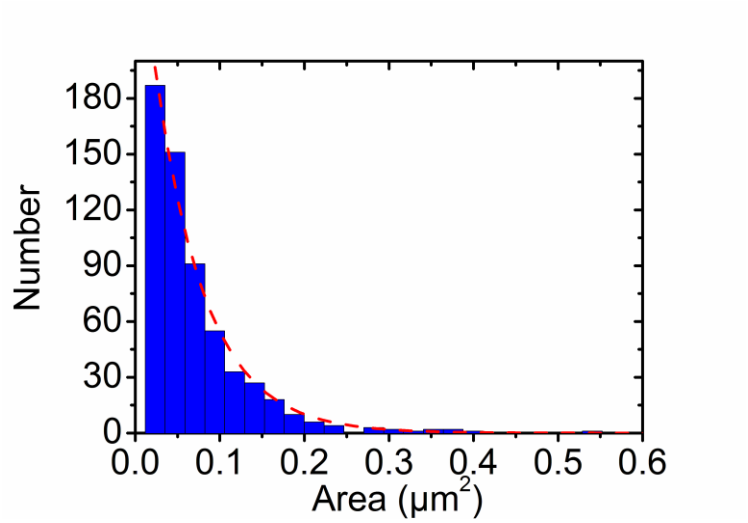

Fig.4.22 Number of the nanoparticle clusters versus their area obtained from AFM measurements (Fig. 4.21). The cluster size distribution follows an exponential function (red dashed curve) [113].

The radius of the employed AFM tip is less than 10 nm. The occurrent distortion due to the tip geometry was neglected; Gwyddion software has the possibility to use the tip parameters during the analysis, but the conclusions, fitting parameters and exponential curve did not change significantly. I excluded the possibility of a contious layer formation of nanoparticles during these measurements. My first experiments with higher nanoparticle concentrations suggested that a countinous gold nanolayer can completely eliminate the waveguide mode of OWLS. Furthermore, Dr. Jeremy Ramsden (Cranfield University, unpublished results) did similar OWLS experiments, and he also found that a 5 nm thick, continous metal nanolayer caused the same phenomenon. It should be mentioned as well that repulsion will be occur between nanoparticles with the same charging (positive or negative), thus, continous layer can not be formed on the OWLS chip surface. The negatively charged gold nanoparticles could not adsorb to the negative biosensor chip.

Based on the above considerations, the adsorption mechanism can be illustrated as in Fig.4.23.

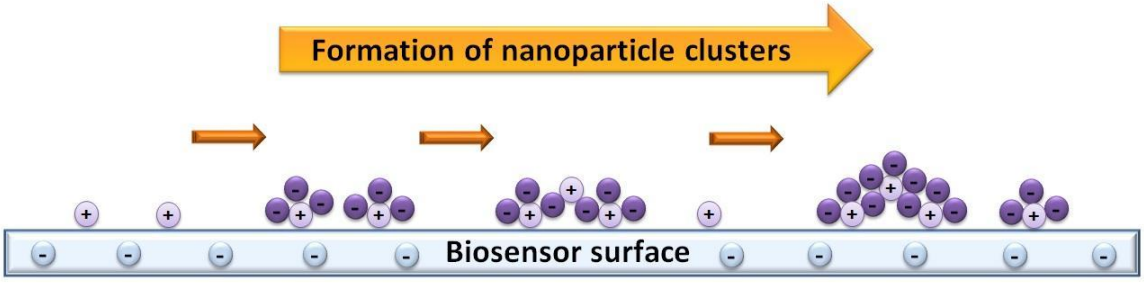

Fig.4.23 Illustration of nanoparticle cluster build up from oppositely charged particles [113].

The size distribution and the relative size could affect the film formation. Previous studies have shown in a liquid phase that if the size distributions of the oppositely charged nanoparticles fully overlap, the nanoparticles can self-assemble into stable nanocrystals [113]. However, if the average sizes of oppositely charged particles are different, this can provide formation of not well defined crystals. Changes in relative size can also affect the mechanism through the interplay between the electrostatic and vdW interactions, and this will be the topic of the further investigations [113]. For example these types of clusters can be a basis of theoretical calculations and models. In the future, nanoparticle clusters may be used for delivery of EGCg, and probably it can be created these types of clusters in solutions as well.

5. SUMMARY AND OUTLOOK

Though a lot of papers and experiments have been published on the biophysical effects of EGCg and green tea polyphenols, there are still remaining fields to study and factors to consider. For example, although most of published studies in cell culture systems used 10-100 μM (= 4.58-45.8 μg/ml) of EGCg, its level in blood after consuming the equivalent of 2-3 cups of green tea was 0.1-0.6 μM (= 0.0458-0.274 μg/ml) and for an equivalent of 7-9 cups was still lower than 1 μM (= 0.458 μg/ml) [5][1]. The concentrations of EGCg shown to have an effect (20-100 μM/ 9.16-45.8 μg/ml) in most previous studies are much higher than the concentrations observed in the plasma or tissues of animals or in human plasma (usually lower than 1 μM/ 0.458 μg/ml) after tea ingestion [5][1][11][12][36]. The rather poor bioavailability of tea catechins needs to be considered as well when we extrapolate results obtained *in vitro* to situations *in vivo* [5][1][9]. In the studies, in general there is no information about the EGCg solutions; they are freshly created, just before the measurement or they are stored. It is very important because of its instability and oxidation. The incubation time in cell media with cells also can be very significant factor for the same reason. Due to the complex conditions (for example the particle pressure in oxygen, the activity of antioxidant enzymes, stability of pH, etc.) found *in vivo* are difficult to replicate, the traditional culture condition can be inappropriate model for EGCg activity [17]. In the *in vitro* experiments with cell lines, there are often studies with only cancerous cells, without normal, healthy cell culture control. It would be useful, if one could compare the effects on both types of cells under the same experimental circumstances. EGCg has an influence on cell viability as well. The most used method for this effect is MTT assay (3-(4,5-Dimethylthiazol-2-yl)-2,5-diphenyltetrazolium bromide), however, both MTT and MTS (3-(4,5-dimethylthiazol-2-yl)-5-(3-carboxymethoxyphenyl)-2-(4-sulfophenyl)-2H-tetrazolium)-based assays provides an underestimation of the anti-proliferative effect of EGCg. This phenomenon is probably due to the increased activity of mitochondrial dehydrogenase in response to EGCg treatment, as well as the intrinsic potential of EGCg to reduce MTT and MTS and increase the formation of formazan [141]. Because of this, careful evaluation of the method is significant for *in vitro* assessment of cell viability and proliferation [141]. Until this time, a lot of papers and results have been published about the beneficial effects of EGCg [1].

I report on the successful application of the M4 Holomonitor to monitor cancer cell motility, migration, motility speed, and the spreading of preosteoblast cells on a nanostructured titanate coating [54]. The M4 Holomonitor, applied in the present study, has a small size, and it is making it feasible to be directly put into a humidified cell culture incubator. This technique is completely noninvasive and label-free, therefore, nothing disturbs the cells during their movements. A special mechanical stage was also developed in order to position the sample into that range of the optical arrangement where digital autofocusing works with high reproducibility and precision [54]. This new development significantly improved image quality. With the help of this novel development, I could perform two successful measurements demonstrating the capabilities of our

novel arrangement [54]. The Holomonitor was used to analyze the morphology and movements of living cells in a way that is automatic, cost efficient, and causes the cells no harm [54][142]. It is demonstrated that the movement of HeLa cells was temperately reduced after the addition of polyphenol EGCg [54]. This phenomenon could be monitored in a completely noninvasive and label-free manner. With this experiment, I proved that our recently developed sample stage is an excellent tool for observing cell dynamical changes and monitoring the effects of chemical substances on living cells. Measurements with a Holomonitor can be especially useful in combination with other novel label-free biosensing methods [91][54][143] to obtain a high content analysis of live cell morphology and behavior [54].

I proved that EGCg can bind to synthetic copolymer coatings by using OWLS. Then, for further examinations, Epic BT was used. The speciality of the study with EPIC BT is that the coating fabrication, its treating with EGCg, and the observation of cell adhesion were examined by the same biosensor in one procedure in triplicates and with different EGCg solutions, thus I got representative kinetic curves of the processes. To compare the methods, it should be mentioned that a lot of parallel measurements can be done by using Epic BT with 96 or 384 well plates, while only one measurement can be done by OWLS, without parallels. Thus, Epic BT also saves time; doing the same amount of experiments by OWLS would be taken for weeks or maybe months, conversely, this time is only few hours by Epic. I verified that EGCg binds irreversibly to PP and PP:PPR chains after the buffer wash as well, and multilayer formation of EGCg molecules on these coatings can also occur. Moreover, after this process, these bound EGCg molecules could inhibit the adhesion of HeLa cells onto this (PP:PPR) surface [129].

I proved that EGCg and its oxidized form, especially at higher concentrations can eliminate the cell repellent property of PP, and cell attractive property of PP:PPR. However, the exact background of the processes are hazy, thus further examinations need to be done to explain the received results. The effects of oxidized form of EGCg are neglected in the literature. I showed that oxidized EGCg solutions have greater impacts on coatings and cell adhesion [129].

The knowledge of this interaction can be more and more important in the future, because there are a lot of developments in therapeutics. Studying cell adhesion on different coatings and to examine active substances are very relevant topics. Our new examination method by Epic BT may open new application trends in the future.

I determined the EGCg concentration where the kinetic curves change. We can observe this phenomenon on the measurement curves, while at lower values than 20 μg/ml of EGCg I received spreading curves, and above this value, adsorption curves. I get this result by MTT cell viability assay as well.

I calculated that 27.3 ± 10 μg/ml is a transition concentration between the two types of kinetic curves by a simple equation. This value is the starting point of the increasing part of the fitted cytotoxicity curve. These convincing results show that the high-throughput Epic BT biosensor

can be applied in cytotoxicity assays, too. This may be an alternative way to carachterize cell viability in a label-free way [123].

I investigated alternating adsorption of oppositely charged gold nanoparticles (stabilized with self-assembled monolayers of positively charged TMA and negatively charged MUA) onto a negatively charged substrate. I used optical waveguide ligthmode spectroscopy (OWLS) to study the kinetic process of deposition of nanoparticles onto the substrate surface. This method provides a convenient means for such investigations owing to a label-free surface. Our results revealed that already adsorbed positively charged particles considerably increase the adsorption of negatively charged particles. Investigation of the morphology of the created surface by AFM revealed that deposited nanoparticles form clusters with various sizes and heights [113]. Kinetic information on cluster formation from nanoobjects can help to design and engineer nanostructured films and materials by self-assembly. Clusters are not just active substance transfering nanoparticles. They are bigger, but still small, and it is not a monocomponent system; thus more active substance can be transported, and there are more opportunities and potentials in carrier design as well. Clusters may be created by biocompatible materials in the future.
My results prove that label-free optical biosensors, so far explored to monitor proteins and living cells [100][143][113] could also be useful in investigating selfassembly processes in nanotechnology, especially when the kinetics of adsorption of nanoscopic components play a crucial role in the formation of nanostructured materials [113].

There are numerous studies in the literature about the antioxidant, antimicrobial, anticancer activity of EGCg, and about its biophysical and biological effects in general. These results are promising, but one should take into account the special properties of EGCg much more carefully during the evaluations. This specific active substance may still has surprises to store for scientists, and with or without further developments (for example with nanoparticles) some time or other could be the most applied natural compound against several illnesses, and it can became the most used chemical for being healthy for a long time.

6. THESIS HIGHLIGHTS

1. I demonstarted for the first time that the novel, miniaturized, quantitative phasecontrast microscope, the Holomonitor M4, is capable of investigating the movement of the epigallocatechin-gallate (EGCg) green tea polyphenol treated cells.

1.a. I applied a new setting with a unique sampe stage to investigate HeLa cervical cancer cells in humified incubator. I employed the Holomonitor M4 with the sample stage fot the first time to examine the effects of EGCg on single cell movements.

1.b. I proved that 500 μg/ml EGCg solution inhibits the movement of HeLa cervical cancer cells. It induced 35% reduction inmotility speed, and 25% reduction in motility, and the migrative behavior almost disappeared due to the EGCg treatment.

2. I revealed that EGCg binds irreversibly to two synthetic copolymer coatings, the poly(L-lysine)-*graft*-poly(ethylene glycol) (PLL-*g*-PEG) anti-adhesive, and its mixed solution with RGD functionalized counterpart, PLL-*g*-PEG/PEG-GGGGYGRGDSP (PLL-*g*-PEG-RGD) in 1:1 ratio, which has cell attractive properties. Furthermore, I investigated by using OWLS (Optical Waveguide Lightmode Spetroscopy) and Epic BT, that EGCg and oxidized EGCg form multilayers with the polymer coatings and the EGCg treatement affects the cellular adhesion properties of the polymer films in a concentration dependent manner.

2.a. I applied the Epic BT biosensor for the first time in measurements, where the effect of EGCg on coatings, and the cellular adhesion on these treated coatings were both investigated in the same process. In my experiments I online monitored the coating formation, the interaction of EGCg with the coatings and subsequent adhesion of HeLa cells on these layers, measured by Epic BT all along. Due to the high-throughput property of this appliance I could examine a lot of concentrations and parallels at the same condition of the cells.

2.b. I proved for the first time by employing label-free optical biosensors, that the oxidized form (brown liquid, where EGCg is in dimerized or in polymerized form) of EGCg has a 1.8 times larger inhibitory impact on HeLa cell adhesion in solution, and three times more binds to the copolymer coatings from the oxidized form compared to the EGCg molecules adsorbing from the freshly created EGCg solution. It has been mentioned for the first time that the freshness of the created EGGg solutions is highly important during the experiments and it can strongly affect the results.

2c. In the case of 500 μg/ml EGCg solution, approximately 5 layers, while in the case of oxidized EGCg solution at the same concentration, approximately 10 layers can be formed with both types of coatings.

2.d. I showed, that the adhesive properties of the PLL-*g*-PEG and PLL-*g*-PEG:PLL-*g*-PEG-RGD coatings change due to the EGCg binding; the cells can not adhere to these surfaces. Thus, the EGCg inhibits HeLa cell adhesion to the PLL-*g*-PEG:PLL-*g*-PEG-RGD coating, however, it has got some cell attractive properties (the inhibition depends on the concentration of EGCg). At the same time, EGCg destroys the cell repellent properties of the PLL-*g*-PEG.

3. I verified with MTT assay, that the cell viability of HeLa cells starts to decrease at around 20 μg/ml EGCg concentration. I recorded cell adhesion kinetic curves by using Epic BT, and I got the same results. At lower values than 20 μg/ml of EGCg, I received spreading curves (active, living process), and above this value, adsorption curves (dead process). I calculated that 27.3 ± 10 μg/ml is a transition concentration between the two types of kinetic curves by developing a simple equation. According to these results, the mentioned method is capable of carachterizing cell viability in an alternative, completely label-free way.

4. I proved by OWLS (Optical Waveguide Lightmode Spectroscopy) and AFM (Atomic Force Microscopy) that the positively charged N,N,N-trimethyl(11-mercaptoundecyl)ammonium chloride (AuTMA) and the negatively charged mercaptoundecanoic acid (AuMUA) gold nanoparticles create clusters with each other on the OWLS chip surfaces during alternating deposition by self-assembly. I determined the concentration which is optimal for the OWLS measurements (AuTMA: 1.58×10^{-6} mM and AuMUA: (2.5×10^{-6} mM).

4.a. I revealed that already adsorbed positively charged particles considerably increase the adsorption of negatively charged particles.

4.b. Investigation of the morphology of the created surface using AFM revealed that the deposited nanoparticles form clusters with various sizes and heights, and not homogeneous layers. These types of clusters can be a basis of further theoretical calculations and models. In the future, these types of clusters may be created in solutions, too, and may be applied in nanomedicine loaded by EGCg as well.

TÉZISPONTOK

1. Bebizonyítottam, hogy a Holomonitor M4 új, miniatürizált, kvantitatív digitális holografikus mikroszkóp kiválóan alkalmazható a zöld tea polifenol epigallokatekin-galláttal (EGCg) kezelt sejtek vizsgálatára.

1.a. A HeLa méhnyakrák sejtek inkubátorban történő vizsgálatához egy új mérési elrendezést alkalmaztam egyedi mintatartó állvánnyal. A Holomonitor M4 berendezést a mintatartó állvánnyal én alkalmaztam elsőként az EGCg sejtmozgásra gyakorolt hatásának kimutatására.

1.b. Holomonitor M4 berendezés segítségével bebizonyítottam, hogy az EGCg 500 µg/ml-es oldata gátolja a HeLa méhnyakrák sejtek mozgását. A sejtek motilitási sebessége 35%-kal, a motilitása 25%-kal csökkent, illetve migrációs hajlandóság csaknem eltűnik a kezelést követően.

2. Feltártam, hogy az EGCg irreverzibilisen kötődik két szintetikus kopolimerhez, az anti-adhezív PLL-g-PEG-hez (poli-L-lizin-*g*-polietilénglikol) és az RGD motívummal ellátott módosulatával, a PLL-*g*-PEG-RGD-vel (PLL-*g*-PEG/PEG-GGGGYGRGDSP) 1:1-ben vegyített, sejtadhéziót elősegítő bevonathoz (PLL-*g*-PEG:PLL-*g*-PEG-RGD). Továbbá az OWLS és Epic BT műszerek segítségével kimutattam, hogy az EGCg, és oxidált formája multiréteget alakít ki ezen polimerekkel, és a kezelt bevonatok befolyásolják a sejtadhéziót.

2.a. Először alkalmaztam az Epic BT RWG bioszenzort olyan méréseknél, ahol az EGCg hatását a bevonatokra, és e kezelt rétegre történő sejtadhéziót is ugyanazon, egymást követő folyamat során vizsgáltam. Kísérleteim során online követtem a bevonat képződést, EGCg interakcióját a bevonattal, és a kezelt felületre történő sejtadhéziót, mindvégig Epic BT műszerrel. A készülék nagy áteresztőképességének köszönhetően többféle EGCg koncentrációt tudtam vizsgálni párhuzamos mérésekkel, a sejtek ugyanazon állapotában.

2.b. Először bizonyítottam be jelölésmentes bioszenzorok alkalmazásával, hogy az EGCg oxidált formája (barna folyadék, ahol az EGCg dimerizálódott vagy polimerizálódott) 1,8-szor erőteljesebb gátló hatást fejt ki a Hela sejtek adhéziójára és háromszor nagyobb mennyiségben kötődik a bevonatokra, mint az EGCg molekulák a frissen készített EGCg oldatból. Először került említésre, hogy az elkészített EGCg oldat frissesége kritikus tényező a mérések és azok eredményei szempontjából.

2c. Kimutattam, hogy 500 µg/ml EGCg oldat esetén körülbelül 5, míg ugyanilyen koncentrációjú oxidált EGCg oldat megközelítőleg 10 réteget tud képezni mind a két típusú bevonat esetében.

2.d. Megmutattam, hogy a PLL-*g*-PEG és PLL-*g*-PEG:PLL-*g*-PEG-RGD bevonatok tulajdonságai megváltoznak az EGCg bekötődése következtében, az alkalmazott koncentrációktól függően; a sejtek nem tudnak hozzákötődni ezekhez a kezelt felületekhez. Így tehát, annak ellenére, hogy a PLL-*g*-PEG:PLL-*g*-PEG-RGD réteg sejteket vonzó tulajdonságokkal rendelkezik, az EGCg a koncentráció függvényében meggátolja a HeLa sejtek adhézióját. Ugyanakkor az EGCg tönkreteszi a PLL-*g*-PEG sejteket taszító tulajdonságát is.

3. MTT teszttel igazoltam, hogy a HeLa sejtek életképessége 20 μg/ml EGCg jelenlétében kezd el csökkenni. Epic BT segítségével kinetikai görbéket rögzítettem, és hasonló eredményeket kaptam. 20 μg/ml EGCg koncentráció alatt szigmoid jellegű kiterülési görbéket kaptam (aktív, élő folyamat jele), míg ezen érték felett adszorpciós jellegű görbéket (halott, élettelen folyamat jele). Egy egyszerű képlet segítségével kiszámoltam, hogy az átmenti koncentráció a két fajta kinetikai görbe között 27,3 ± 10 μg/ml. Eredményeim alapján az általam kidolgozott módszer alkalmasnak tűnik egy alternatív életképesség-vizsgálatként történő széleskörű felhasználásra, amely kiiktatja a potenciálisan zavaró jelölők alkalmazását.

4. Bebizonyítottam OWLS-sel (Optical Waveguide Lightmode Spectroscopy) és AFM-mel (Atomic Force Microscopy), hogy a pozitív töltésű N,N,N-trimetil(11-merkaptoundecil)ammónium-klorid (AuTMA) és a negatív töltésű merkaptoundekánsav (AuMUA) arany nanorészecskék klasztereket formálnak egymással és önszerveződnek az OWLS chipen a váltakozó depozíciós eljárás (alternating deposition) során. Meghatároztam az OWLS méréseknél alkalmazható optimális nanorészecske koncentrációt (AuTMA: 1.58×10^{-6} mM és AuMUA: 2.5×10^{-6} mM).

4.a. Feltártam, hogy a már adszorbeálódott pozitív töltésű részecskék jelentősen elősegítik a negatív töltésű részecskék adszorpcióját.

4.b. Az AFM-mel történt morfológiai vizsgálatok alapján elmondható, hogy a nanorészecskék nem homogén rétegeket, hanem klasztereket képeznek az alkalmazott felületen, és ezek a képződmények különböző méretűek és magasságúak. Ezek az új típusú klaszterek a későbbiekben alapjául szolgálhatnak elméleti számításoknak és modelleknek. A jövőben lehetségessé válhat ilyen jellegű klaszterek kialakítása folyadékokban is, illetve EGCg-vel feltöltve a nanogyógyászatban történő felhasználásuk is ígéretes lehet.

7. ACKNOWLEDGEMENTS

First and foremost I thank my supervisor, Dr. Róbert Horváth. It has been an honor to be his student and to be the part of the Nanobiosensorics Lendület research team. I am very thankful for his support, patience, advices, benign attitude and for giving me freedom in my work.

I am also grateful to all of my colleges in the laboratory for the good, happy company and mood.

Special thanks to Dr. Dániel Patkó and Norbert Orgován for their cheerful help and teaching. I am also thankful to Dr. Sándor Kurunczi for his advices in occurrent chemical problems.

I appreciate the work of Dr. Inna Székács. She helped us a lot in our experiments (for example cell breeding). Her job is essential in our laboratory.

I would like to thank the other PhD students in our group their help and company: Rita Ungai-Salánki, Enikő Farkas, Boglárka Kovács, Judit Nádor and András Saftics.

I am grateful that I had been the consultant of two very clever, hard-working, diligent BSc students; Ágnes Dobos and Enikő Forgács during my PhD student period.

I thank Béla Plósz for creating the sample stage.

I would like to thank all of my co-authors, Dr. István Lagzi, Dr. Bartlomiej Kowalczyk, Dr. Zoltán Rácz, Dr. Bartosz A. Grzybowski, Dr. Eleni Makarona, Dr. Christos Tsamis, Krisztina Juhász, László Kőrösi, for their work and co-operation in my published articles as first author. Special thanks to Szilvia Bősze, her advices and work were essential in my publications. I would like to thank the co-operation of Dr. István Kurucz as well.

I am also grateful to Prof. Dr. István Bársony (director of MFA), Prof. Dr. Ferenc Vonderviszt (head of Doctoral School of Molecular- and Nanotechnologies), Zita Vereskuti (ex coordinator of administration of the doctoral school), Dr. Hajnalka Jankovich (present coordinator of administration of the doctoral school) for their support and for providing the necessary background to my research and PhD studies. This work was supported by the Lendület project.

Last but not least, I would like to thank my family for all their love and support. I am very grateful to my parents who helped me become the person I am today. I am especially thankful to my boyfriend for his love and support, he understood and helped me, and gave me strength in the hard and less hard times. And finally, I am thankful to my friends as well for their support.

8. LIST OF PUBLICATIONS

8.1. Papers used to compose the thesis highlights

{T0-Introduction chapter} Beatrix Peter, Szilvia Bosze, Robert Horvath: Biophysical characteristics of proteins and living cells exposed to the green tea polyphenol epigallocatecin-3-gallate (EGCg): Review of recent advances from molecular mechanisms to nanomedicine and clinical trials. *Europan Biophysics Journal, DOI: 10.1007/s00249-016-1141-2* (2016) [1]

{T1} Beatrix Peter, Judit Nador, Krisztina Juhasz, Agnes Dobos, Laszlo Körösi, Inna Székács, Daniel Patko, and Robert Horvath: Incubator proof miniaturized Holomonitor to in situ monitor cancer cells exposed to green tea polyphenol and preosteoblast cells adhering on nanostructured titanate surfaces: validity of the measured parameters and their corrections. *Journal of Biomedical Optics 20(6), 067002* (2015) [54]

{T2} Beatrix Peter, Eniko Farkas, Eniko Forgacs, Andras Saftics, Sandor Kurunczi, Inna Szekacs, Szilvia Bosze and Robert Horvath: Label-free optical biosensor to real-time study multicomponent model system of cell-surface interactions: polymer coatings exposed to EGCg and their interactions with living cells.Under submission. [129]

{T3} Beatrix Peter, Rita Salanki, Inna Szekacs, Szilvia Bősze and Robert Horvath: Label-free cytotoxicity assay using the kinetic cell spreading data. Under preparation. [123]

{T4} Beatrix Peter, Sandor Kurunczi, Daniel Patko, Istvan Lagzi, Bartlomiej Kowalczyk, Zoltán Rácz, Bartosz A. Grzybowski, and Robert Horvath: Label-Free in Situ Optical Monitoring of the Adsorption of Oppositely Charged Metal Nanoparticles. *Langmuir 30, 13478−13482* (2014) [113]

8.2. Other papers

1. Norbert Orgovan, Beatrix Peter, Szilvia Bősze, Jeremy J Ramsden, Bálint Szabó, Robert Horvath: Dependence of cancer cell adhesion kinetics on integrin ligand surface density measured by a high-throughput label-free resonant waveguide grating biosensor. *Scientific Reports 4: 4034. 8 p.* (2014)

2. Salanki R, Hos C, Orgovan N, Peter B, Sandor N, Bajtay Z, Erdei A, Horvath R, Szabo B: Single Cell Adhesion Assay Using Computer Controlled Micropipette. *Plos One* 9:(10) *p. e111450. 12 p.* (2014)

3. Salánki R, Gerecsei T, Orgovan N, Sándor N, Péter B, Bajtay Z, Erdei A, Horvath R, Szabó B. Automated single cell sorting and deposition in submicroliter drops. *Applied Physics Letters 105:(8) Paper 083703.* (2014)

4. Norbert Orgovan, Beatrix Peter, Szilvia Bősze, Jeremy J. Ramsden, Bálint Szabó, and Robert Horvath: Label-free profiling of cell adhesion: determination of the dissociation constant for native cell membrane adhesion receptor - ligand interaction (23rd chapter). Methods in Pharmacology and Toxicology: Label-free Biosensor Methods in Drug Discovery, Springer, USA. (2015)

5. Eleni Makarona, Beatrix Peter, Inna Szekacs, Christos Tsamis and Robert Horvath: ZnO Nanostructure Templates as a Cost-Efficient Mass-Producible Route for the Development of Cellular Networks. *Materials 9 (256)* (2016)

6. Istvan Kurucz, Beatrix Peter, Aurel Prosz, Inna Szekacs, Anna Erdei, Robert Horvath: Label-free optical biosensor for on-line monitoring the integrated response of human B cells upon the engagement of stimulatory and inhibitory immune receptors. Under submission.

8.3. Participation in conferences

Poster presentations

1. R. Salánki , N. Orgován, B. Péter, N. Sándor, R. Horváth, B. Szabó: Automated single cell sorting and deposition. Single Cell Analysis Europe, Barcelona, Spain. 5-6th March 2013

2. Péter Beatrix, Patkó Dániel, Kőrösi László, Kovács Tamás és Horváth Róbert: Vírusok és baktériumok vizsgálata jelölésmentes optikai bioszenzorral. A Magyar Biofizikai Társaság XXIV. Kongresszusa, Veszprém, Hungary. 27-30th August 2013

3. Nádor Judit, Patkó Dániel, Orgován Norbert, Péter Beatrix, Kőrösi László, Fried Miklós, Petrik Péter, Horváth Róbert: Titanát-nanocsövekből készített nanostruktúrált bioszenzor bevonatok előllítása, karakterizálása és alkalmazása. A Magyar Biofizikai Társaság XXIV. Kongresszusa, Veszprém, Hungary. 27-30th August 2013

4. Salánki Rita, Orgován Norbert, Péter Beatrix, Sándor Noémi, Bajtay Zsuzsa, Erdei Anna, R. Horváth, B. Szabó: Élő emlős sejtek automatikus detektálása és válogatása mikroszkópon. A Magyar Biofizikai Társaság XXIV. Kongresszusa, Veszprém, Hungary. 27-30th August 2013

5. Patkó Dániel, Kovács Boglárka, Péter Beatrix, Kaspar Cottier, Vonderviszt Ferenc, Kőrösi László, Kovács Tamás, és Horváth Róbert: Nagy érzékenységű optikai szenzor biológiai részecskék jelölésmentes vizsgálatára. A Magyar Biofizikai Társaság XXIV. Kongresszusa, Veszprém, Hungary. 27-30th August 2013

6. Rita Salánki, Norbert Orgován, Beatrix Péter, Noémi Sándor, Zsuzsa Bajtay , Anna Erdei, Róbert Horváth , Bálint Szabó: Automated single cell sorting and deposition of live mammalian cells on microscope. Single Cell Genomics, Rehovot, Izrael. 1-3rd October 2013

7. N. Orgovan, R. Salánki, N. Sándor, Zs. Bajtay, A.Erdei, B. Peter, Sz. Bősze, J.J. Ramsden, B. Szabó, R. Horvath: Label-free optical monitoring of the adhesion and spreading of human primary immune cells and human tumor cells. XII EUROPT(R)ODE, XII Conference on Optical Chemical Sensors & Biosensors, Athens, Greece. 13-16th April 2014

8. A. Kritharidou, B. Peter, T. Kyrasta, R. Horvath, C. Tsamis, Z. Georgoussi, and E. Makarona: Cost-efficient Templatesof ZnO-based Nanostructures for Cellular Networks. Micro and Nano Engineering 2014, Lausanne, Switzerland. 22-26th September 2014

9. B. Peter, I. Szekacs, R. Ungai-Salánki, N. Orgovan, S. Bosze, R. Horvath: Label-free invesztigationsof the effect of green tea polyphenolson the dynamics of living cells. 4th International Conference on Bio-Sensing Technology, Lisbon, Portugal. 10-13th May 2015

10. Péter Beatrix, Székács Inna, Ungai-Salánki Rita, Orgován Norbert, Bősze Szilvia, Horváth Róbert: Zöld tea polifenolok élő sejtek adhéziós dinamikájára gyakorolt hatásának jelölésmentes vizsgálata. *45.* Membrán-Transzport Konferencia, Sümeg, Hungary. 19-22nd May 2015

11. Péter Beatrix, Székács Inna, Ungai-Salánki Rita, Orgován Norbert, Bősze Szilvia, Horváth Róbert: EGCG élő sejtek adhéziós dinamikájára és mozgására gyakorolt hatásának vizsgálata jelölésmentes technikákkal. A Magyar Biofizikai Társaság XXV. Kongresszusa, Budapest, Hungary. 25-28th August 2015

12. Istvan Kurucz, Beatrix Peter, Anna Erdei, Robert Horvath: A novel, label-free technique to monitor the integrated cellular response of immunocompetent cells. 4th European Congress of Immunology (ECI 2015), Vienna, Austria. 6-9th September 2015

Oral presentations

1. Salánki Rita, Orgován Norbert, Péter Beatrix, Sándor Noémi, Bajtay Zsuzsa, Erdei Anna, Róbert Horváth, Bálint Szabó: Számítógépes látással detektált egyedi sejtek válogatása. A Magyar Biofizikai Társaság XXIV. Kongresszusa, Veszprém, Hungary. 27-30th August 2013

2. Horváth Róbert, Farkas Enikő, Kovács Boglárka, Péter Beatrix, Patkó Dániel, Orgován Norbert, Vonderviszt Ferenc: Nagy érzékenységű optikaiszenzorok nanostruktúrált bevonatok és élő sejtek tanulmányozására. A Magyar Biofizikai Társaság XXIV. Kongresszusa, Veszprém, Hungary. 27-30th August 2013

3. Orgován Norbert, Salánki Rita, Péter Beatrix, Sándor Noémi, Bajtay Zsuzsa, Erdei Anna, Bálint Szabó és Horváth Róbert: Vérből izolált humán monociták adhéziójának vizsgálata OWLS-sel. A Magyar Biofizikai Társaság XXIV. Kongresszusa, Veszprém, Hungary. 27-30th August 2013

4. Beatrix Peter, Sandor Kurunczi, Daniel Patko, Istvan Lagzi, Bartlomiej Kowalczyk, Bartosz A. Grzybowski and Robert Horvath: Label-free in-situ optical monitoring of the adsorption of gold nanoparticles. Japanese-Hungarian Conference on Applied Mathematics and Nonlinear Dynamics, Budapest, Hungary. 12th December 2013

5. Rita Salánki, Tamás Gerecsei, Norbert Orgovan, Noémi Sándor, Beatrix Péter, Zsuzsa Bajtay, Anna Erdei, Bálint Szabó, Robert Horvath: Automated single cell sorting and deposition in submicroliter drops. Single Cell Genomics, Stockholm, Sweden. 9-11th September 2014

6. Péter Beatrix: Ellentétes töltésű arany nanorészecskék adszorpciójának vizsgálata OWLS-sel. MTA Természettudományi Kutatóközpont Doktori Konferencia, Budapest, Hungary. 10-12th December 2014

9. REFERENCES

1. Peter, B.; Bosze, S.; Horvath, R. Biophysical characteristics of living cells exposed to the green tea polyphenol epigallocatecin-3-gallate (EGCg): Review of recent advances from molecular mechanisms to clinical trials. *Eur. Biophys. J.* **2016**, DOI 10.1007/s00249-016-1141-2 (and the references therein)

2. Dufresne, C. J.; Farnworth, E. R. A review of latest research findings on the health promotion properties of tea. *J. Nutr. Biochem.* **2001**, *12*, 404–421. (and the references therein)

3. Singh, B. N.; Shankar, S.; Srivastava, R. K. Green tea catechin, epigallocatechin-3-gallate (EGCG): Mechanisms, perspectives and clinical applications. *Biochem. Pharmacol.* **2011**, *82*, 1807–1821. (and the references therein)

4. Mukhtar, H.; Ahmad, N. Tea polyphenols: Prevention of cancer and optimizing health. *Am. J. Clin. Nutr.* **2000**, *71*, 1698–1702. (and the references therein)

5. Tachibana, H. Green tea polyphenol sensing. *Proc. Japan Acad. Ser. B* **2011**, *87*, 66–80. (and the references therein)

6. Suzuki, Y.; Isemura, M. Binding interaction between (-)-epigallocatechin gallate causes impaired spreading of cancer cells on fibrinogen. *Biomed. Res.* **2013**, *34*, 301–8. (and the references therein)

7. Mereles, D.; Hunstein, W. Epigallocatechin-3-gallate (EGCG) for clinical trials: More Pitfalls than Promises? *Int. J. Mol. Sci.* **2011**, *12*, 5592–5603. (and the references therein)

8. Yang, C. S.; Wang, X.; Lu, G.; Picinich, S. C. Cancer prevention by tea: animal studies, molecular mechanisms and human relevance. *Nat. Rev. Cancer* **2009**, *9*, 429–39. (and the references therein)

9. Vaidyanathan, J. B.; Walle, T. Cellular uptake and efflux of the tea flavonoid (-)epicatechin-3-gallate in the human intestinal cell line Caco-2. *J. Pharmacol. Exp. Ther.* **2003**, *307*, 745–752. (and the references therein)

10. Yang, C.S.; Chen, L.;Lee, M.J.; Balentine, D.; Kuo, M.C.; Shantz, S.P. Blood and urine levels of tea catechinsafter ingestion of different amounts of green tea by human volunteers. *Cancer Epidemiol. Biomark.* **1998**, 7 351-354

11. Hong, J.; Lu, H.; Meng, X.; Colon, H.-H.; Ryu, J.; Hara, Y.; Yang, C. S. Stability, Cellular Uptake, Biotransformation, and Efflux of Tea Polyphenol (-)-Epigallocatechin-3-Gallate in HT-29 Human Colon Adenocarcinoma Cells Stability, Cellular Uptake, Biotransformation, and Efflux of Tea Polyphenol. *Cancer Res.* **2002**, *62*, 7241–7246. (and the references therein)

12. Kim, H. S.; Quon, M. J.; Kim, J. a. New insights into the mechanisms of polyphenols beyond antioxidant properties; lessons from the green tea polyphenol, epigallocatechin 3-gallate. *Redox Biol.* **2014**, *2*, 187–195. (and the references therein)

13. Ahmad, N.; Gupta, S.; Mukhtar, H. Green tea polyphenol epigallocatechin-3-gallate differentially modulates nuclear factor kappaB in cancer cells versus normal cells. *Arch. Biochem. Biophys.* **2000**, *376*, 338–346. (and the references therein)

14. Hirun, S.; Roach, P. D. A study of stability of (-)-Epigallocatechin gallate (EGCG) from green tea in a frozen product. *Int. Food Res. J.* **2011**, *18*, 1261–1264.

15. Mizooku, Y.; Yoshikawa, M.; Tsuneyoshi, T.; Arakawa, R. Analysis of oxidized epigallocatechin gallate by liquid chromatography/ mass spectrometry. *Rapid Commun. Mass Spectrom.* **2003**, *17*, 1915–1918.

16. Zhou, Q.; Chiang, H.; Portocarrero, C.; Zhu, Y.; Hill, S.; Heppert, K.; Jayaratna, H.; Davies, M.; Janle, E.; Kissinger, P. Investigating the Stability of EGCg in Aqueous Media. *Current Separations* **2003**, *3*, 83–86.

17. Song, S.; Huang, Y.-W.; Tian, Y.; Wang, X.-J.; Sheng, J. Mechanism of action of (–)-epigallocatechin-3-gallate: auto-oxidation-dependent activation of extracellular signal-regulated kinase 1/2 in Jurkat cells. *Chin. J. Nat. Med.* **2014**, *12*, 654–662.

18. Fujimura, Y.; Umeda, D.; Yano, S.; Maeda-Yamamoto, M.; Yamada, K.; Tachibana, H. The 67 kDa laminin receptor as a primary determinant of anti-allergic effects of O-methylated EGCG. *Biochem. Biophys. Res. Commun.* **2007**, *364*, 79–85.

19. Hou, Z.; Sang, S.; You, H.; Lee, M. J.; Hong, J.; Chin, K. V.; Yang, C. S. Mechanism of action of (-)-epigallocatechin-3-gallate: Auto-oxidation- dependent inactivation of epidermal growth factor receptor and direct effects on growth inhibition in human esophageal cancer KYSE 150 cells. *Cancer Res.* **2005**, *65*, 8049–8056. (and the references therein)

20. Ishii, T.; Ichikawa, T.; Minoda, K.; Kusaka, K.; Ito, S.; Suzuki, Y.; Akagawa, M.; Mochizuki, K.; Goda, T.; Nakayama, T. Human serum albumin as an antioxidant in the oxidation of (-)-epigallocatechin gallate: participation of reversible covalent binding for interaction and stabilization. *Biosci. Biotechnol. Biochem.* **2011**, *75*, 100–106.

21. Davies, H. S.; Pudney, P. D. a.; Georgiades, P.; Waigh, T. a.; Hodson, N. W.; Ridley, C. E.; Blanch, E. W.; Thornton, D. J. Reorganisation of the Salivary Mucin Network by Dietary Components: Insights from Green Tea Polyphenols. *PLoS One* **2014**, *9*, e108372. (and the references therein)

22. Georgiades, P.; Pudney, P. D. a.; Rogers, S.; Thornton, D. J.; Waigh, T. a. Tea Derived Galloylated Polyphenols Cross-Link Purified Gastrointestinal Mucins. *PLoS One* **2014**, *9*, e105302.

23. Mccoll, J.; Horvath, R.; Yakubov, G. E; Ramsden, J. J. The adsorption of EGCG – mucin complexes on biomimetic surfaces. **2016**, 1–18. To appear.

24. Zhao, Y.; Chen, L.; Yakubov, G.; Aminiafshar, T.; Han, L. Experimental and Theoretical Studies on the Binding of Epigallocatechin Gallate to Puri fi ed Porcine Gastric Mucin. *J. Phys. Chem. B* **2012**, *116*, 13010−13016.

25. Horvath, R.; McColl, J.; Yakubov, G. E.; Ramsden, J. J. Structural hysteresis and hierarchy in

adsorbed glycoproteins. *J. Chem. Phys.* **2008**, *129*, 1–5.

26. Sazuka, M.; Itoi, T.; Suzuki, Y.; Odani, S.; Koide, T.; Isemura, M. Evidence for the interaction between (-)-Epigallocatechin Gallate and Human Plasma Proteins Fibronectin, Fibrinogen, and Histadine-rish Glycoprotein. *Biosci. Biotechnol. Biochem.* **1996**, *60*, 1317 – 1319.

27. Zhao, Y.; Chen, L.; Han, L.; Marzinek, J.K.; Mantalaris, A.; Pistikopoulos, E.N.; Lian, G.; Bond, P.J.; Noro, M.G. Molecular and Thermodynamic Basis for EGCG-Keratin Interaction-Part II: Experimental Investigation . *AIChE J.* **2013**, *59*, 4824–4827.

28. Hudson, S. a.; Ecroyd, H.; Dehle, F. C.; Musgrave, I. F.; Carver, J. a. (-)-Epigallocatechin-3-Gallate (EGCG) Maintains κ-Casein in Its Pre-Fibrillar State without Redirecting Its Aggregation Pathway. *J. Mol. Biol.* **2009**, *392*, 689–700.

29. Mandel, S. a.; Amit, T.; Weinreb, O.; Reznichenko, L.; Youdim, M. B. H. Simultaneous manipulation of multiple brain targets by green tea catechins: A potential neuroprotective strategy for Alzheimer and Parkinson diseases. *CNS Neurosci. Ther.* **2008**, *14*, 352–365.

30. Nelson, J.; McFerran, N. V; Pivato, G.; Chambers, E.; Doherty, C.; Steele, D.; Timson, D. J. The 67 kDa laminin receptor: structure, function and role in disease. *Biosci. Rep.* **2008**, *28*, 33–48. (and the references therein)

31. Patra, S.K.; Rizzi, F.; Silva, A.; Rugina, D.O.; Bettuzzi, S. *J.* Molecular targets of (-)-epigallocatechin-3-gallate (EGCG): Specifity and interaction with membrane lipid rafts. *Physicol. Pharmacol.* **2014**, 217–235. (and the references therein)

32. Fujimura, Y.; Sumida, M.; Sugihara, K.; Tsukamoto, S.; Yamada, K.; Tachibana, H. Green tea polyphenol EGCG sensing motif on the 67-kDa laminin receptor. *PLoS One* **2012**, *7*.

33. Tachibana, H.; Koga, K.; Fujimura, Y.; Yamada, K. A receptor for green tea polyphenol EGCG. *Nat. Struct. Mol. Biol.* **2004**, *11*, 380–381.

34. Suzuki, Y.; Isemura, M. Inhibitory effect of epigallocatechin gallate on adhesion of murine melanoma cells to laminin. *Cancer Lett.* **2001**, *173*, 15–20.

35. Umeda, D.; Yano, S.; Yamada, K.; Tachibana, H. Involvement of 67-kDa laminin receptor-mediated myosin phosphatase activation in antiproliferative effect of epigallocatechin-3-O-gallate at a physiological concentration on Caco-2 colon cancer cells. *Biochem. Biophys. Res. Commun.* **2008**, *371*, 172–176.

36. Umeda, D.; Yano, S.; Yamada, K.; Tachibana, H. Green tea polyphenol epigallocatechin-3-gallate signaling pathway through 67-kDa laminin receptor. *J. Biol. Chem.* **2008**, *283*, 3050–3058. (and the references therein)

37. Byun, E. H.; Omura, T.; Yamada, K.; Tachibana, H. Green tea polyphenol epigallocatechin-3-gallate inhibits TLR2 signaling induced by peptidoglycan through the polyphenol sensing molecule 67-kDa laminin receptor. *FEBS Lett.* **2011**, *585*, 814–820. (and the references therein)

38. Fujimura, Y.; Umeda, D.; Yamada, K.; Tachibana, H. The impact of the 67 kDa laminin

receptor on both cell-surface binding and anti-allergic action of tea catechins. *Arch. Biochem. Biophys.* **2008**, *476*, 133–138. (and the references therein)

39. Lu, Y.-C.; Luo, P.-C.; Huang, C.-W.; Leu, Y.-L.; Wang, T.-H.; Wei, K.-C.; Wang, H.-E.; Ma, Y.-H. Augmented cellular uptake of nanoparticles using tea catechins: effect of surface modification on nanoparticle-cell interaction. *Nanoscale* **2014**, *6*, 10297–306.

40. Zheng, F. J.; Shi, L.; Yang, J.; Deng, X. H.; Wu, Y. Q.; Yan, X. Q.; Huang, N. Effect of tea polyphenols on the adhesion of highly metastatic human lung carcinoma cell lines to endothelial cells in vitro. *Asian Pacific J. Cancer Prev.* **2012**, *13*, 3751–3755.

41. Lo, H. M.; Hung, C. F.; Huang, Y. Y.; Wu, W. Bin Tea polyphenols inhibit rat vascular smooth muscle cell adhesion and migration on collagen and laminin via interference with cell-ECM interaction. *J. Biomed. Sci.* **2007**, *14*, 637–645.

42. Takahashi, A.; Watanabe, T.; Mondal, A.; Suzuki, K.; Kurusu-Kanno, M.; Li, Z.; Yamazaki, T.; Fujiki, H.; Suganuma, M. Mechanism-based inhibition of cancer metastasis with (-)-epigallocatechin gallate. *Biochem. Biophys. Res. Commun.* **2014**, *443*, 1–6.

43. Punathil, T.; Tollefsbol, T. O.; Katiyar, S. K. EGCG inhibits mammary cancer cell migration through inhibition of nitric oxide synthase and guanylate cyclase. *Biochem. Biophys. Res. Commun.* **2008**, *375*, 162–167.

44. Gu, J.; Makey, K. L.; Tucker, K. B.; Chinchar, E.; Mao, X.; Pei, I.; Thomas, E. Y.; Miele, L. EGCG , a major green tea catechin suppresses breast tumor angiogenesis and growth via inhibiting the activation of HIF-1 α and NF κ B , and VEGF expression. *Vasc. Cell* **2013**, *5*, 1–10.

45. Weber, A. A.; Neuhaus, T.; Skach, R. A.; Hescheler, J.; Ahn, H. Y.; Schrör, K.; Ko, Y.; Sachinidis, A. Mechanisms of the inhibitory effects of epigallocatechin-3 gallate on platelet-derived growth factor-BB-induced cell signaling and mitogenesis. *FASEB J.* **2004**, *18*, 128–130. (and the references therein)

46. McColl, J.; Horvath, R.; Aref, A.; Larcombe, L.; Chianella, I.; Morgan, S.; Yakubov, G. E.; Ramsden, J. J. Polyphenol control of cell spreading on glycoprotein substrata. *J. Biomater. Sci. Polym. Ed.* **2009**, *20*, 841–851.

47. Chan, C.-M.; Huang, J.-H.; Chiang, H.-S.; Wu, W.-B.; Lin, H.-H.; Hong, J.-Y.; Hung, C.-F. Effects of (-)-epigallocatechin gallate on RPE cell migration and adhesion. *Mol. Vis.* **2010**, *16*, 586–595.

48. Melgarejo, E.; Medina, M. Á.; Sánchez-Jiménez, F.; Urdiales, J. L. Epigallocatechin gallate reduces human monocyte mobility and adhesion in vitro. *Br. J. Pharmacol.* **2009**, *158*, 1705–1712.

49. Tudoran, O.; Soritau, O.; Balacescu, O.; Balacescu, L.; Braicu, C.; Rus, M.; Gherman, C.; Virag, P.; Irimie, F.; Berindan-Neagoe, I. Early transcriptional pattern of angiogenesis induced by EGCG treatment in cervical tumour cells. *J. Cell. Mol. Med.* **2012**, *16*, 520–530.

50. El-Schish, Z.; Mölder, A; Sebesta, M.; Gisselsson, L.; Alm, K.; a, G. W. Digital holographic microscopy – innovative and non-destructive analysis of living cells. *Microsc. Sci. Technol. Appl.*

Educ. **2010**, 1055–1062.

51. Persson, J.; Mölder, A.; Pettersson, S.; Alm, K. Cell motility studies using digital holographic microscopy. *Education* **2010**, 1063–1072.

52. Zhang, Q.; Tang, X.; Lu, Q.; Zhang, Z.; Rao, J.; Le, A. D. Green tea extract and (-)-epigallocatechin-3-gallate inhibit hypoxia- and serum-induced HIF-1alpha protein accumulation and VEGF expression in human cervical carcinoma and hepatoma cells. *Mol. Cancer Ther.* **2006**, *5*, 1227–1238.

53. Hellmann, J. K.; Münter, S.; Wink, M.; Frischknecht, F. Synergistic and additive effects of epigallocatechin gallate and digitonin on Plasmodium sporozoite survival and motility. *PLoS One* **2010**, *5*, 1–7.

54. Peter, B.; Nador, J.; Juhasz, K.; Dobos, A.; Korosi, L.; Székács, I.; Patko, D.; Horvath, R. Incubator proof miniaturized Holomonitor to *in situ* monitor cancer cells exposed to green tea polyphenol and preosteoblast cells adhering on nanostructured titanate surfaces: validity of the measured parameters and their corrections. *J. Biomed. Opt.* **2015**, *20*, 067002. (and the references therein)

55. Sugisawa, A.; Umegaki, K. Physiological concentrations of (-)-epigallocatechin-3-O-gallate (EGCg) prevent chromosomal damage induced by reactive oxygen species in WIL2-NS cells. *J. Nutr.* **2002**, *132*, 1836–1839.

56. Tran, P. L. C. H. B.; Kim, S.-A.; Choi, H. S.; Yoon, J.-H.; Ahn, S.-G. Epigallocatechin-3-gallate suppresses the expression of HSP70 and HSP90 and exhibits anti-tumor activity in vitro and in vivo. *BMC Cancer* **2010**, *10*, 276.

57. Hayakawa, S.; Saeki, K.; Sazuka, M.; Suzuki, Y.; Shoji, Y.; Ohta, T.; Kaji, K.; Yuo, a; Isemura, M. Apoptosis induction by epigallocatechin gallate involves its binding to Fas. *Biochem. Biophys. Res. Commun.* **2001**, *285*, 1102–1106.

58. Siddiqui, I. a; Asim, M.; Hafeez, B. B.; Adhami, V. M.; Tarapore, R. S.; Mukhtar, H. Green tea polyphenol EGCG blunts androgen receptor function in prostate cancer. *FASEB J.* **2011**, *25*, 1198–1207.

59. Kiss, A.; Bécsi, B.; Kolozsvári, B.; Komáromi, I.; Kövér, K. E.; Erdodi, F. Epigallocatechin-3-gallate and penta-O-galloyl-β-d-glucose inhibit protein phosphatase-1. *FEBS J.* **2013**, *280*, 612–626.

60. D'Agostino, E. M.; Rossetti, D.; Atkins, D.; Ferdinando, D.; Yakubov, G. E. Interaction of tea polyphenols and food constituents with model gut epithelia: The protective role of the mucus gel layer. *J. Agric. Food Chem.* **2012**, *60*, 3318–3328.

61. Scarpa, E.-S.; Ninfali, P. Phytochemicals as Innovative Therapeutic Tools against Cancer Stem Cells. *Int. J. Mol. Sci.* **2015**, *16*, 15727–15742. (and the references therein)

62. Tao, L.; Park, J.-Y.; Lambert, J. D. Differential prooxidative effects of the green tea polyphenol, (-)-epigallocatechin-3-gallate, in normal and oral cancer cells are related to differences in sirtuin 3 signaling. *Mol. Nutr. Food Res.* **2015**, *59*, 203–211.

63. Lu, L. Y.; Ou, N.; Lu, Q.-B. Antioxidant induces DNA damage, cell death and mutagenicity in human lung and skin normal cells. *Sci. Rep.* **2013**, *3*, 3169.

64. Das, S.; Tanwar, J.; Hameed, S.; Fatima, Z.; Manesar, G. Antimicrobial potential of epigallocatechin-3- gallate (EGCG): a green tea polyphenol. **2014**, *2*, 167–174. (and the references therein)

65. Anand, P. K.; Kaul, D.; Sharma, M. Green tea polyphenol inhibits Mycobacterium tuberculosis survival within human macrophages. *Int. J. Biochem. Cell Biol.* **2006**, *38*, 600–609. (and the references therein)

66. Sharma, S. K.; Kumar, G.; Kapoor, M.; Surolia, A. Combined effect of epigallocatechin gallate and triclosan on enoyl-ACP reductase of Mycobacterium tuberculosis. *Biochem. Biophys. Res. Commun.* **2008**, *368*, 12–17. (and the references therein)

67. Fatima, Z.; Hameed, S.; Islam, N. Expression of Mycobacterium tuberculosis 85B and proinflammatory TNF-α in human monocytes. **2012**, *2*, 1–6.

68. Patil, P. R.; Gemma, S.; Campiani, G.; Craig, A. G. Broad inhibition of plasmodium falciparum cytoadherence by (+)-epigallocatechin gallate. *Malar. J.* **2011**, *10*, 348.

69. Chandrashekaran, I. R.; Adda, C. G.; Macraild, C. a; Robin, F.; Norton, R. S. EGCG disaggregates amyloid-like fibrils formed by *Plasmodium falciparum* merozoite surface protein 2. *NIH Public Access*. **2012**, *513*, 153–157. (and the references therein)

70. Lambert, J.D.; Lee, M-J.; Diamond, L.; Ju, J.; Hong, J.; Bose, M.; Newmark, H.L.; C.S. Yang, C.S. Dose-dependent levels of epigallocatechin-3-gallate in human colon cancer cells and mouse plasma and tissues. *Drug Metab. Dispos.*, **2006**, *34*, 8–11.

71. Kim, S.; Lee, M. J.; Hong, J.; Li, C.; Smith, T. J.; Yang, G. Y.; Seril, D. N.; Yang, C. S. Plasma and tissue levels of tea catechins in rats and mice during chronic consumption of green tea polyphenols. *Nutr. Cancer* **2000**, *37*, 41–48. (and the references therein)

72. Li, W.; Zhu, S.; Li, J.; Assa, A.; Jundoria, A.; Xu, J.; Fan, S.; Eissa, N. T.; Tracey, K. J.; Sama, A. E.; Wang, H. EGCG stimulates autophagy and reduces cytoplasmic HMGB1 levels in endotoxin-stimulated macrophages. *Biochem. Pharmacol.* **2011**, *81*, 1152–1163.

73. Fujiki, H.; Sueoka, E.; Watanabe, T.; Suganuma, M. Synergistic enhancement of anticancer effects on numerous human cancer cell lines treated with the combination of EGCG, other green tea catechins, and anticancer compounds. *J. Cancer Res. Clin. Oncol.* **2014**. (and the references therein)

74. Hu, F.; Wei, F.; Wang, Y.; Wu, B.; Fang, Y.; Xiong, B. EGCG synergizes the therapeutic effect of cisplatin and oxaliplatin through autophagic pathway in human colorectal cancer cells. *J. Pharmacol. Sci.* **2015**, *128*, 27–34.

75. Song, Q.; Li, D.; Zhou, Y.; Yang, J.; Yang, W.; Zhou, G.; Wen, J. Enhanced uptake and transport of (+) -catechin and (−) -epigallocatechin gallate in niosomal formulation by human intestinal Caco-2 cells. **2014**, 2157–2165.

76. Wang, S.; Su, R.; Nie, S.; Sun, M.; Zhang, J.; Wu, D.; Moustaid-Moussa, N. Application of nanotechnology in improving bioavailability and bioactivity of diet-derived phytochemicals. *J. Nutr. Biochem.* **2014**, *25*, 363–376. (and the references therein)

77. Ding, J.; Kong, X.; Yao, J.; Wang, J.; Cheng, X.; Tang, B.; He, Z. Core–shell mesoporous silica nanoparticles improve HeLa cell growth and proliferation inhibition by (−)-epigallocatechin-3-gallate by prolonging the half-life. *J. Mater. Chem.* **2012**, *22*, 19926.

78. de Pace, R. C. C.; Liu, X.; Sun, M.; Nie, S.; Zhang, J.; Cai, Q.; Gao, W.; Pan, X.; Fan, Z.; Wang, S. Anticancer activities of (-)-epigallocatechin-3-gallate encapsulated nanoliposomes in MCF7 breast cancer cells. *J. Liposome Res.* **2013**, *23*, 187–96.

79. Luo, X.; Guan, R.; Chen, X.; Tao, M.; Ma, J.; Zhao, J. Optimization on condition of epigallocatechin-3-gallate (EGCG) nanoliposomes by response surface methodology and cellular uptake studies in Caco-2 cells. *Nanoscale Res. Lett.* **2014**, *9*, 291. (and the references therein)

80. Hu, B.; Ting, Y.; Yang, X.; Tang, W.; Zeng, X.; Huang, Q. Nanochemoprevention by encapsulation of (−)-epigallocatechin-3-gallate with bioactive peptides/chitosan nanoparticles for enhancement of its bioavailability. *Chem. Commun.* **2012**, *48*, 2421.

81. Dube, A.; Nicolazzo, J. a.; Larson, I. Chitosan nanoparticles enhance the intestinal absorption of the green tea catechins (+)-catechin and (-)-epigallocatechin gallate. *Eur. J. Pharm. Sci.* **2010**, *41*, 219–225.

82. Shukla, R.; Chanda, N.; Zambre, a.; Upendran, a.; Katti, K.; Kulkarni, R. R.; Nune, S. K.; Casteel, S. W.; Smith, C. J.; Vimal, J.; Boote, E.; Robertson, J. D.; Kan, P.; Engelbrecht, H.; Watkinson, L. D.; Carmack, T. L.; Lever, J. R.; Cutler, C. S.; Caldwell, C.; Kannan, R.; Katti, K. V. Laminin receptor specific therapeutic gold nanoparticles (198AuNP-EGCg) show efficacy in treating prostate cancer. *Proc. Natl. Acad. Sci.* **2012**, *109*, 12426–12431.

83. Landis-Piwowar, K.; Chen, D.; Foldes, R.; Chan, T.-H.; Dou, Q. P. Novel epigallocatechin gallate analogs as potential anticancer agents: a patent review (2009 - present). *Expert Opin. Ther. Pat.* **2013**, *23*, 189–202. (and the references therein)

84. Chung, J. E.; Tan, S.; Gao, S. J.; Yongvongsoontorn, N.; Kim, S. H.; Lee, J. H.; Choi, H. S.; Yano, H.; Zhuo, L.; Kurisawa, M.; Ying, J. Y. Self-assembled micellar nanocomplexes comprising green tea catechin derivatives and protein drugs for cancer therapy. *Nat. Nanotechnol.* **2014**, *9*, 907–912.

85. Haratifar, S.; Meckling, K. A.; Corredig, M. Antiproliferative activity of tea catechins associated with casein micelles, using HT29 colon cancer cells. *J. Dairy Sci.* **2014**, *97*, 672–678.

86. Hsieh, D. S.; Wang, H.; Tan, S. W.; Huang, Y. H.; Tsai, C. Y.; Yeh, M. K.; Wu, C. J. The treatment of bladder cancer in a mouse model by epigallocatechin-3-gallate-gold nanoparticles. *Biomaterials* **2011**, *32*, 7633–7640.

87. Li, N.; Chen, Y.; Zhang, Y.-M.; Yang, Y.; Su, Y.; Chen, J.-T.; Liu, Y. Polysaccharide-gold nanocluster supramolecular conjugates as a versatile platform for the targeted delivery of anticancer drugs. *Sci. Rep.* **2014**, *4*, 4164.

88. Croissant, J. G.; Zhang, D.; Alsaiari, S.; Lu, J.; Deng, L.; Tamanoi, F.; AlMalik, A. M.; Zink, J. I.; Khashab, N. M. Protein-gold clusters-capped mesoporous silica nanoparticles for high drug loading, autonomous gemcitabine/doxorubicin co-delivery, and in-vivo tumor imaging. *J. Control. Release* **2016**, *229*, 183–191.

89. McIntosh, C. M.; Esposito, E. A.; Boal, A. K.; Simard, J. M.; Martin, C. T.; Rotello, V. M. Inhibition of DNA transcription using cationic mixed monolayer protected gold clusters. *J. Am. Chem. Soc.* **2001**, *123*, 7626–7629.

90. Koehn, F. E.; Carter, G. T. The evolving role of natural products in drug discovery. *Nat. Rev. Drug Discov.* **2005**, *4*, 206–220. (and the references therein)

91. Orgovan, N.; Peter, B.; Bősze, S.; Ramsden, J. J.; Szabó, B.; Horvath, R. Dependence of cancer cell adhesion kinetics on integrin ligand surface density measured by a high-throughput label-free resonant waveguide grating biosensor. *Sci. Rep.* **2014**, *4*, 4034. (and the references therein)

92. Zhang, X.; Deng, H.; Xiao, Y.; Xue, X.; Ferrie, A. M.; Tran, E.; Liang, X.; Fang, Y. Label-free cell phenotypic profiling identifies pharmacologically active compounds in two traditional Chinese medicinal plants. *RSC Adv.* **2014**, *4*, 26368.

93. Stephens, D. J.; Allan, V.J. Light Microscopy Techniques for Live Cell Imaging. *Sci. (New York, NY)* **2003**, *300*, 82–86.

94. Székács, I.; Horvath, R.; Székács; A. Label-Free Optical Biosensors for Monitoring Cellular Processes and Cytotoxic Agents at Interfaces Using Guided Modes and Advanced Phase-Contrast Imaging Techniques. *Biosensors for Security and Bioterrorism Applications, Advanced Sciences and Technologies for Security Applications (Springer)* **2016**, 443-468. (and the references therein)

95. Székács, I.; Fejes, Á.; Klátyik, S.; Takács, E.; Patkó, D.; Pomóthy, J.; Mörtl, M.; Horváth, R.; Madarász, E.; Darvas, B.; Székács, A. Environmental and Toxicological Impacts of Glyphosate with Its Formulating Adjuvant. *Int. Sch. Sci. Res. Innov.* **2014**, *8*, 19–24.

96. Tóth, A. E.; Walter, F. R.; Bocsik, A.; Sántha, P.; Veszelka, S.; Nagy, L.; Puskás, L. G.; Couraud, P. O.; Takata, F.; Dohgu, S.; Kataoka, Y.; Deli, M. A. Edaravone protects against methylglyoxal-induced barrier damage in human brain endothelial cells. *PLoS One* **2014**, *9*, 1–14.

97. Mitchell, J. Small molecule immunosensing using surface plasmon resonance. *Sensors* **2010**, *10*, 7323–7346.

98. Yetisen, A. K.; Naydenova, I.; da Cruz Vasconcellos, F.; Blyth, J.; Lowe, C. R. Holographic sensors: three-dimensional analyte-sensitive nanostructures and their applications. *Chem. Rev.* **2014**, *114*, 10654–10696.

99. Cooper, M. A. Optical biosensors: where next and how soon? *Drug Discov. Today* **2006**, *11*, 1061–1067.

100. Vörös, J.; Ramsden, J. J.; Csúcs, G.; Szendro, I.; De Paul, S. M.; Textor, M.; Spencer, N. D. Optical grating coupler biosensors. *Biomaterials* **2002**, *23*, 3699–3710. (and the references therein)

101. Kurrat, R.; Textor, M.; Ramsden, J. J.; Böni, P.; Spencer, N. D. Instrumental improvements in optical waveguide light mode spectroscopy for the study of biomolecule adsorption. *Rev. Sci. Instrum.* **1997**, *68*, 2172–2176.

102. Kurrat, R. Adsorption of Biomolecules on Titanium Oxide Layers in Biological Model Solutions. **1998**, 1–103.

103. Ramsden, J. J.; Li, S. Y.; Heinzle, E.; Prenosil, J. E. Optical method for measurement of number and shape of attached cells in real time. *Cytometry* **1995**, *19*, 97–102.

104. Hug, T. S.; Prenosil, J. E.; Morbidelli, M. Optical waveguide lightmode spectroscopy as a new method to study adhesion of anchorage-dependent cells as an indicator of metabolic state. *Biosens. Bioelectron.* **2001**, *16*, 865–874.

105. Székács, A.; Adányi, N.; Székács, I.; Majer-Baranyi, K.; Szendro, I. Optical waveguide light-mode spectroscopy immunosensors for environmental monitoring. *Appl. Opt.* **2009**, *48*, B151–8.

106. Shamah, S. M.; Cunningham, B. T. Label-free cell-based assays using photonic crystal optical biosensors. *Analyst* **1090**, *136*, 1090–1102.

107. Patko, D.; Cottier, K.; Hamori, A.; Horvath, R. Single beam grating coupled interferometry: high resolution miniaturized label-free sensor for plate based parallel screening. *Opt. Express* **2012**, *20*, 23162.

108. Fang, Y. Resonant Waveguide Grating Biosensor for Microarrays. *Optical Guided-wave Chemical and Biosensors II., Chemical Sensors and Biosensors 8 (Springer)* **2010**. (and the references therein)

109. Fang, Y. Probing cancer signaling with resonant waveguide grating biosensors. *Expert Opin. Drug Discov.* **2010**, *5*, 1237–1248.

110. Fang, Y. Label-free cell-based assays with optical biosensors in drug discovery. *Assay Drug Dev. Technol.* **2006**, *4*, 583–595.

111. Fang, Y.; Ferrie, A. M.; Fontaine, N. H.; Mauro, J.; Balakrishnan, J. Resonant waveguide grating biosensor for living cell sensing. *Biophys. J.* **2006**, *91*, 1925–40.

112. Hassanzadeh, A.; Azami, D. Waveguide evanescent field fluorescence microscopy: theoretical investigation of optical pressure on a cell. *J. Nanophotonics* **2014**, *8*, 083076.

113. Peter, B.; Kurunczi, S.; Patko, D.; Lagzi, I.; Kowalczyk, B.; Grzybowski, B. A.; Horvath, R. Label-Free in Situ Optical Monitoring of the Adsorption of Oppositely Charged Metal Nanoparticles. *Langmuir* **2014**, *30*, 13478-13482. (and the references therein)

114. Millipore Actin Cytoskeleton and Focal Adhesion Staining Kit Cat. No. FAK100 manual

2009, 1–7.

115. Liu, Y.; Peterson, D. A.; Kimura, H.; Schubert, D. Mechanism of cellular 3-(4,5-dimethylthiazol-2-yl)-2,5-diphenyltetrazolium bromide (MTT) reduction. *J. Neurochem.* **1997**, *69*, 581–93.

116. Supino, R. MTT Assays. *In Vitro Toxicity Testing Protocols, Methods in Molecular Biology (Humana Press),* **1995**, 43, 137-149.

117. Morgan, D. M. Tetrazolium (MTT) assay for cellular viability and activity. *Methods Mol. Biol.* **1998**, *79*, 179–183.

118. Horobin, R. W. Selection of optimum tetrazolium salts for use in histochemistry: the value of structure-staining correlations. *Histochem. J.* **1982**, *14*, 301–310.

119. Slater, T. F.; Sawyer, B.; Straeuli, U. Studies on Succinate-Tetrazolium Reductase Systems. Iii. Points of Coupling of Four Different Tetrazolium Salts. *Biochim. Biophys. Acta* **1963**, *77*, 383–393.

120. Mosmann, T. Rapid colorimetric assay for cellular growth and survival: application to proliferation and cytotoxicity assays. *J. Immunol. Methods* **1983**, *65*, 55–63.

121. Altman, F. P. *Tetrazolium salts and formazans.*; Gustav Fischer Verlag · Stuttgart, 1976; Vol. 9.

122. Denizot, F.; Lang, R. Rapid colorimetric assay for cell growth and survival. Modifications to the tetrazolium dye procedure giving improved sensitivity and reliability. *J. Immunol. Methods* **1986**, *89*, 271–277.

123. Peter, B.; Salanki, R.; Szekacs, I.; Bősze, S.; Horvath, R. Label - free cytotoxicity assay using the kinetic cell spreading data . Under preparation.

124. Tiefenthaler, K.; Lukosz, W. Sensitivity of grating couplers as integrated-optical chemical sensors. *J. Opt. Soc. Am. B* **1989**, *6*, 209.

125. MicroVacuum Ltd. Optical Waveguide Lightmode Spectroscopy System OWLS210 Hardware Operator's Manual **2014**.

126. Physics, S.; March, R.; Chemistry, B.; Engineering, C. Review of New Experimental Techniques for Investigating Random Sequential Adsorption.Pdf. **1993**, *73*, 853–877.

127. Ramsden, J. J.; Horvath, R. Optical biosensors for cell adhesion. *J. Recept. Signal Transduct. Res.* **2009**, *29*, 211–223.

128. Orgovan, N.; Kovacs, B.; Farkas, E.; Szabó, B.; Zaytseva, N.; Fang, Y.; Horvath, R. Bulk and surface sensitivity of a resonant waveguide grating imager. *Appl. Phys. Lett.* **2014**, *104*, 1–5.

129. Peter, B.; Farkas, E.; Forgacs, E.; Saftics, A.; Kurunczi, S.; Szekacs, I. Label-free optical biosensor to real-time study multicomponent model system of cell-surface interactions : a case study on polymer coatings exposed to EGCg and their interactions with living cells. Under

submission. 1–21.

130. Lee, S.; Spencer, N. D. Adsorption properties of poly(L-lysine)-graft-poly(ethylene glycol) (PLL-g-PEG) at a hydrophobic interface: Influence of tribological stress, pH, salt concentration, and polymer molecular weight. *Langmuir* **2008**, *24*, 9479–9488.

131. Orgovan, N.; Peter, B.; Bősze, S.; Ramsden, J. J.; Szabó, B.; Horvath, R. Dependence of cancer cell adhesion kinetics on integrin ligand surface density measured by a high-throughput label-free resonant waveguide grating biosensor. *Sci. Rep.* **2014**, *4*, 4034. (and the references therein)

132. VandeVondele, S.; Voros, J.; Hubbell, J. A. RGD-grafted poly-L-lysine-graft-(polyethylene glycol) copolymers block non-specific protein adsorption while promoting cell adhesion. *Biotechnol. Bioeng.* **2003**, *82*, 784–790.

133. Tosatti, S.; Schwartz, Z.; Campbell, C.; Cochran, D. L.; Vandevondele, S.; Hubbell, J. A.; Denzer, A.; Simpson, J.; Wieland, M.; Lohmann, C. H.; Textor, M.; Boyan, B. D. RGD-containing peptide GCRGYG RGD SPG reduces enhancement of osteoblast differentiation by poly (L - lysine) - graft -poly (ethylene glycol) -coated titanium surfaces. *J Biomed Mater Res A.* **2004**, *68*, 458-72.

134. Kunzler, T. P.; Huwiler, C.; Drobek, T.; Vörös, J.; Spencer, N. D. Systematic study of osteoblast response to nanotopography by means of nanoparticle-density gradients. *Biomaterials* **2007**, *28*, 5000–5006.

135. Pasche, S.; Textor, M.; Meagher, L.; Spencer, N. D.; Griesser, H. J. Relationship between interfacial forces measured by colloid-probe atomic force microscopy and protein resistance of poly(ethylene glycol)-grafted poly(L-lysine) adlayers on niobia surfaces. *Langmuir* **2005**, *21*, 6508–6520.

136. Bretscher, A.; Drees, B.; Harsay, E.; Schott, D.; Wang, T. What are the basic functions of microfilaments? Insights from studies in budding yeast. *J. Cell Biol.* **1994**, *126*, 821–825.

137. Yamada, K. Molecular interactions in cell adhesion complexes. *Curr. Opin. Cell Biol.* **1997**, *9*, 76–85.

138. Burridge, K.; Nuckolls, G.; Otey, C.; Pavalko, F.; Simon, K.; Turner, C. Actin-membrane interaction in focal adhesions. *Cell Differ. Dev.* **1990**, *32*, 337–342.

139. Turner, E.; Burridge, K. Transmembrane molecular matrix assemblies interactions in cell-extracellular. *Curr. Opin. Cell Biol.* **1991**, *3*, 849–53.

140. Orgovan, N.; Patko, D.; Hos, C.; Kurunczi, S.; Szab??, B.; Ramsden, J. J.; Horvath, R. Sample handling in surface sensitive chemical and biological sensing: A practical review of basic fluidics and analyte transport. *Adv. Colloid Interface Sci.* **2014**, *211*, 1–16.

141. Wang, P.; Henning, S. M.; Heber, D. Limitations of MTT and MTS-based assays for measurement of antiproliferative activity of green tea polyphenols. *PLoS One* **2010**, *5*.

142. Alm, K.; El-Schich, Z.; Miniotis, M.F.; Wingren, A.G.; Janicke, B.; Oredsson, S. Cells and Holograms-Holograms and Digital Holographic Microscopy as a Tool to Study the Morphology of Living Cells. *Holography – Basic Principles and Contemporary Applications (InTech)*, **2013**, 335-351.

143. Orgovan, N.; Salánki, R.; Sándor, N.; Bajtay, Z.; Erdei, A.; Szabó, B.; Horvath, R. In-situ and label-free optical monitoring of the adhesion and spreading of primary monocytes isolated from human blood: Dependence on serum concentration levels. *Biosens. Bioelectron.* **2014**, *54*, 339–344.

REFERENCES FROM THE INTERNET

I1. http://www.phiab.se/technology/phase-contrast-microscopy

I2.http://zeiss-campus.magnet.fsu.edu/articles/basics/contrast.html

I3. https://commons.wikimedia.org/wiki/File:Phase_shift_image_of_cells_in_3D.jpg

I4. http://www.phiab.se/products/products

I5. http://www.phiab.se/technology/holographic-microscopy

I6. http://www.accela.eu/phase-holographic-imaging/holomonitor-m3

I7. http://www.owls-sensors.com/pdf/OWLS_Standard_System.pdf